Investigation of Interface modelling techniques using finite element analysis with ATENA

Arjun Vithalkar

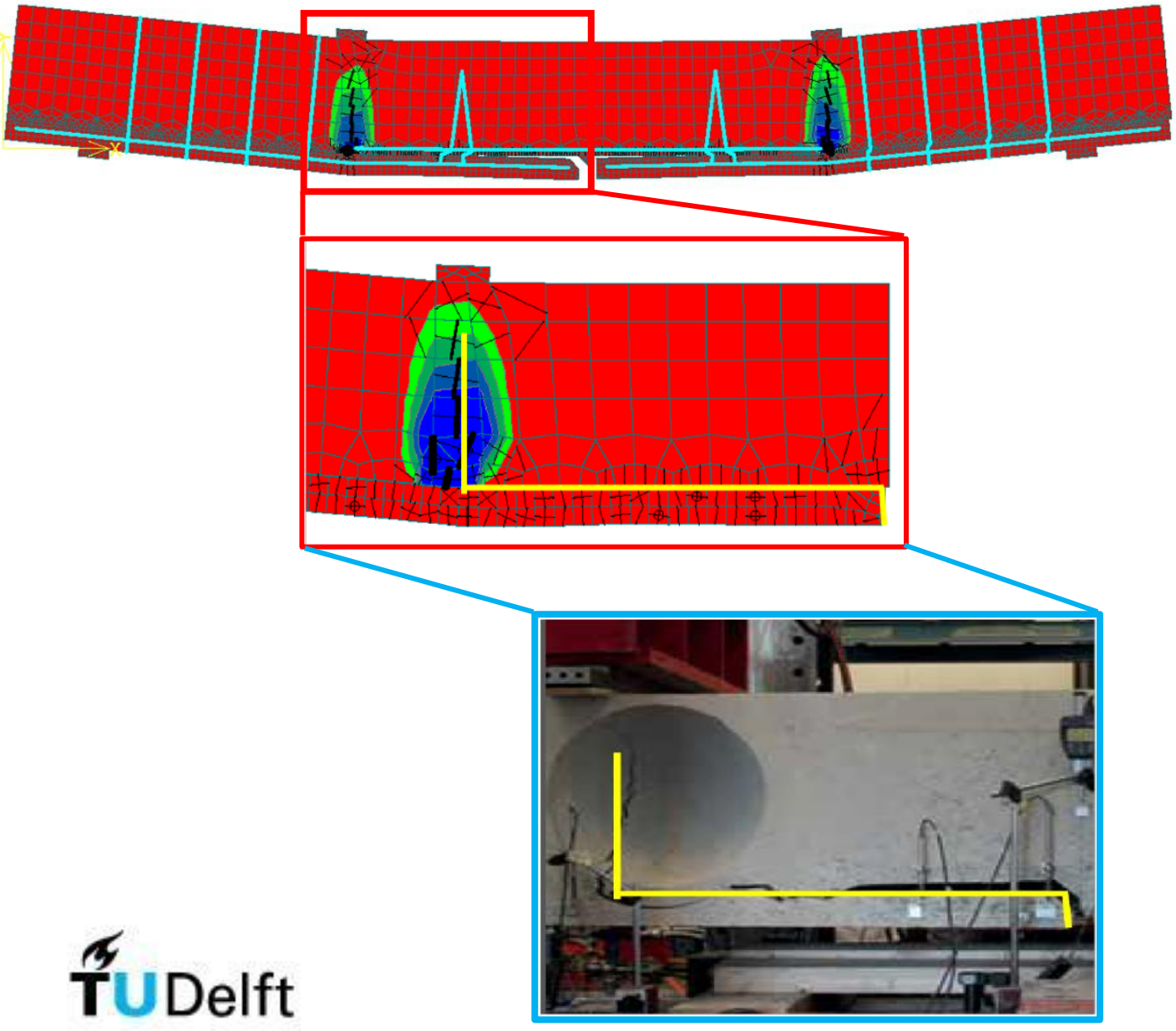

TU Delft

Investigation of interface modelling techniques using finite element analysis with ATENA

by

Arjun Vithalkar

Research proposal
in partial fulfillment of the requirements for the degree of

Master of Science
in Structural Engineering

at the Delft University of Technology,

Student number	: 4623894
Chairman	: Dr. ir. drs. C.R. Braam
Daily Supervisor	: Mrs. dr. ir. M. Lukovic
Committee member	: Ir. L. J. M. Houben

Abstract

Study of interface behavior has been the primary area of focus for researchers in the field of concrete science and technology. This interface between two concrete elements becomes important for prefabricated systems, combination of precast and in-situ concrete elements, combinations of concrete cast at different times, repairs of existing concrete structures, strengthening of a structural element such as beam or slab and so on. In this research an attempt is made to check if the interface behavior is reliably predicted using finite element analysis in ATENA with the help of standard elements available in the software. Validation of the numerical results is performed by simulating an experimental bond test and structural test and conclusions are drawn based on the response of these numerical models.

Strength of the interface is mainly governed by the roughness of the adjacent surfaces. In the literature study, a chronological overview of the development of shear models is presented that make use of these roughness parameters in calculating shear capacity of the interface. A finite element analysis is performed using standard elements available in ATENA. ATENA interface material model (ATENA IMM), present in the software uses 2D line interface elements having zero thickness to model an interface. Roughness parameters assigned to this model are based on the guidelines proposed in different design codes. Many parameters need to be defined in this interface that are difficult to measure accurately from experiments. For this, a 5 mm thick artificial interface layer is created by using 2D linear quadrilateral material elements. This technique is named as artificial interface model (ArtIM) that uses physical material properties to define the interface. Since, cohesion and friction coefficient parameters cannot be specifically defined in ArtIM unlike in ATENA IMM, an explicit roughness is incorporated by designing the interface layer in a wave pattern with certain wavelength and amplitude depending on the different surface roughness classes as defined in the Model Code 2010.

A check is performed for the assigned input parameters for the two interface modelling techniques, by simulating bond tests (direct tension test and shear load test) on a small scale composite concrete specimen. Furthermore, validation of the two interface modelling techniques is carried out by comparing the numerical results to experimental findings for a bond test performed by T. Paulay, R. Park and M. H. Phillips [1] and for a structural test case of the Eindhoven airport car park garage failure [2], [3]. ATENA IMM rightly predicts the initial response of the interface but does not comply with the experimental results once the interface fails. With the use of ArtIM, an overestimation of the shear strength is exhibited and the conventional ratio of 2 between the shear and tensile strength [4], [5] cannot be obtained. Moreover, once the material in the interface layer fails, a brittle behavior is exhibited pertaining to the concrete properties assigned to the interface material layer.

Different reinforcement modelling techniques are studied using ATENA IMM with a very low bond strength (no bond condition). The default 1-D reinforcement (RF) bar element when modelled perpendicular to the interface does not reliably predict the response of loading. Hence, other RF modelling techniques are discussed among which, 1-D RF bar elements modelled in cross pattern reliably predict the initial stiffness of the RF bars. The inclination of the RF bars was tested for different angles to comply with the experimental results. However, further research is required to calculate appropriate inclination of the RF bars. In this case the optimum angle between the cross RF bars and interface is around 80°.

In the structural test, interface behavior is investigated for a specimen with (fully reinforced) and without (partially reinforced) shear reinforcement in the flexural span. ATENA IMM safely predicts the bond strength in case of both, partially reinforced and fully reinforced models. However, by using ArtIM, an overestimation of the interface strength is observed. The important aspect in the structural model is the shear strength of the interface and since, while using an artificial material element for the interface the shear strength obtained is almost 40% higher than the experimental results, the ultimate load carrying capacity of the whole model increases manifold.

After investigating the two interface modelling techniques, on bond level and structural level, it can be

concluded that, the ATENA interface material model (IMM) as well as the artificial interface model (ArtIM) do not predict the interface behavior reliably. However, by using ATENA IMM a conservative response is obtained as opposed to the ArtIM which overestimates the shear capacity of the interface.

Acknowledgement

My time in TU Delft till now has been very insightful and full of new experiences. The lessons I learnt here, will help me not only until my graduation period but also for the rest of my life. I thank you TU Delft and especially Concrete Structures track for making my dream come true.

First of all, I would like to thank my supervisor Mrs. dr. ir. Mladena Luković for her support and for providing me with all the resources that were needed during this master thesis work. Her enthusiasm and support in every aspect motivated me to take up this project and successfully carry it to the end.

I would also like to thank my chairman Dr. ir. drs. René Braam for helping me with some important aspects of my thesis work. His contribution in the progress meetings really helped me understand the topic more clearly.

Moreover, I would like to thank my friends Prajakta, Srinidhi, Nikhil, Kshiteej, Sakshi, Nilaya, Rucha, Ajinkya and Rajashree for supporting me and for providing valuable inputs throughout my graduation journey.

Last, but not the least, I would like to thank my sister, brother-in-law, my parents and my grandparents for their trust and continuous support in all the situations. Their love has always motivated me to give my best performance.

List of Figures

List of Tables

Contents

1

Introduction

1.1. In general

With the increasing demand of concrete structures interaction between the old and new concrete has become a primary area of concern for many researchers around the globe. The most important aspect in the interaction between two adjacent concrete elements is the bond between them at the interface level. Thus, study of interface behavior has been the main area of focus. This interface between two concrete elements becomes important for prefabricated systems, combination of precast and in-situ concrete elements, combinations of concrete cast at different times, repairs of existing concrete structures, strengthening of a structural element such as beam or slab and so on.

Study of interfaces is not a straightforward topic. Many aspects influence the strength of interfaces such as surface roughness of the adjacent concrete elements, aggregate size used in the concrete, surface preparation techniques, mechanical devices crossing the interface, concrete strength of the adjacent elements etc. Design codes developed to this day (ACI 318, Eurocode 2, Model Code 2010), propose guidelines to determine the strength of the interface. As per the advancement of these codes very few parameters are considered for calculating the interface strength. However, interaction between different factors, as mentioned earlier, and sometimes combinations of some of these factors ultimately account for the strength of this interface.

Out of all the factors mentioned earlier, an attempt is made to understand the influence of roughness parameters like, cohesion, tensile strength and coefficient of friction at the interface level. These parameters define the interaction at the interface, between two concrete elements. Moreover, effect of reinforcement bars crossing the interface is studied by using different design techniques proposed in this research to model these bars. To validate the use of these reinforcement modelling techniques, the numerical results obtained in this research are compared directly to the experimental findings produced by T. Paulay, R. Park and M. H. Phillips [1]. Guidelines from the different design codes are used as a basis for the analyses presented in this report. Since, the design codes provide guidelines on structural level, these analytical models are not always useful to perform complex analyses on the entire structure. To perform a complete analyses of a structure, for example a bridge or a building, these structures need to be divided into small structural elements like slabs, beams and columns. Analyses of these individual elements can be performed, using the analytical formulae but without 100% accuracy. Performing a numerical analysis using various finite element software packages has proven to be very successful in order to reduce such intense labor and to improve the accuracy of these analyses. Although, FEA may not estimate the structural response perfectly, it still gives a conservative approach while designing.

The numerical analysis is performed by using ATENA finite element software specifically developed for concrete and reinforced concrete structures. The standard elements available in this software, such as 2D interface elements used in interface material model (IMM) and quadrilateral material elements used for developing an artificial interface (ArtIM), are used for the analysis in this research. However, the ATENA IMM has a dependency on many parameters pertaining to the roughness of the adjacent concrete surfaces. It is difficult to accurately measure the roughness parameters with experiments. Hence, another artificial

interface model (ArtIM) is proposed in this research which uses quadrilateral material elements to create an artificial interface layer with a certain thickness. Physical concrete properties such as elastic modulus, compressive and tensile strength of the material, are defined for the artificial interface layer. To incorporate the roughness effect, the artificial interface layer is modelled in a wave pattern with certain wave length and amplitude. Effect of this explicit roughness profile is studied in detail.

The numerical analyses of different composite concrete specimens using the two interface models in performed in three parts. In the first part, verification of the ATENA Interface Material Model (IMM) and the Artificial Interface Model (ArtIM) is carried out by subjecting a small scale bond model to direct tension test and shear load test. Parametric analysis is performed by varying different parameters involved in the interaction. The next two stages after verification of the interface models, are the validation of the numerical models. First validation is performed on a material model by comparing numerical results to the experimental observations established T. Paulay, R. Park and M. H. Phillips. The second validation is performed on a structural model which involves the comparison of numerical results to the research performed in the case study of Eindhoven car parking garage.

This research thus provides guidelines on the methodology of modelling an interface and analyses of the observations obtained by making use of the two interface models are presented to justify these guidelines.

In the next section, outline of the entire research and flow of the report is discussed for better understanding.

1.2. Outline of Master Thesis

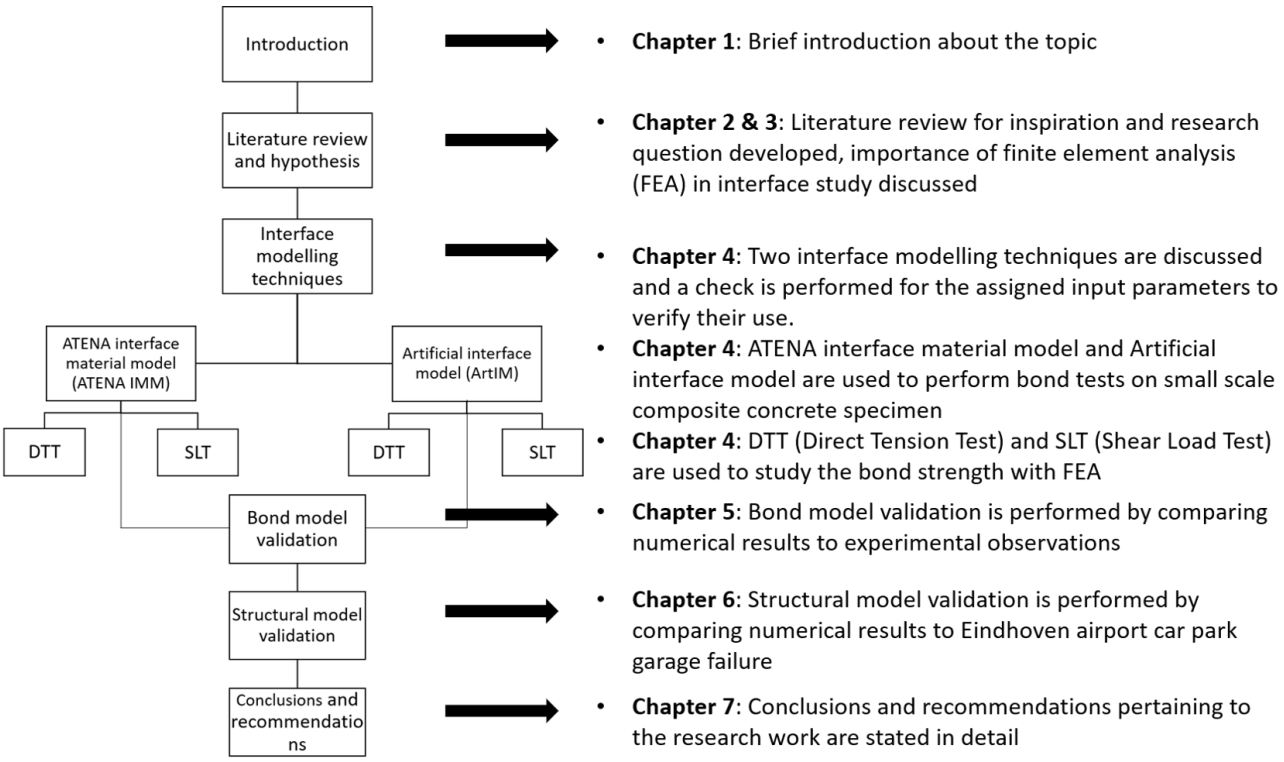

Figure 1.1: Flow of the research work

2

Literature review

In the study of interfaces it is noted that, various factors have a combined effect on the overall strength of the interface. These factors include the roughness of the adjacent concrete surfaces, workability of concrete, shrinkage and deformation compatibility, temperature effects and cement to aggregate bond in concrete. In this research main focus is given to the roughness characteristics that affect the bond strength between two concrete layers. A detailed literature study regarding interface strength and the different shear models proposed by various scientists is discussed in this chapter. Limited information is present on the shear capacity of composite concrete structures specifically focusing on the influence of bond strength. Considering the various guidelines proposed by the old design codes, an estimate about the bond strength and its relevance with respect to the shear capacity of a composite concrete model can be estimated.

2.1. Shear Models: A chronological overview

Many researchers are still working to understand the influence of interface characteristics on the shear capacity of a composite concrete section. This section presents a chronological development of the design codes and the factors which these codes focus upon, to establish guidelines to calculate shear strength at the interface.

Shear Friction Theory (SF)

In design codes, such as ACI 318 [11], Eurocode 2 and fib Model Code 2010, prediction of the longitudinal shear strength of the interface between two concrete layers cast at different times, is made using the shear friction theory. The bond strength between these two concrete layers depends mainly on the following parameters,

- *substrate roughness*, the cohesion and friction parameters contribute to the surface roughness in the models
- *material strength* of adjacent concrete layers along-with the aggregate interaction with the concrete is crucial for the bond between the two concrete layers
- *shear connectors* crossing the interface are mainly activated once the bond breaks. Nevertheless they provide higher ductility to the composite concrete section along-with a rise in the final shear capacity of the interface

However, there are many others factors such as, differential shrinkage due to varying curing conditions and differential stiffness due to different concrete Young's modulus of different layers, which are not accounted in the design codes and separate research is to be carried out in these respective areas.

An attempt to include the effect of the aforementioned three main parameters, in a more accurate prediction of longitudinal shear strength is made by Santos and Júlio [12]. Their research signifies that, the load transfer mechanism of shear forces between concrete parts cast at different times results from the combination of three main parameters: cohesion, friction and dowel action. Although, this cohesion parameter is considered

in many design guidelines, dowel action is usually neglected. Only the shear-friction parameter is considered in all design provisions. A 'saw-tooth model' is shown in Figure 2.1a to exemplify this concept.

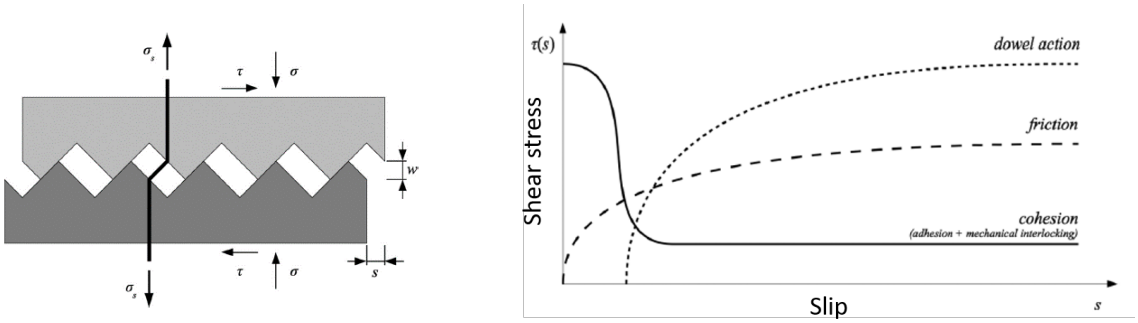

(a) Saw-tooth model

(b) Shear stress - slip behavior [12]

Figure 2.1: Load transfer mechanisms

Figure 2.1b, shows the contribution of roughness parameters with the increment in slip according to Santos and Júlio [12]. In the initial phase, Van der Waals forces acting between the particles are very strong which results in the adhesion and aggregate interlocking effect. Major contribution to the shear stress transfer is made by these cohesion parameters at low slip values. The frictional resistance provided due to the interaction between the two concrete layers increases gradually as the stress increases. However, once the interface reaches the peak shear capacity failure at the interface occurs. This results in stress redistribution and effect of Van der Waals forces almost diminishes (drop in stress value). At his stage, the stress transfer mainly takes place due to the reinforcement bars/dowels crossing the interface. Depending on the material strength of the dowels a bending resistance is provided in order to transfer the shear stress. This leads to a gradual increase in the dowel action phenomenon, with a subsequent stability in shear stress transfer until development of kinks in the dowels.

The "shear friction theory" was first proposed by Birkeland and Birkeland [13], for the prediction of ultimate longitudinal shear stress at concrete-to-concrete interfaces in the presence of reinforcement bars crossing the interface. The shear stress expression is given in Equation 2.1. The coefficient of friction varies as per the surface preparation methods and has different values in different interface combinations.

1. $\mu = 1.7$, monolithic concrete,
2. $\mu = 1.4$, artificially roughened construction joints,
3. $\mu = 0.8$ to 1.0, ordinary construction joints or steel-to-concrete interfaces

$$v_u = \mu \rho f_y \tag{2.1}$$

where,

v_u : shear capacity
μ : coefficient of friction
ρ : reinforcement ratio
f_y : yield strength of reinforcement bars

This expression only considers the contribution of friction thus, neglecting other important parameters namely, adhesion and aggregate interlocking, concrete strength of the weakest layer and dowel action due to deformation of reinforcing bars. Hence, further important models were proposed by various scientists.

Modified Shear Friction Theory (MSF)

One such modification to the shear-friction theory, also called as, "Modified shear friction theory" proposed by Mattock and Hawkins [14], gives an expression (Equation 2.2) for the prediction of longitudinal shear

stress at the interface.

$$v_u = 1.38 + 0.8(\rho f_y + \sigma_n)(MPa) \tag{2.2}$$

The assumed constant $1.38\ N/mm^2$, gives the contribution of the cohesion between the two concrete layers. Whereas, the second term in the expression gives the contribution of the clamping stresses. When rebars are assumed to yield in tension, a compressive stress perpendicular to the interface plane is exerted which is known as the clamping stress. A constant value of 0.8 is assumed for the coefficient of friction. σ_n is the external compression acting on the specimen.

Another model was proposed by Loov [15], which includes the influence of concrete compressive strength, on the shear strength of the interface.

$$v_u = k\sqrt{f_c(\rho f_y + \sigma_n)} \tag{2.3}$$

For uncracked interfaces the value of the constant k was considered as 0.5.

Major contribution after the modified shear friction theory was done by Walraven [6] [16], who developed a "sphere model" which considered the interaction between the aggregates, the binding paste and the interface zone. This is also known as the aggregate interlock effect (Figure 2.2). This model, was mainly developed for cracked concrete surfaces, which provides a more accurate prediction of the shear-friction capacity and the shear-slip behaviour of the cracked concrete surfaces [9].

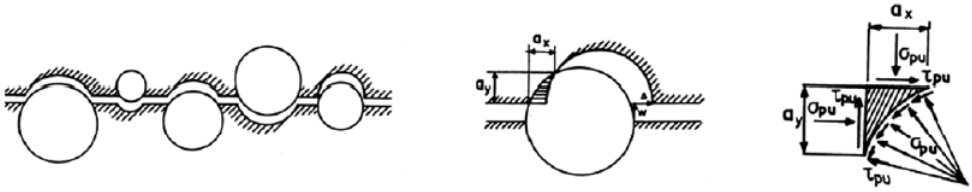

Figure 2.2: Aggregate interlock effect by Walraven [6]

A large experimental study was conducted to derive some expressions considering the aggregate interlock effect. This lead to the following nonlinear design expressions given in Equations 2.4 - 2.6.

$$v_u = C_1\left(\rho f_y\right)^{C_2}(MPa) \tag{2.4}$$

$$C_1 = 0.822 f_c^{0.406}(MPa) \tag{2.5}$$

$$C_2 = 0.159 f_c^{0.303}(MPa) \tag{2.6}$$

Walraven's model was credited as the best one till that time until research was not done on another important parameter called the dowel action. Even with such an accuracy, the contribution of dowel action was still not considered in the evaluation of shear capacity of the interface. Tsoukantas and Tassios [17] were the first ever researchers to consider this dowel action phenomenon. However, this theory was not much refined. Later on, Randl [9] proposed a further modified version of the shear theory, also known as the "Extended Shear Friction Theory" which is incorporated in the fib Model Code 2010.

Design recommendations in existing codes

ACI318 [11], proposes guidelines considering mainly the friction effect, thus developing an expression given in Equation 2.7.

$$v_u = \rho f_y(\mu \sin\alpha + \cos\alpha) \tag{2.7}$$

The values for coefficient of friction used in this case, depend on a modification factor. This modification factor is directly related to concrete density. Moreover, there is a limitation on the yield strength of reinforcement to be used. Angle α is the same as used in Eurocode 2 defined in Figure 2.3.

In order to include the influence of cohesion parameter, a new set of design guidelines are proposed in Eurocode 2 [7]. In this design code, the contribution of friction and cohesion is exclusively considered without including the dowel action phenomenon, which is later discussed in the "extended shear friction theory". The expression for shear resistance proposed in Eurocode 2 is given in Equation 2.8.

$$v_u = c f_{ctd} + \mu\sigma_n + \rho f_y(\mu \sin\alpha + \cos\alpha) \leq 0.5\nu f_{cd} \tag{2.8}$$

In the Eurocode 2 expression (Equation 2.8), first term gives the contribution of cohesion. Whereas, the other two terms show the contribution of friction due to external compression stresses and the compression developed in the connectors, if any, crossing the interface respectively. The angle $'\alpha'$ is defined in Figure 2.3 and should be limited by $45° \leq \alpha \leq 90°$.

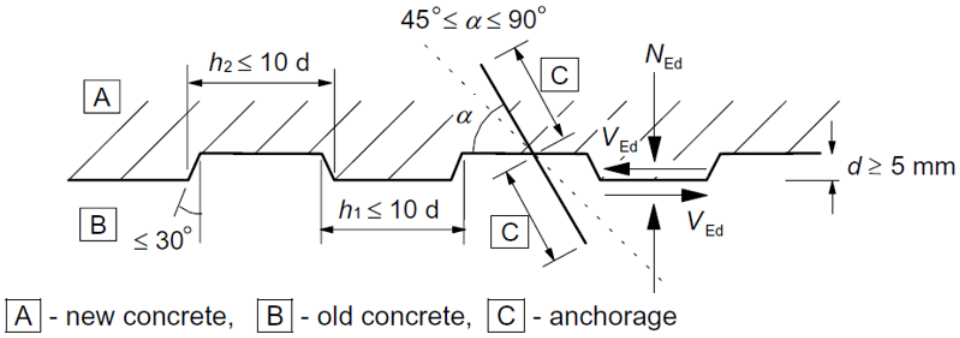

Figure 2.3: Indented construction joint [7]

The constant values for cohesion and friction are different than the ones considered in ACI 318[11]. Thus, different bond strength values were obtained with every other design code. To overcome this issue and to include some other parameters in the shear resistance of the interface such as, differential shrinkage, differential stiffness and exact surface treatment procedure, *Santos* and *Júlio* [12], developed a non-destructive technique to calculate the exact topography of the surface. A 2D Laser Roughness Analyser (2D-LRA method) is used to gauge the exact surface profile.

Various roughness parameters were calculated using the LRA device, among all, the mean valley depth R_{vm}, gave the best correlation between the shear resistance and roughness (cohesion and friction coefficient calculated using Equations 2.12-2.13). A highest coefficient of correlation was obtained for the mean valley depth ($R^2 > 0.95$) [18]. Expression for mean valley roughness is given by the scientists in Equation 2.9. Figure 2.4 shows the roughness profile and peaks and valley depth used for the roughness calculation.

$$R_{vm} = \frac{1}{5}\sum_{i=1}^{5} |v_i| \tag{2.9}$$

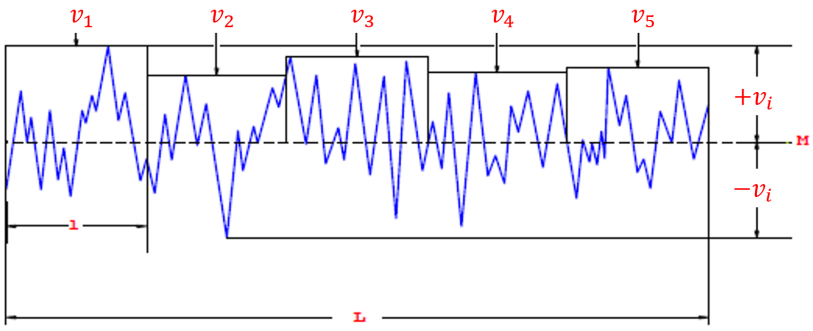

Figure 2.4: Roughness profile and mean valley depth

A total of 300 test specimens and 5 small test specimens for slant shear testing and splitting tensile strength testing each were considered by the authors *Santos and Júlio*. These specimens were prepared by using different surface preparation techniques and changing the difference between the ages of substrate and overlay concrete. Moreover, two different curing conditions were adopted; inside the laboratory and exterior conditions. Thus, because of varying temperature and relative humidity the differential shrinkage phenomenon was incorporated in to the test results. From the results obtained on testing these specimens, two different failure modes were observed, namely adhesive failure and cohesive failure. Adhesive failure is when the bond at the interface breaks while, cohesive failure happens due to crushing of concrete as shown in Figure 2.5.

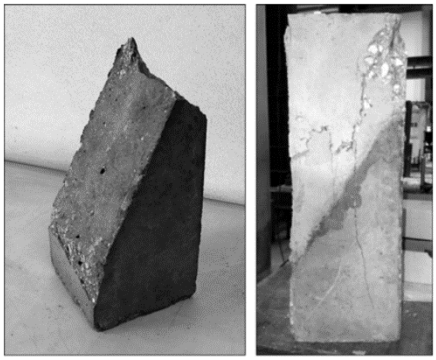

Figure 2.5: Failure modes for slant shear test (a) adhesive; and (b) cohesive [8]

The initial conclusions of the experiments also show that, the bond strength of the interface, increases with increase in the surface roughness value in both indoor and outdoor curing conditions. Moreover, an unexpected observation was made about the correlation between bond strength and difference of ages between the substrate and overlay concrete layer. This ambiguity was later explained by a particular stress state, induced by differential shrinkage, opposite in sign to the stress induced by loading conditions. This stress due to shrinkage causes the bond strength of the interface to increase with time [12]. Furthermore, number of failures occurring due to cohesive failure criterion increase with the increase of the difference between the Young's modulus of both concrete layers. Thus, the effect of differential stiffness is also observed in the experimental results performed by *Santos* and *Júlio*.

Hence, to further improve the accuracy of results and dependency of aforementioned parameters, the scientists proposed a new design approach based on two main principles,

- Measurement and characterization of surface roughness to calculate both coefficients of cohesion and friction, without imposing a minimum roughness amplitude for each surface condition (unlike in Eurocode 2, where different surface classes are distinguished depending on the roughness amplitude; for example for rough surface, minimum roughness amplitude must be 3 mm below which the surface is classified as smooth and also in case of Model Code 2010, where roughness is classified as smooth $R < 1.5$ mm, slightly rough 1.5 mm $\leq R < 3.0$ mm and rough $R \geq 3.0$ mm and for any amplitude in the respective roughness range, the cohesion and friction coefficients are constant).
- Two separate shear stresses are obtained at the interface, with and without the need to provide shear reinforcement.

Based on the Eurocode 2 approach, the coefficient of cohesion is obtained by the Equation 2.10.

$$c = \frac{v_u}{f_{ctm}} \tag{2.10}$$

Whereas, the coefficient of friction is calculated using the Equation 2.11.

$$\mu = \frac{v_u - c f_{ctm}}{\sigma_n} \tag{2.11}$$

Furthermore, a function is obtained considering the correlation between mean valley depth R_{vm} and coefficients of cohesion and friction. These functions have the best coefficients of correlation for cohesion and friction (R^2) - 0.92 and 0.94 respectively [12]. Thus, the new expressions for design values of coefficients of cohesion and friction are given in Equations 2.12 - 2.13.

$$c_d = \frac{1.06 R_{vm}^{0.15}}{\gamma_{coh}} \ (mm) \tag{2.12}$$

$$\mu_d = \frac{1.37 R_{vm}^{0.04}}{\gamma_{fr}} \ (mm) \tag{2.13}$$

Due to the uncertainty of these models, partial safety factors are introduced in the expressions in accordance with the Eurocode 2. This partial safety factor is calculated using the Equation 2.14.

$$\gamma = \frac{\mu - k \cdot \sigma}{\mu - \alpha \cdot \beta \cdot \sigma} = \frac{1 - k \cdot V_R}{\mu - \alpha \cdot \beta \cdot V_R} \tag{2.14}$$

where,

k : 1.65 for 5 % fractile of normal distribution
V_R : coefficient of variation
α : weighting factor (0.8 for partial safety factors)
β : reliability factor (3.8)
μ : average coefficient of friction
σ : standard deviation

Thus, with all these observations, it can be safely concluded that the surface roughness has a significant influence on the bond strength of the interface between two concrete layers. The different load transfer mechanisms are cohesion, friction and dowel action. fib Model Code 2010, is the first design code to consider the effect of dowel action in the shear resistance of the interface in an "extended shear friction theory" explained in the next section.

Extended Shear Friction Theory (ESF)

According to *Dr. Randl*, regarding the most general situation of a shear interface with connectors and possibly also external compression forces acting perpendicular to the shear plane, it is possible to identify the following mechanisms contributing to the interface shear resistance [9].

A Mechanical interlock and adhesive bonding

B Friction

C Dowel action

D Interaction

A) Mechanical interlock and adhesive bonding

The forces acting due to chemical and physical bond between the two layers, create an adhesive bond in the interface layer. This adhesive bond is governing and active at very low slip values (s ≤ 0.05 mm). In case of high slip, the effect of adhesive bond would be negligible, since, the bond would have already broken down. This is evident from Figure 2.1b shown in the beginning where the "shear friction theory" is explained.
The "Van der Waals forces" acting due to the chemical and physical bonding can transfer shear force through the interface in case of a smoother surface. For this purpose, the most important parameter is the surface topography. Like in the research of Santos and Júlio [12], where a 2D Laser Roughness Analyser (2D-LRA) method is used to determine the exact topography of the concrete surface, in this case also, laser profilometry techniques are used to identify the detailed topography of the substrate surface.

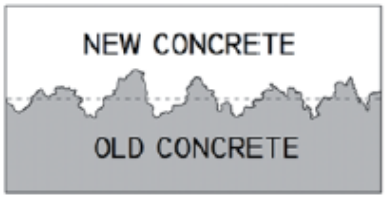

Figure 2.6: Mechanical interlock and adhesive bonding [9]

Tests were performed with surfaces that were treated with high pressure water (HPW)-blasted joints. Another factor was decisive for the shear resistance, despite careful treatment with a bond separator and with very low amounts of reinforcement (< 0.05 %). This factor was called the "interlocking effect". This effect is prominent in cases when surfaces are irregular and when the aggregates protrude sufficiently from the surface, i.e. $R_t \geq 1.5\ mm$. Figure 2.6 shows the mechanical interlocking and adhesive bonding at the interface between two concrete layers cast at different times.

B) Friction

This phenomenon gets activated due to compressive forces acting perpendicular to the interface. These compressive forces may be generated due to external compression action, prestressing forces or due to the clamping effect caused by the connectors crossing the interface. At a low slip value, stresses due to friction start developing and eventually at higher slip values, contribution of this parameter is almost constant which is evident from the Figure 2.1b.

In case of connectors crossing the interface, the influence of friction is very less in case the roughness amplitude is very low (R < 1.0 mm). The coefficient of friction value recommended by Eurocode 2 for very smooth surface is 0.5, which is already very low if strengthening of interface is considered. The value of *w* (joint widening) shown in Figure 2.7 is also very low because of low roughness amplitude, thus reducing the overall shear capacity of the composite concrete specimen. When the

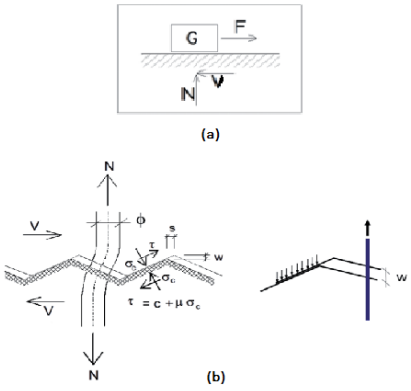

Figure 2.7: Friction (a) Interface without connectors, (b) Interface with connectors [9]

interface does not have connectors crossing through it, the friction is activated by the self weight of the overlay concrete layer [9].

This frictional resistance is directly proportional to the compressive forces acting perpendicular to the interface. Friction is considered in almost all the previously stated design codes. This effect is shown in Figure 2.7.

C) Dowel action (bending resistance of steel connectors)

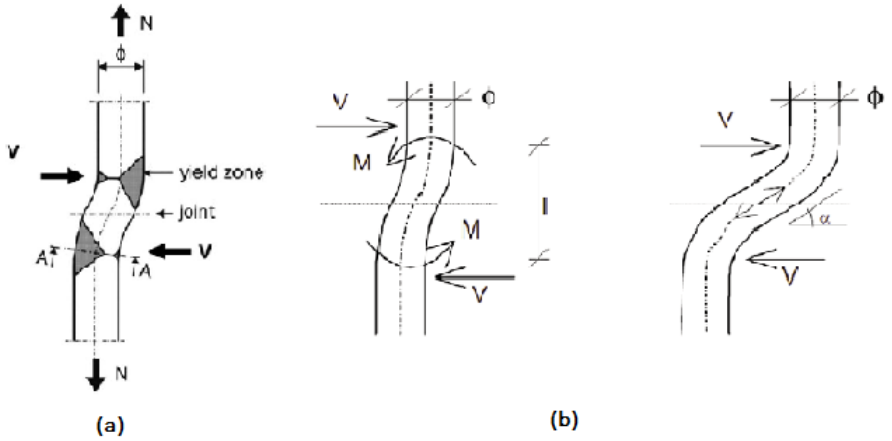

Figure 2.8: (a) Superposition of bending and tension in interface shear connectors, (b) Bending (dowel action) and kinking of connectors [9]

This phenomenon activates in case, shear connectors are crossing interface and when top and bottom parts of connector move in opposite directions. Due to this movement, bending stresses are developed in the connectors as shown in Figure 2.8. This resistance to bending is known as the "dowel action". Moreover, due to widening of the joint, axial tension is generated in the connectors as well.

At very low slip values (usually for $s \leq 0.05$ mm), adhesion and friction parameters govern the shear capacity at the interface. The reinforcement bars/connectors crossing the interface are not activated unless the interface elements attain their respective bonding strength and this happens at relatively higher slip values ($s \geq 0.05$ mm). Hence, there is no transfer of shear by dowel action mechanism at lower slip values (Figure 2.1b). Once, the dowel action is activated, the bending resistance offered by these connectors contribute to the shear resistance at the interface. As the slip further increases, kinks are developed in the connectors which also influence the shear resistance but not as much as the bending resistance provided at relatively lower slip values. This is because, the maximum bending stresses are developed at some distance from the interface joint, whereas, shear forces are present at the interface layer itself. Hence, even at large displacements, an increase in the shear resistance is observed [9] but in a very gradual manner (Figure 2.1b).

D) Interaction

In real life situation, the structures exhibit a combination of all the aforementioned phenomenons in different proportions. As the shear slip changes, the effect on each parameter is observed. For example, when the shear slip increases, the adhesive bond breaks and furthermore, the aggregate interlocking effect also decreases, since the protruding aggregates get crushed [9].

The contribution of each mechanism greatly depends on the surface roughness, bond strength and the amount of connectors crossing the interface, if any. If connectors are not present at the interface, then the failure can be regarded as brittle with loss of adhesion.

Whereas, in case of connectors crossing the interface, a more ductile behaviour is observed and failure occurs at larger slips [9]. In such cases, friction and dowel action mechanisms are more prominent.

fib Model Code 2010 design approach

All the aforementioned mechanisms are not incorporated in the previously mentioned design codes. $Dr.Randl$ developed the extended shear friction theory to propose changes in the *fib* Model Code 2010, considering effects of the four main parameters. The recommendations according to the *fib* Model Code 2010 design approach are as follows,

Adhesive bond, aggregate interlocking and friction

As mentioned earlier in section 2.1, the adhesive bonding, aggregate interlocking and friction have a combined effect on the shear resistance of the interface. Moreover, these parameters greatly depend on the roughness of the surface. Here, the roughness is determined by sand patch method. In this method, certain amount of fine sand is spread concentrically on the surface until all the surface undulations are filled with sand. The mean surface roughness R_t, is determined by dividing the volume of sand required to cover the surface by the diameter of the circle formed by spreading the fine sand.

The values recommended by performing various tests on concrete specimens, for the adhesive bond and friction coefficient are given in Table 2.1. Please note, these values are valid for concrete material strength less than or equal to C50/60.

Table 2.1: Mean shear resistance of interface with respect to surface roughness (≤ C50/60) [9]

Roughness	**Adhesive Bond**	**Coefficient of friction**
Smooth	0.5 - 1.5 N/mm^2	0.5 - 0.7
Slightly roughened ($R_t = 0.5 - 1.0\ mm$)	1.5 - 2.5 N/mm^2	0.8 - 1.0
Very rough ($R_t = 2.5 - 3.0\ mm$)	2.5 - 3.5 N/mm^2	1.1 - 1.4

There is a lot of variation in the friction coefficient values obtained, depending on the confining stresses perpendicular to the interface. The values in the above Table are obtained from a large number of test results and the range mentioned for each roughness is considered to be a reference for calculating shear stress at the interface. According to the *fib* Model Code 2010, values in Table 2.1 are considered final.

Dowel action

According to a lot of literature, for estimating the shear bearing capacity of the connectors crossing the interface, $Huber/von\ Mises$ failure criteria is referred [9]. As per this criteria, the ultimate shear load obtained must be equal to $(A_s \cdot f_y)/\sqrt{3}$, which is usually not the case, since the concrete plasticizes, which leads to bending of the connector.

A semi-empirical approach was first proposed by $Rasmussen$ [19], in which he uses the average values of concrete stresses at the lower part of the connector. Thus, assuming that at the point of maximum bending moment, shear force will be zero. The ultimate load can thus, be calculated using Equation 2.15.

$$V_{f,max} = k \cdot \phi^2 \cdot \sqrt{f_{c,cyl} \cdot f_y} \tag{2.15}$$

Experiments show that the value of the constant k is 1.3. In another model, proposed by $Vintzeleou$ and $Tassios$ [20], for more accuracy in the results, an eccentricity is considered between the point of maximum bending moment and the point of maximum shear force (at the surface level). This is shown in Figure 2.9.

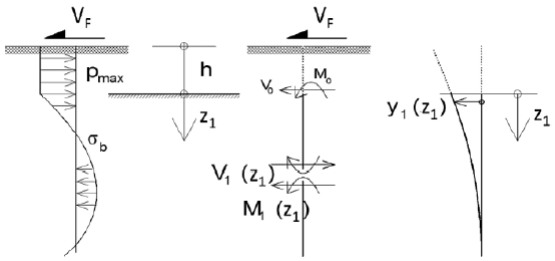

Figure 2.9: Modeling a cast-in dowel under shear loading [9]

The ultimate load bearing capacity in this case is given by the Equation 2.16.

$$V_{f,max} = 1.5 \cdot \frac{\phi^2 \cdot \pi}{4} \cdot \sqrt{f_{c,cube} \cdot f_y} \tag{2.16}$$

Based on these two and some other researcher's work, $Dr.Randl$ developed a parabolic expression to represent the behaviour of load vs. horizontal displacement (slip) for the dowel action effect. This parabolic expression is given in Equation 2.17.

$$V_F(s) \approx V_{F,max} \cdot \left(\frac{s}{s_{max}}\right)^{0.5} \leq \frac{A_s \cdot f_y}{\sqrt{3}} \tag{2.17}$$

where, s_{max} is the slip when $V_{F,max}$ value is attained. Also, $s \leq s_{max} \approx 0.10\phi - 0.20\phi$.

Interaction between the joint opening and dowel action

In case, when a dowel crosses the interface, some tensile stresses are developed in the dowel due to widening of the joint, as described in section 2.1. Bending resistance of these connectors, i.e. the dowel action effect has to be reduced, because the concrete will crush before the dowel attains it's maximum bending capacity. Thus, a new formulation for the $M-N$ interaction is proposed in the Model Code 2010, given by Equation 2.18.

$$V_F(s) = V_{F,max} \cdot \left(\frac{s}{s_{max}}\right)^{0.5} \cdot \sqrt{1 - \left(\frac{\sigma_s}{f_y}\right)^2} \tag{2.18}$$

The axial stress σ_s acting in the dowel greatly depends on the surface roughness, joint opening and the anchorage of the connector in the concrete layer. The maximum axial stress in case of high pressure water-blasted surface and sand-blasted surfaces is about 50 % of f_y. Thus, a value of 0.5 for σ_s / f_y is recommended [9].

Superposition of different load mechanisms

For superimposition of different mechanisms, various aspects have to be taken into account.

- Horizontal displacement or slip of the interface, greatly influences the contribution of the load mechanisms.
- All load mechanisms are inter-related and influence each other.
- In dowel action mechanism, the interaction between the tension and bending in the connectors.

Considering all these effects, two cases are developed [9]:

- Case 1: Rigid bond-slip (brittle behaviour):
  $\tau_{Ru}\ (s \leq 0.05mm) = \tau_{R,adhesion} + \tau_{R,friction}$
- Case 2: Non-rigid bond-slip (ductile behaviour):
  $\tau_{Ru}\ (s > 0.05mm) = \tau_{R,interlocking} + \tau_{R,friction} + \tau_{R,dowel\ action}$

In Case 1, a strong bond is present between the two concrete surfaces. There are no connectors crossing the interface in this situation. Adhesion between the surfaces is the main criteria contributing to the shear resistance of the joint. Moreover, friction develops due to external compression confinement. This situation is prominent in cases having very less slip ($s \leq 0.05\ mm$). Thus, the shear resistance in this case is given by Equation 2.19 which considers $Coulomb's$ shear friction hypothesis.

$$\tau_{Rd} = c_a \cdot f_{ctd} + \mu \cdot \sigma_n \leq 0.5 \cdot \nu \cdot f_{cd} \tag{2.19}$$

In this equation, the constant c_a is the adhesion constant proposed in the Model Code 2010.

Table 2.2: Design values for adhesive bond effect [9]

Surface characteristics of interface	$\mathbf{c}_a$
Very smooth (steel, plastic, specially treated timber formwork)	0.025
Smooth (concrete surface slightly roughened, R_t <1.5 mm)	0.20
Rough (intensely roughened surface, $R_t \geq$ 1.5 mm)	0.40
Very rough (Including shear keys, $R_t \geq$ 3.0 mm)	0.50

The values proposed in the Table 2.2, agree with the results of a study done by $Zilch$ [21] based on the EC2 approach. Although, the c_a values vary with different scientists' results, Model Code 2010 recommendations are significantly accurate as per reality.

Furthermore, when the failure occurs due to higher shear loading, Case 1 is no longer applicable. Now, Case 2 explains the resistance more accurately as it considers the effect of connectors crossing the interface. According to $Dr.\ Randl$ [9] Case 2 will be the governing case when following situations occur:

- The shear load is so high that the adhesive bonding is not able to resist the entire load.
- In case of contamination of the substrate surface, before casting the new concrete overlay, the adhesive bond is weaker that expected.
- The reinforcement crossing the interface is always greater than 0.05 %, hence, a more ductile behaviour is expected.

A new formula (Equation 2.20) is proposed as a modification to the one given in Equation 2.19.

$$\tau_{Ru} = \tau_{R,interlock} + \mu \cdot (\sigma_n + \kappa_1 \cdot \rho \cdot f_y) + \kappa_2 \cdot \rho \cdot \sqrt{f_{c,cube} \cdot f_y} \tag{2.20}$$

The values of κ_1 and κ_2 are influenced by the fact that,

– A combination of bending moment and axial stresses develop in the reinforcement or connectors crossing the interface.

– The maximum contributions by each parameter occurs at different horizontal displacements.

The constant κ_1 considers the extent of tensile stress that can be attained with the simultaneous bending action. Usually the value is less than 1, $\kappa_1 = \sigma_s / f_y \leq 1.0$. For rough interfaces this value is assumed to be 0.5 as per experimental validations [9].

Whereas, the $\tau_{R,interlock}$, μ and κ_2 values are back calculated by using numerous test results via regressive analyses. Furthermore, to derive the material design characteristics, the friction and dowel action terms in Equation 2.20 are divided by partial safety factors $\gamma_c = 1.5$ for concrete and $\gamma_s = 1.15$ for steel. For the interlocking term in the formula, a factor c_r is multiplied to the cubic root of concrete strength. This is done as the aggregate interlock effect varies as per the cubic root of the concrete strength [9].

$$\tau_{Rd} = c_r \cdot f_{ck}^{1/3} + \mu \cdot (\sigma_n + \kappa_1 \cdot \rho \cdot f_{yd}) + \kappa_2 \cdot \rho \cdot \sqrt{f_{cd} \cdot f_{yd}} \leq \beta_c \cdot \nu \cdot f_{cd} \tag{2.21}$$

where,
μ : coefficient of friction
ρ : degree of reinforcement at interface
κ_1 : coefficient of efficiency for tensile force that can be activated in the reinforcement
σ_n : compressive stress due to external normal force
κ_2 : coefficient for flexural resistance of reinforcement (dowel action)
β_c : coefficient allowing for angle of diagonal concrete strut
ν : reduction factor for strength of diagonal concrete strut: $\nu = 0.55 \cdot (30/f_{ck})^{1/3} \leq 0.55$

Table 2.3: Values for constants in design for Equation 2.21 [9]

Surface roughness	$\mathbf{c_r}$	κ_1	κ_2	β_c	μ	
					$\mathbf{f_{ck} \geq 20}$	$\mathbf{f_{ck} \geq 35}$
Very rough: $R_t \geq 3.0\ mm$	0.2	0.5	0.9	0.5	0.8	1.0
Rough: $R_t \geq 1.5\ mm$	0.1	0.5	0.9	0.5	0.7	0.7
Smooth	0	0.5	1.1	0.4	0.6	0.6
Very smooth	0	0	1.5	0.3	0.5	0.5

The extended shear friction theory proposed in fib Model Code 2010, in accordance with the explanations provided by $Dr.\ Randl$ [9], give two critical limit situations depending on the bond strength of interface between the two concrete layers, namely rigid and non-rigid bond. Thus, a more realistic approach to calculate the shear resistance of the interface is proposed in this design code depending on different mechanisms - aggregate interlock, adhesion and friction between concrete layers and dowel action.

The guidelines provided by all the aforementioned design codes are mainly related to the calculation of shear strength on a structural level. However, it is not always possible to analyse a specific structure, for example, a bridge or a building, by applying analytical models on the whole structure. Analysis of an entire structure is a very complex process involving the interaction between many different structural elements. Hence, to minimize the efforts required to analyse a structure by reducing errors and achieving efficiency in the analyses, computational modelling or FEM analysis is essential.

2.2. Need for Finite Element analysis in interface study

According to the new fib Model Code 2010, the design shear resistance of a reinforced concrete (RC) structure can be evaluated through analytical and numerical calculation methods that fall into four different levels of approximations. The complexity and the accuracy of the calculated shear resistance increase with increasing the level of approximation. Nonlinear finite element analysis (NLFEA) belongs to the highest level of approximation (Level IV) because of their advantage to consider real material properties and some more 'hidden' capacities of the structure [22]. In today's world NLFEA is used as a basic step to simulate real-life situations. Since in olden times such advanced models were not developed, to check the service life and durability of existing structures, many companies especially in Netherlands, are using NLFEA.

ATENA is a finite element software package specifically developed for concrete and reinforced concrete structures. This software provides ease in developing a numerical model with concrete material properties and gives accurate results while studying the stress-strain relationship, creep, shrinkage and strength properties. While developing a model using ATENA, there are many parameters which are to be considered in order to understand the behavior of interfaces, which is the area of concern for this research. As a test case, ATENA interface material model (IMM), which is available in this software package, is verified to understand its response towards direct tension test and shear load test. Once the verification is carried out successfully, actual material and structural models from the corresponding experiments are designed and the analyses of these results are accomplished. Moreover, another artificial interface model (ArtIM) is proposed in this report which uses the material properties and quadrilateral finite elements to develop an interface and to thoroughly understand the response of the composite concrete models at the interface level.

It is very important that the appropriate design rules that are proposed by different codes get reflected into the numerical models. Many parameters are involved in the NLFEA of interface study. A specific procedure

to design the models using a FEM software is not readily available. Moreover, due to involvement of various parameters affecting the interface strength a detailed understanding about the topic is essential. Hence, an attempt is made to investigate with the existing numerical models, whether the behavior of the interface can be reliably predicted using material and structural tests.

3

Hypothesis

In this chapter, a brief description about the research question is presented. Inspiration for the thesis topic and the research questions is derived from the literature study completed in the previous chapter.

3.1. Research question

From the guidelines proposed by different design codes it is evident that, in the study of interface behavior, the most important characteristic associated with the interface is the roughness of the adjacent concrete elements. This roughness influences the two most important properties, adhesion and cohesion, which represent the total bond strength between the two concrete layers. The theoretical explanation of these characteristics is already given in the literature chapter. However, it is not always convenient to apply the analytical approach to understand the response of an entire structure. Advanced calculation techniques are required to accurately predict the response of structure subjected to any load combinations. Hence, to understand the influence of different interface parameters on the shear capacity of a composite concrete specimen, a computational study is performed with the use of finite element analysis.

One such FEM software package, *ATENA* is specifically developed for concrete and reinforced concrete structures. This FEM software program is used for the non-linear analyses of various composite concrete models in order to study the interface behavior. ATENA has a default interface material model (IMM) which is tested under different boundary conditions in this report. These models are verified by subjecting them to direct tension test and shear load test. A variation of this interface model is proposed in the form of an artificial interface model (ArtIM), which is developed as an alternative to the default ATENA IMM. This is done in order to precisely understand the crack propagation at the interface level and to investigate whether the effects of the interface parameters involved in ATENA IMM (tensile strength, cohesion and coefficient of friction) can be modelled manually without using the interface material model (IMM).

Thus, the research topic to be examined is framed as follows.

Can Finite element Analysis using ATENA reliably predict the interface behavior?

To answer this question, a detailed study of the interface models is necessary along-with a validation by comparing the numerical models to certain experimental findings. Ultimately, this thesis will lay a foundation for future research pertaining to interface study using computational modelling. Moreover, the report provides details of the numerical models studied by using 2D interface elements and 2D quadrilateral material elements to understand the interface behavior using material and structural tests. Some of the other important outcomes of this study, as discussed further, will also be answered along-with the main research topic.

- *Can the standard materials and element libraries of ATENA be used to model the interface behavior?*
- *Does the behavior of the interface model agree well with the experimental results?*
- *Can a structural interface failure be simulated using the interface modelling techniques in ATENA?*

An attempt is made to successfully answer these research questions hereafter.

4

Verification of Interface Models

In order to use finite element analysis (FEA), to predict response of a structure, first a verification of the numerical models is necessary. As a test case, a small scale composite concrete bond model is tested using numerical analysis to verify the use of designated parameters . Inspiration for this specific model is taken from the ATENA documentation manual. Guidelines from the manual are adopted to design the numerical model. The test case model is subjected to a direct tension test (DTT) and a shear load test (SLT). Two different interface models are introduced in the next section, that are the focal points of this numerical study. The mechanical models used for the analysis are shown in Figures 4.2 and 4.15.

4.1. Interface Models

In order to verify the test case, two interface models are chosen for the analyses.

- ATENA Interface Material Model (IMM)
- Artificial Interface Model (ArtIM)

First, a default interface material model (IMM) provided in ATENA is used to model the interface between two concrete elements. In this model 2D line 4-node interface elements are used to model the interface. The main parameters to be defined are normal and tangential stiffness, tensile strength, cohesion and coefficient of friction at the interface. The element has zero thickness in this model. Whereas, if use of ATENA interface material model (IMM) is to be avoided, then an alternate artificial interface model (ArtIM) is proposed in this research. Unlike ATENA IMM, the artificial interface model is based on standard material properties that are to be defined for the interface layer. The various roughness parameter inputs in ATENA IMM cannot be obtained accurately in all experimental cases. Hence, by using the standard ATENA material elements, an attempt is made to design an artificial interface layer, that can act as an interface between the two adjacent concrete elements. In this model 4-noded linear quadrilateral elements are used to define the artificial interface layer. A certain thickness is provided to the interface layer corresponding to, for example, a mortar joint between two bricks. By providing thickness to the interface, the exact cracking pattern at this level can be observed clearly. Effects of cohesion and friction (roughness parameters) can be incorporated in the ArtIM, by designing the interface layer with an explicit roughness (wave pattern of interface elements). The direct tension and shear load tests are performed using both these interface models starting with the IMM and then ArtIM. In the following sections, a detailed discussion about these interface models and the numerical analyses are performed on a small scale composite concrete model.

4.2. ATENA Interface Material Model (IMM)

The Interface Material Model (IMM) is designed for the purpose of simulating a contact surface between two adjacent materials, for example, a construction joint or contact between foundation and concrete structure. This interface model is based on Mohr-Coulomb criterion with tension cut-off [10]. The failure surface for the interface elements is shown in Figure 4.1a.

Important parameters in IMM

The ATENA Interface Material Model (IMM) has two types of parameters. First set of parameters describe the real physical properties of the interface: tensile strength (f_t), cohesion (c) and coefficient of friction (μ). These properties correspond to real material properties.

The second set of parameters are the stiffness coefficients, which are defined for numerical purposes: normal and tangential stiffness. Each coefficient has two values, basic (K_{nn} & K_{tt}) that represent stiffness of the interface in elastic state, and minimal K_{nn}^{min} & K_{tt}^{min} that serves for numerical purposes in order to preserve the positive definiteness of the global system of equations. However, these values cannot be assigned arbitrarily. There is a certain dependence of these parameters on each other as described in Equation 4.1. Moreover, according to the guidelines of ATENA manual and as a thumb-rule of computational design, the interface tensile strength should be kept approximately half of the cohesion, if the interface is expected to fail before the concrete itself [23] which is generally the case.

The basic stiffness coefficients should have a high value in order to represent well a rigid body and the minimal stiffness coefficients should be very low in order to represent an open contact. The minimum values to be maintained for the basic stiffness are of the order $K_{nn} = E/t$, & $K_{tt} = G/t$, where E and G are the elastic modulus and shear modulus of the adjacent concrete elements and t is the element mesh size. Hence, a same value of $K_{nn} = K_{tt} = \frac{E}{t} = \frac{30000\ N/mm^2}{10\ mm} = 3\times10^6\ MN/m^3$, is assigned to the normal and tangential stiffness coefficients. Whereas, the minimal stiffness coefficients are in the order of 0.001 times the basic stiffness values.

$$\begin{aligned} f_t &< \frac{c}{\mu}, \quad f_t < c \\ c &> 0, \quad f_t > 0, \quad \mu > 0 \end{aligned} \tag{4.1}$$

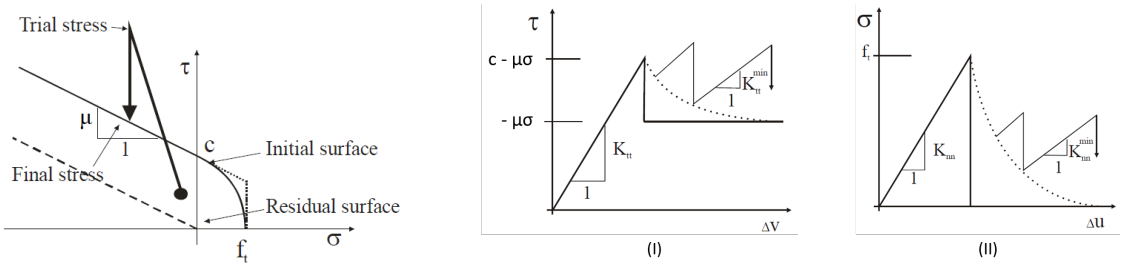

(a) Failure surface for interface elements

(b) Typical interface model behavior in (I) shear and (II) tension

Figure 4.1: (a) Mohr-Coulomb failure criteria and (b) interface model behavior in ATENA [10]

In ATENA, the evolution law depends on the equivalent nonlinear interface relative displacement

$$\Delta u_{eq}^{f} = \sqrt{\Delta u_f^2 + \Delta v_f^2} \text{ in 2D}$$

Where Δu_f and Δv_f are the inelastic components of the relative interface displacement on the decomposition into elastic and fracturing (nonlinear) part (Equation 4.2).

$$\begin{aligned} \Delta u &= \Delta u_e + \Delta u_f \\ \Delta v &= \Delta v_e + \Delta v_f \end{aligned} \tag{4.2}$$

The above relation shows the dependency of tensile strength and shear strength on each other. Typical softening behavior for the interface model (IMM) is shown in Figure 4.1 by dotted lines. When no softening law is defined, the default behavior of the curves is brittle and is shown in the same Figure 4.1 by solid lines. In this research, the softening laws are not defined explicitly and hence, the effect of minimal stiffness after interface failure is insignificant and brittle behavior is expected from the numerical models.

Preparation of numerical model

The model used for the verification, is made up of two rectangular concrete elements with same concrete material properties. The overlay concrete layer is assumed to be cast after the substrate concrete layer starts hardening. Moreover, the substrate layer has different roughness characteristics corresponding to various surface preparation techniques which will not be discussed here. However, a clear distinction in the surface properties is made based on the guidelines of fib Model Code 2010 [16] for smooth, slightly rough and rough surfaces. A steel plate is designed on top of the overlay concrete layer to ensure uniform distribution of stresses. Dimensions of the model are shown in the mechanical model in Figure 4.2.

The model is first subjected to a tensile load (Direct Tension Test). In this test, uniformly distributed load is enforced as prescribed deformation on the top edge of the steel plate. Whereas, the bottom edge of substrate concrete is completely fixed. In the second case, the model is tested for its shear behavior and is subjected to a lateral load (Shear Load Test). A point load is enforced as prescribed deformation on top left corner of the steel plate. Specific characteristics of the numerical model are discussed further.

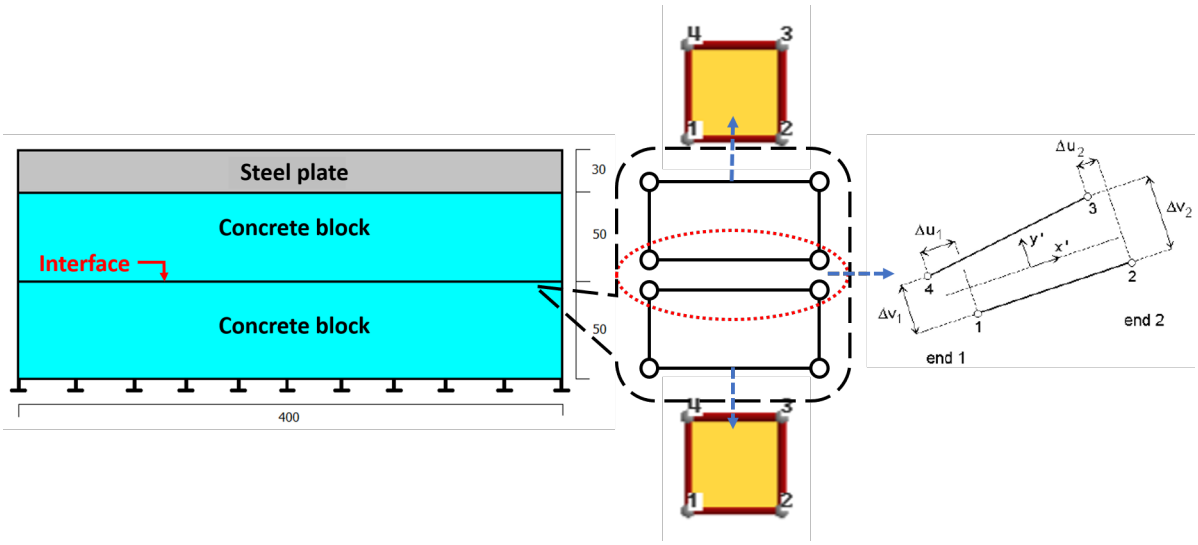

Figure 4.2: Schematization of small scale composite concrete model and finite element types used for numerical analysis (all dimensions are in mm) using ATENA IMM

- The structure is made up of 2D elements in a 2D environment. Thickness of the elements is 300 mm;
- The steel plate is modelled as *plane stress elastic isotropic* elements with elastic modulus E = 210,000 N/mm^2 and Poisson's ratio = 0.3;
- The concrete block elements are modelled as *3D Non Linear Cementitious 2* elements, with exponential tension stiffening behavior, cube compressive strength of 50 MPa, Poisson's ratio = 0.2 and remaining properties defined as per Eurocode guidelines;
- The interface is modelled as *2D line 4 node interface* elements with previously defined stiffness coefficients and different set of physical properties depending on the roughness class that are defined in the direct tension test section;
- The mesh is generated using quadrilateral elements with an element size of 10 mm for steel and concrete elements and mesh refinement of 5 mm is applied at the interface;
- The bottom edge of the substrate concrete layer is restrained in both x- and y-direction.
- Self-weight of the elements is disregarded in this analysis,
- Newton-Raphson solution method is used for the calculation of the numerical results

In the next sections, detailed discussion about the direct tension test (DTT) and shear load test (SLT) is performed.

4.2.1. Direct Tension Test (DTT)

A direct tension test (DTT) explains the behavior of a model when it undergoes tensile stresses. In many instances, this can be useful to have a complete perspective of what is happening in a structure. Hence, a DTT is carried out using numerical simulations on the small scale composite concrete model. For the analysis, half of the geometry is modelled considering symmetry about the vertical axis going through the mid-plane of the body. This is done to reduce the computational time of the analysis. Mechanical model for this test is shown in Figure 4.3a and Figure 4.3b shows the numerical model developed for the analysis. Mesh size used for the analysis is 10 mm for the macro-elements and 5 mm near the interface. A constant vertical force is applied on top edge of the steel plate in the form of a prescribed deformation (LC-2)[1] of magnitude 0.0001 mm in every load step. Reason to choose such small load step size is to avoid convergence problems and maintain accuracy of results. The bottom-most edge of the concrete specimen is constrained in the y-direction (LC-1). Whereas, the right edge of the specimen is constrained in x-direction (LC-3) on account of symmetry, thus, making this model statically determinate.

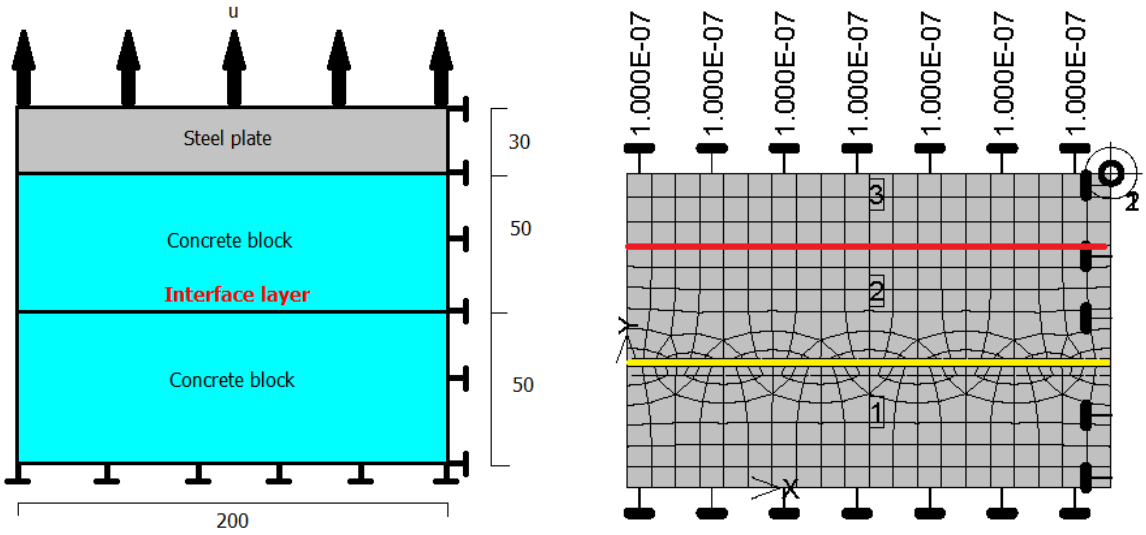

(a) Mechanical model (b) Numerical model

Figure 4.3: Mechanical and numerical model developed with ATENA IMM using symmetry
(All dimensions are in mm)

The model is tested with different parametric combinations pertaining to the bond strength of the concrete layers (interface strength). These cases are listed below.

- **Perfect Bond (PB)** The two concrete layers are rigidly connected to each other (By assigning rigid connection type to the interface line element)
- **Smooth Interface** The interface properties correspond to a smooth substrate surface ($f_t = 0.5MPa,\ c = 1.0MPa,\ \mu = 0.6$)
- **Slightly Rough Interface** The interface properties correspond to a slightly rough substrate surface ($f_t = 1.0MPa,\ c = 2.0MPa,\ \mu = 0.9$)
- **Rough Interface** The interface properties correspond to a rough substrate surface ($f_t = 1.5MPa,\ c = 3.0MPa,\ \mu = 1.3$)

The values used for the interface parameters correspond with the guidelines proposed in fib Model Code 2010 as described in Table 2.1.

[1] LC-# denotes the load case number used in the ATENA simulations

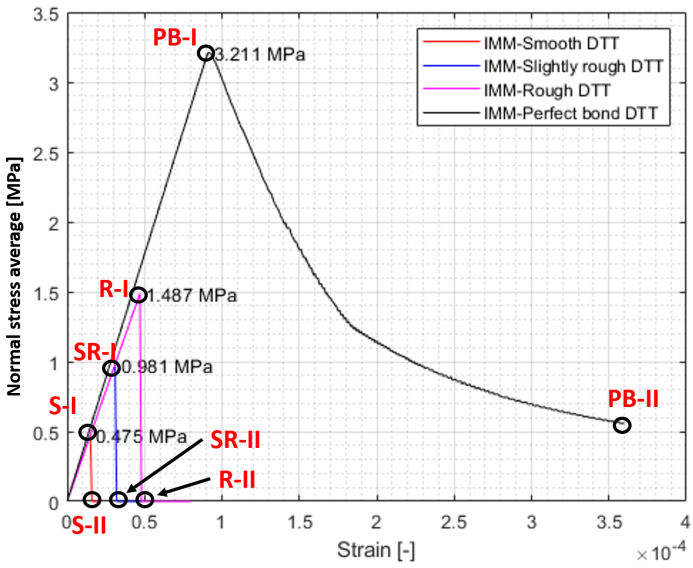

Figure 4.4: Stress - Strain curve for different bond strength models undergoing direct tension test using ATENA IMM

Figure 4.4 shows the response of DTT to the different values of bond strengths. The stress and strain values correspond to the reaction force and vertical displacement of the model respectively. Reaction at the top edge of the steel plate is monitored. Whereas, for the vertical displacement a monitoring point is set at the top right node of the model as shown in Figure 4.3b. The average normal stress developed at the interface is calculated by dividing the reaction force in each load step by the normal area (perpendicular to the prescribed displacement, in this case $200 \times 300 = 60000\ mm^2$) of the model. Similarly, strain is calculated by dividing the vertical displacement by the vertical height of the model (in this case $100\ mm$). Since, the stress distribution is uniform along the length of the model (Figure **??**), this method of stress and strain calculation is acceptable.

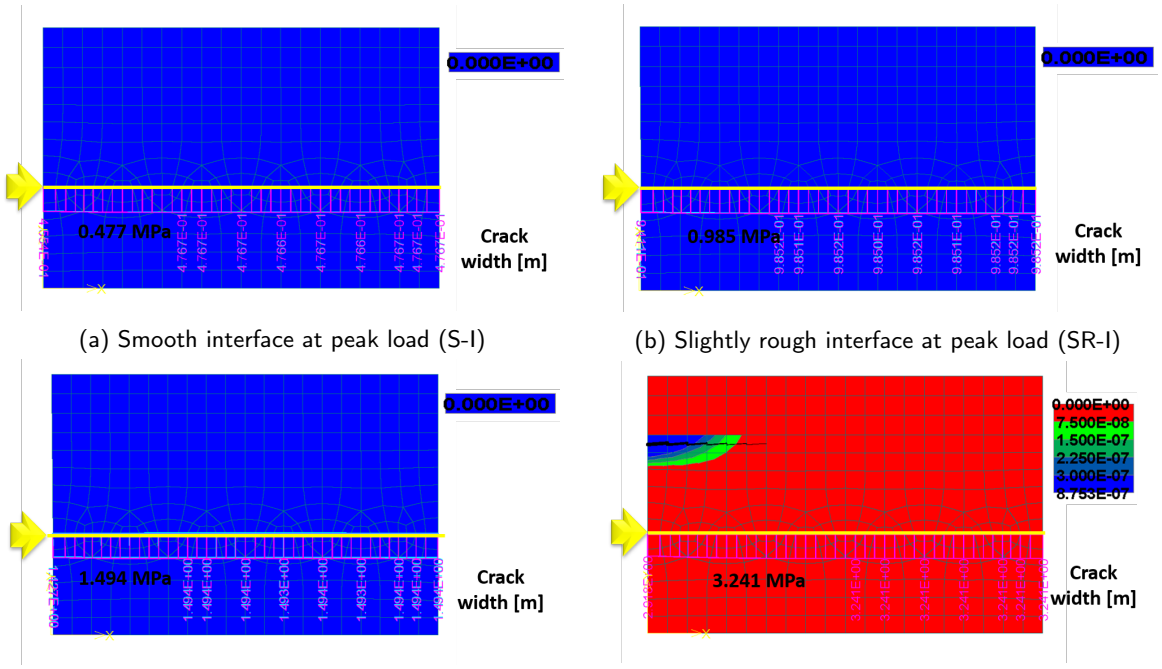

(a) Smooth interface at peak load (S-I)

(b) Slightly rough interface at peak load (SR-I)

(c) Rough interface at peak load (R-I)

(d) Perfectly bonded interface at peak load (PB-I)

Figure 4.5: Crack distribution and normal stress at interface at peak load step using ATENA IMM

Crack distribution and normal interface stress distribution is shown in Figure 4.5[2] at their respective peak load step, for the four models with different bond strengths. An uniform stress distribution is observed at the interface with maximum stress equal to the tensile strength of the respective roughness cases.

For non-rigid bond cases (smooth, slightly rough and rough interface Figures 4.5a - 4.5c), cracks cannot be observed in the adjacent concrete elements. This is because, these elements are in elastic state on account of a very high tensile strength with respect to the interface strength. The uniform stress distribution at the interface is shown with pink color with the maximum stress value written in black. These stress values correspond with the tensile strength assigned to the respective models.

For a rigid bond/perfectly bonded case, the crack width distribution and the normal stress distribution at the interface level is shown in Figure 4.5d at the peak load step. Interface is very strong in this case, thus resisting the tensile stresses and eventually resulting in material failure. The crack initiates from the rear end of the specimen, near the steel plate-concrete interface on account of the model attaining the peak tensile strength.

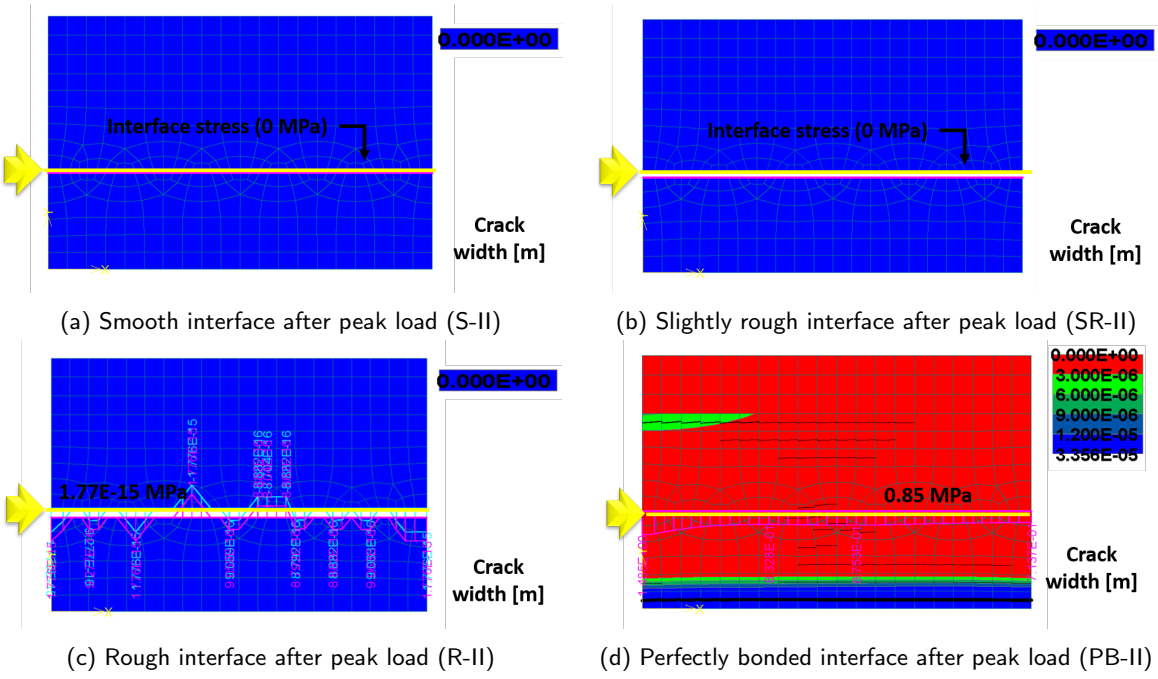

(a) Smooth interface after peak load (S-II)

(b) Slightly rough interface after peak load (SR-II)

(c) Rough interface after peak load (R-II)

(d) Perfectly bonded interface after peak load (PB-II)

Figure 4.6: Crack distribution and normal stress at interface after peak load step using ATENA IMM

With further increment of load, stresses at interface drop to zero for non-rigid bond cases as can be seen in Figures 4.6a - 4.6b. For smooth and slightly rough interface, normal stress at interface drops to zero and hence it is not visible in the figure. However, for rough interface, before reaching absolute zero a stress distribution can be observed at the next load step after attaining peak tensile strength (Figure 4.6c). Nevertheless, this value is very small and it is safe to assume that normal stress at the interface drops to zero once peak tensile strength of the interface is achieved.

For the perfectly bonded model, significant crack distribution and normal stress at the interface can be clearly observed in Figure 4.6d. This figure shows the stress state at the last load step. Tensile stress at the interface drops to almost 0.85 MPa as can also be verified from the graph 4.4. Eventually, after the initial cracks near the edge, tensile stresses near the middle of the specimen increases (right edge of the symmetric model) thus inducing cracks near the bottom fixed edge of the specimen.

In case of non-rigid bond cases, as the stresses at the interface reach its tensile capacity, the interface breaks. The stress at the interface becomes zero once it has failed and the top concrete layer lifts up, thus breaking

[2] yellow arrows in figures denote location of the interface

any contact with the bottom layer. Since, any special softening law was not defined in the models (Figure 4.1), the stress value simply dropped to zero with a brittle failure response.

In case of perfectly bonded concrete layers, a linear behavior is observed (Figure 4.4) in the initial stage of the analysis until the model reaches its peak tensile strength. As the curve reaches its peak at the tensile strength of the material, an exponential tension softening post peak response of the specimen is obtained as expected from the analytical models. Since, in this case, on account of a very strong interface concrete material failure occurs, the post-peak response follows the standard exponential softening law defined in ATENA for the 3D Non Linear cementitious element type. Thus, the input parameters assigned to the model are verified by the results obtained from the direct tension test.

4.2.2. Shear Load Test (SLT)

Shear capacity along the interface is a very important characteristic of a composite concrete specimen. This adhesive bond strength along the interface, is a result of interaction between various parameters involved at the interface like cohesion and friction as discussed earlier in the different design codes. To understand the co-relation between various parameters with the help of FEM analysis, a shear load test is simulated on a numerical model. This section mainly focuses on the basic principles involved in the modelling of a small scale concrete bond model using ATENA and the verification of results obtained from this numerical analysis.

Here, the same composite concrete model, as the one used in the DTT, is subjected to a shear load test (loading parallel to the interface) (SLT). The boundary conditions assigned are identical to the previous test. A lateral load is applied to the top left corner of the steel plate in the form of prescribed deformation and of magnitude $0.003\ mm$ in incremental load steps. Moreover, the top edge of the steel plate is kept fixed in order to avoid any numerical irregularities with the model. A perfect bond is assumed between the steel plate and concrete. Whereas, bond between top and bottom concrete layers is varied as rigid (perfect bond) and non-rigid (weaker bond with different roughness parametric combinations) depending on the model to be verified. Unlike in the DTT, a full length model is simulated in the shear load test (SLT), since the model is not symmetric because of the designated boundary conditions. Mechanical set-up for the shear load test is shown in Figure 4.7.

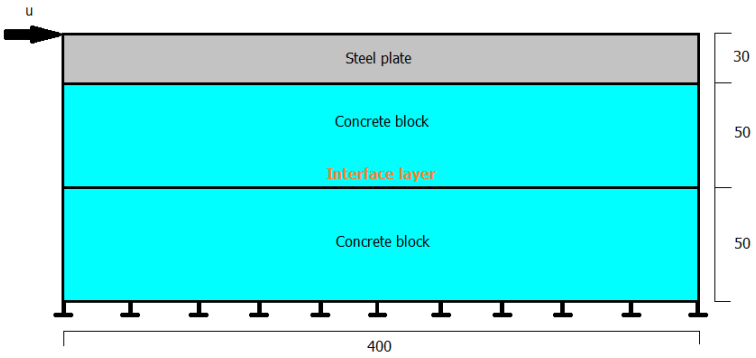

Figure 4.7: Mechanical model for shear load test

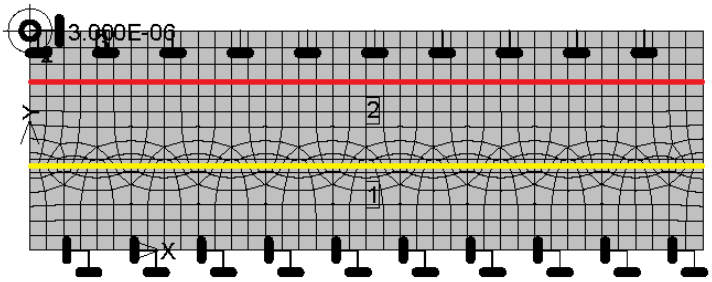

Figure 4.8: Numerical model for shear load test

The mesh size used in the numerical model shown in Figure 4.8 is $10\ mm$ with a finer mesh ($5\ mm$) at the interface. Steel-concrete and concrete-concrete interfaces are denoted with red and yellow lines respectively. The material properties and element types used for the concrete elements and the steel plate are identical as discussed in the direct tension test (DTT).

The parameters directly influencing the surface roughness (in ATENA IMM), as discussed in the beginning of section 4.2, are tensile strength, cohesion and coefficient of friction. In the next few sections, verification of cohesion (along-with tensile strength) and friction parameters is performed by adopting the same surface classification as in the DTT (smooth, slightly rough and rough).

Verification of parameters

Cohesion (c) and tensile strength (f_t)

In order to verify the cohesion and tensile strength parameters in the ATENA interface material model, several simulations are run by changing values for these two parameters. Each set of values represent different surface class and is classified as smooth, slightly rough and rough interface, similar to the case of DTT. These values are assigned according to the Model Code 2010 guidelines and are also shown in Table 4.1. Additionally, bond between the two concrete layers is classified as rigid (perfect bond) and non-rigid (smooth, slightly rough and rough interface characteristics).

Firstly, non-rigid bond properties are assigned to the bond between two concrete layers and later, a rigid bond case is tested. In the next few chapters these same values will be used to validate the experimental results obtained by other researchers pertaining to interface failure in composite concrete structures. Response of the small scale bond model to a shear load test, using the ATENA IMM is shown in Figures 4.9d - 4.9c.

Table 4.1: Input parameters in numerical model for different roughness properties

Parameters	**Symbol**	**Units**	**Smooth Interface**	**Slightly Rough Interface**	**Rough Interface**	**Perfect Bond**
			Fig. 4.9a	Fig. 4.9b	Fig. 4.9c	Fig. 4.9d
Material properties						
Cube compressive strength	f_c	[MPa]	50	50	50	50
Interface parameters						
Tensile strength	f_t	[MPa]	0.50	1.00	1.50	-
Cohesion	c	[MPa]	1.00	2.00	3.00	-
Coefficient of friction	μ	[-]	0.60	0.90	1.30	-

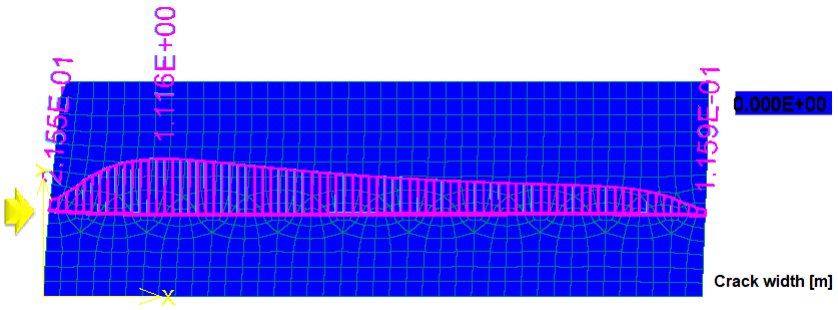

(a) Smooth interface (S-I) (Displacement multiplier - 1000)

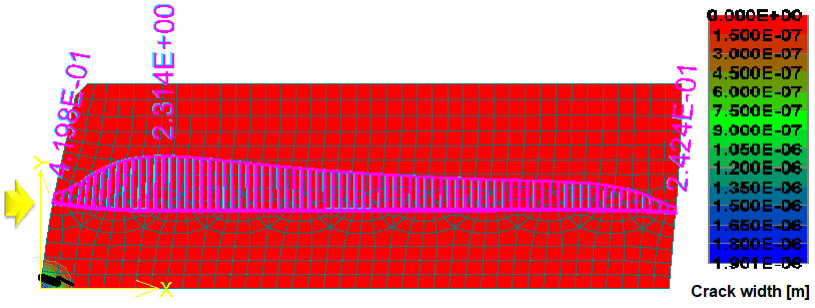

(b) Slightly rough interface (SR-I) (Displacement multiplier - 1000)

Figure 4.9: Crack distribution and interface shear stress for a shear load test using different interface properties with ATENA IMM

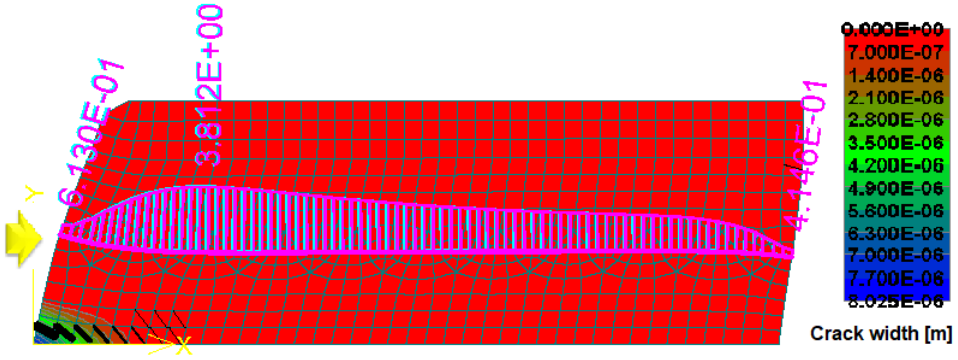

(c) Rough interface (R-I) (Displacement multiplier - 1000)

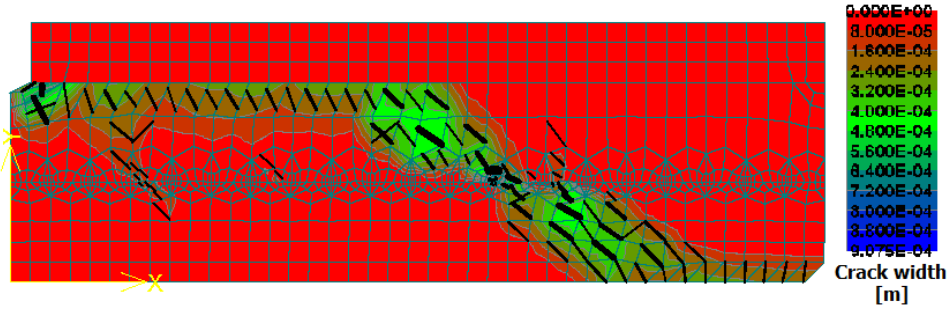

(d) Perfectly bonded concrete layers (PB-I) (Displacement multiplier - 10)

Figure 4.9: Crack distribution and interface shear stress for a shear load test using different interface properties with ATENA IMM

Figure 4.9 shows crack width distribution in the composite concrete model in four different bond cases ([a] Perfect bond, [b] smooth interface, [c] slightly rough interface and [d] rough interface) along-with interface shear stress distribution in the non-rigid cases. The figures show a deformed shape of the respective models at peak load step. The displacement multiplier, chosen to showcase the deformed model results, is 1000 for non-rigid bond models and 10 for perfectly bonded model. This gives a more distinct outlook on the results. Shear stress distribution at the interface is displayed at peak load. In case of perfect bond, the interface is very strong. Hence, cracking in the model is not influenced by interface failure but rather by a material (structural) failure, which occurs as the concrete element reaches its maximum tensile strength. Cracks can be observed in the model starting from the point of application of load to the bottom fixed support in a diagonal cracking pattern. This crack pattern resembles the strut-tie model explained by the theory of plasticity. Whereas, in case of non-rigid bonds, since the interface is weaker in shear than the adjacent concrete elements, a slip occurs immediately after the peak load at the interface is attained. Response of the model at the immediate next load step after the peak load is shown in Figure 4.10. The interface shear stress drops to a very low value (can be approximated to be zero for calculation purpose) with stress concentration at the interface near the left edge of the composite concrete model.

Furthermore, in the non-rigid bond cases, minor cracks can be observed near the bottom fixed support at the left edge (especially in case of slightly rough and rough interfaces). These cracks develop on account of high tensile stresses, induced by the moment (caused by the point load), near the fixed support.

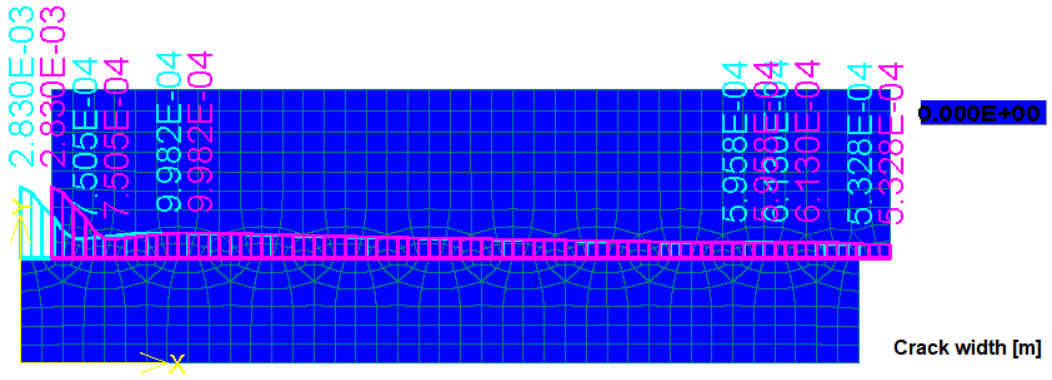

(a) Smooth interface, next load step after S-I (Displacement multiplier - 1000)

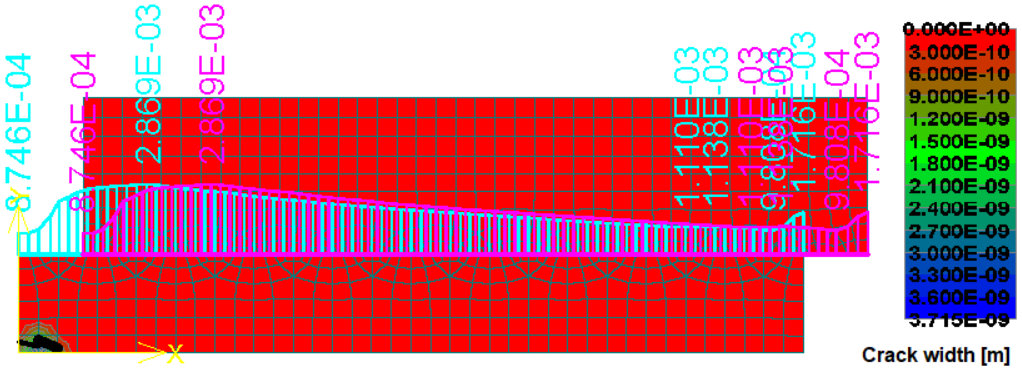

(b) Slightly rough interface, next load step after SR-I (Displacement multiplier - 1000)

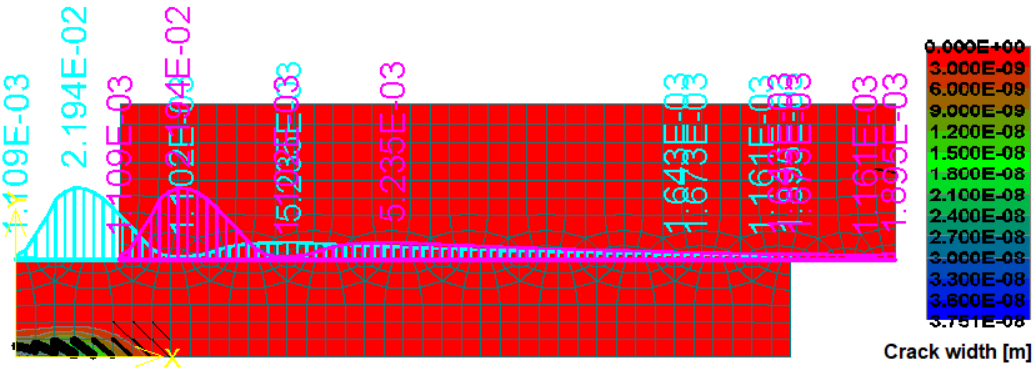

(c) Rough interface, next load step after R-I (Displacement multiplier - 1000)

Figure 4.10: Crack distribution and interface shear stress for a shear load test using different interface properties (Next load step after peak load)

The shear stress drops drastically once the interface reaches its shear capacity in the non-rigid bond models. Due to this brittle behavior the interface breaks and the top concrete layer slides in the direction of application of load. The post peak behavior of the models can be explained by the constitutive relation of the softening law assigned to the models. Since, no external compression is applied, the residual dry friction ('$-\mu\sigma$' in Figure4.1) is equal to zero. Responses shown in Figure 4.11 justify this behavior. Moreover, the graph presents a direct comparison between shear stress - strain relations in different models, with rigid and non-rigid bond strengths.

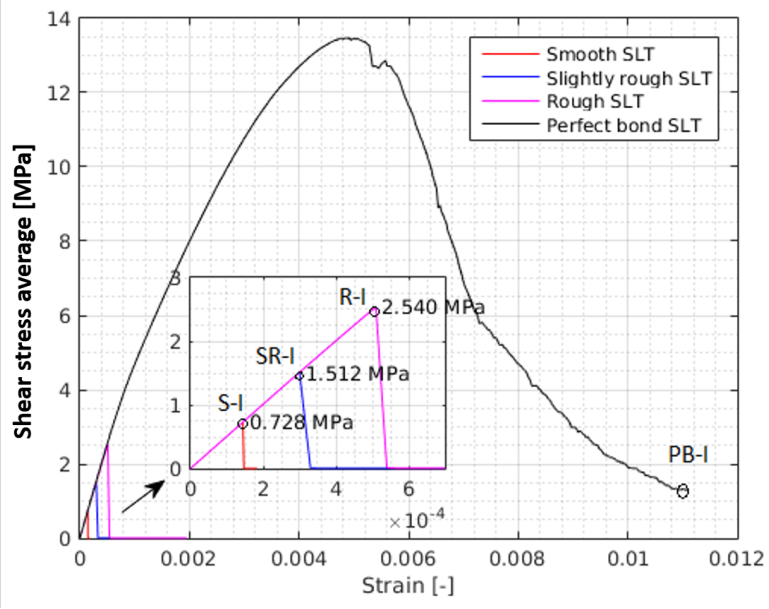

Figure 4.11: Shear stress - strain curve with different bond strength between the concrete layers

From the graph in Figure 4.11, it is observed that shear capacity of a perfectly bonded composite model is much higher than the non-rigid bond cases. The main reason for this is that, instead of interface failure, like in the non-rigid bond cases, the perfectly bonded model undergoes a material (structural) failure. This shows that if the bond between the two concrete layers is strong enough to replicate a perfect bond, then the highest shear capacity for the composite model can be achieved.

Coefficient of friction (μ)

Verification of friction parameter is performed on different roughness classes by comparing the results obtained in this section to the Mohr-Coulomb failure criterion with tension cut-off. An external compressive stress is applied on the top edge of the steel plate using the same numerical model, before applying the lateral loading. In the absence of an external compression, friction parameter is not activated, which is also evident from the formulae proposed by different design codes. With the external compression applied perpendicular to the interface, an increase in the shear capacity is anticipated. A uniformly distributed line load on top edge of the steel plate (magnitudes of $0.0367\ MPa$ *and* $3.67\ MPa$) is applied as the necessary pre-compression. The reason of choosing these specific magnitudes is because of an experimental test setup, which will be introduced in the next chapter. The parameters assigned for this verification are provided in Table 4.1. All the boundary conditions are exactly same as in the previous section.

As the external pressure increases, frictional resistance along the interface also increases, according to the formula 2.20. This gives rise to an increased shear strength of the specimen as explained in the Model Code 2010 [9]. Thus, a higher shear stress can be attained at the interface, as seen from the values in Table 4.2.

Table 4.2: Maximum normal and shear stress values at the interface for different load and roughness combinations (verification of Mohr-Coulomb failure criterion)

Interface property	Friction coefficient	Precompression [MPa]	σ (x) [MPa]	τ (y) [MPa]	tan θ^3 |-m_θ|
Smooth	μ=0.60	0.0367	-0.215	0.929	**0.62**
		3.6700	-4.426	3.585	
Slightly rough	μ=0.90	0.0367	-0.482	2.314	**0.89**
		3.6700	-4.717	6.095	
Rough	μ=1.30	0.0367	-1.093	4.006	**0.62**
		3.6700	-4.717	6.245	

A graphical representation is presented to explain the results. The maximum normal and shear stress values obtained from the analyses (Table 4.2) are plotted with normal stress on the X-axis and shear stress on the Y-axis. The two points are extrapolated to obtain the y-intercept in the graph. This y-intercept is the cohesion at the interface. Whereas, the slope of these line graphs correspond to the coefficient of friction. These line graphs are shown by bold lines in Figure 4.12.

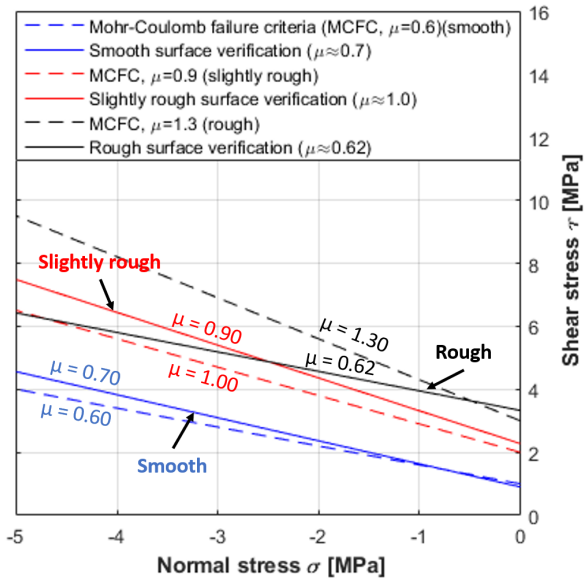

Figure 4.12: Verification of friction coefficient in accordance with the Mohr-Coulomb failure criteria (MCFC) for different roughness classes

The dotted lines in Figure 4.12, represent the Mohr-Coulomb failure criteria (MCFC) for three pre-defined non-rigid bond models (smooth, slightly rough and rough interface) in compression zone. This is also explained in the description of the interface material model (Figure 4.1a) in the beginning of the section. The blue, red and black line graphs represent the smooth, slightly rough and rough interface cases. With the prescribed boundary conditions and pre-compressive loads, an interface failure is achieved for *smooth* and *slightly rough* interface conditions. Slope of the lines obtained after plotting the line graphs (bold lines) and that of the failure surface defined by the MCFC (dotted lines) are nearly equal to the friction coefficient of the respective roughness classes. Hence, it is possible to verify the friction coefficient parameter in these conditions.

However, in case of rough interface, in the presence of an external pre-compression the interface strength increases significantly. Due to a very strong interface, the model no longer demonstrates interface failure, but rather a concrete material failure is observed. This is also evident from the significant difference in slope of line obtained from the line graph and the coefficient of friction assigned to the ATENA IMM. Hence, friction coefficient couldn't be verified in case of rough interface condition.

4.2.3. Reliability of bond tests (DTT and SLT)

There are different types of tests available to estimate the bond strength in tension and shear, for example, pull-off test, wedge splitting test, push-out test, slant shear test etc. Drawing comparisons between tensile and shear bond strength is difficult, as not only are these significantly affected by differences of test setups in tension and shear, but also shear and tensile bond are differently correlated to interfacial factors (e.g. roughness/texture). Nevertheless, for each test set-up and semi-empirical shear approach, Randl and Zanotti in their research [4] obtained a nearly constant cohesion-tensile bond ratio for different concretes with different strengths (normal strength and high strength). Minimum ratio of 0.6 was obtained with push-out test to a maximum of 2.8 with slant shear test. Other researchers work also agreed to this observation, by acquiring this ratio approximately equal to 2.5 like in the case of Peyerl and Steiner [5].

The models designed for direct tension test and shear load test in this report do not exactly correspond to any of the previously mentioned bond tests. However, ratio of bond strength in shear and tension can be calculated using the results obtained from the numerical analysis of DTT and SLT adopted in this research work. Considering the tensile strength and shear strength achieved from the non-rigid bond case models, ratio of shear is to tensile strength is calculated by two methods. First method uses stress values from the stress - strain curves plotted for DTT and SLT. Second method uses the peak stress values at the interface from the crack distribution figures of the respective DTT and SLT results.

[3] θ is the angle of Mohr-Coulomb failure criteria curve with the horizontal (i.e, the coefficient of friction); 'm_θ' is denoting the slope and not unit of length

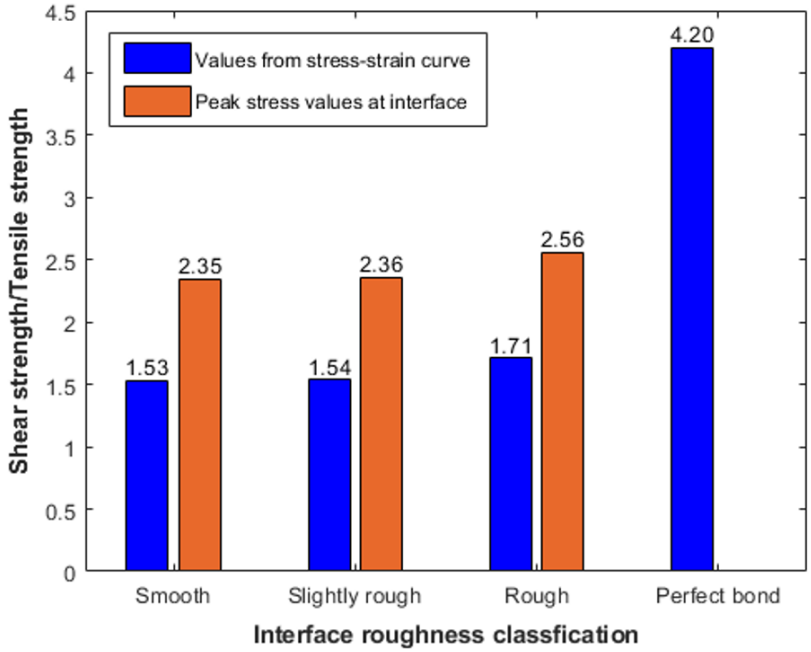

Figure 4.13: Ration between shear strength and tensile strength obtained from two approaches for different interface roughness characteristics

A direct comparison of shear strength to tensile strength ratio across different roughness classes is obtained from the two previously described approaches as shown in Figure 4.13. Blue bar ('*Values from stress - strain curve*') is the ratio obtained by dividing the shear stress values from the stress - strain curves by the tensile strength obtained in DTT. Whereas, the orange bar ('*Peak stress values at interface*') is obtained by dividing the maximum interface shear stress values (Figures 4.9) by the same tensile strength from the DTT. A similar ratio (1.5 - 2.6) is obtained from the comparison thus, complying with the work of other researchers. Therefore, the direct tension and shear load tests adopted for the verification of interface models, are reliable enough to proceed with the finite element analyses.

However, for a same roughness class, difference is observed in the ratio obtained by the two techniques. Ratio calculated using the peak stress values from the interface are obviously higher because, as the name suggests, these are the maximum shear stress values at the interface. Since, shear stress distribution is not uniform along the interface, peak values are used for the comparison. Moreover, in case of perfectly bonded model, the ratio between the shear strength and tensile strength is much higher (≈ 4). Since, in this case bond between the two concrete elements is very strong this leads to a material failure of the adjacent elements. Failure at the interface cannot be achieved in the perfectly bonded model.

After using the *2D line 4-noded interface* elements to model an interface, another alternative approach is proposed using the standard material elements in ATENA. For this, *4-noded quadrilateral* elements are used to design an artificial interface layer. This interface layer has a certain thickness and physical properties corresponding to a concrete material. An attempt is made to model the interface using artificial interface layer by providing explicit roughness and to check reliability of this model. Hence, in the next section, an artificially created interface element model (ArtIM) is studied with similar tests as performed for the ATENA IMM.

4.3. Artificial Interface Model (ArtIM)

The ATENA interface material model has a dependency on many factors pertaining to roughness of the concrete surface. It is not always simple and straightforward to accurately measure these parametric values from experiments. To address this limitation an artificial interface model (ArtIM) is proposed which uses standard material elements available in ATENA. An attempt is made to design this model such that, an artificial interface is created to simulate an actual interface between two concrete elements. To incorporate the effect of different roughness classes, an explicit roughness is provided to the artificial interface layer which uses quadrilateral finite elements shaped in the form of a wave pattern. Similar to the case of ATENA IMM, DTT and SLT are performed using the artificial interface model (ArtIM) to study the interface behavior.

Important parameters in ArtIM

The artificial interface model (ArtIM) uses material elements instead of interface elements to simulate an interface between two adjacent concrete elements. Parameters to be defined for the material element, include the physical properties of a concrete element: elastic modulus (E), Poissons's ratio (ν), tensile strength (f_t) and compressive strength (f_c). In order to ensure localisation of cracks in the interface layer, tensile strength of the artificial interface should be less than that of the adjacent concrete elements.

The nonlinear behavior of concrete in the biaxial stress state is described by means of the effective stress σ_c^{ef} and the uniaxial strain ε^{eq}. The effective stress is nothing but a principal stress in most cases. The complete equivalent uniaxial stress-strain diagram for concrete is shown in Figure 4.14a. Whereas, in the compression stress state the failure function according to Kupfer [24] is used in ATENA. This failure function is shown in Figure 4.14b.

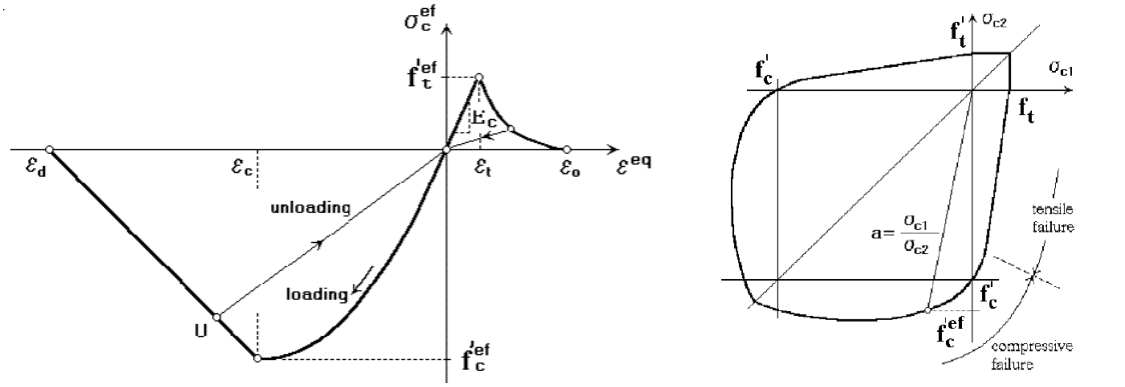

(a) Uniaxial stress-strain law of concrete [10] (b) Biaxial failure function for concrete [10]

Figure 4.14: Stress - strain relationships for concrete material in ATENA

With the use of the above mentioned parameters, an artificial interface layer is created. Unlike in the ATENA IMM, a constant thickness is provided to the interface layer throughout the length of the specimen. Thickness of this layer is chosen to be between $5 - 10\ mm$ (for example, thickness of mortar layer in masonry structures). Specifications of the numerical model are described further.

Preparation of numerical model

Similar to the ATENA IMM, geometry of the concrete elements and steel plate used in this model are identical. Main difference is in the interface layer. Previously interface elements were used to model the interface, whereas, in this model, material elements are used to create an artificial interface layer. For this, a third element is introduced between the two adjacent concrete elements. This third layer represents the artificial interface layer. A constant thickness of 5 mm is maintained throughout the length of the model. To incorporate the effect of different roughness classes, an explicit roughness is provided to the artificial layer. This is done by modelling the layer in a wave pattern with certain wavelength and amplitude depending on the roughness classification provided in *fib* Model Code 2010 [16]. Detailed discussion on this is presented

in the direct tension test section. Figure 4.15 shows the mechanical model used to analyze the Artificial Interface Model (ArtIM) with details about the finite elements used for the analysis. The detailing of the artificial interface created (straight pattern) is shown in Figure 4.16. The black region represents the interface layer whereas, the gray regions are a part of the adjacent concrete elements. Specific characteristics of the numerical model are discussed further.

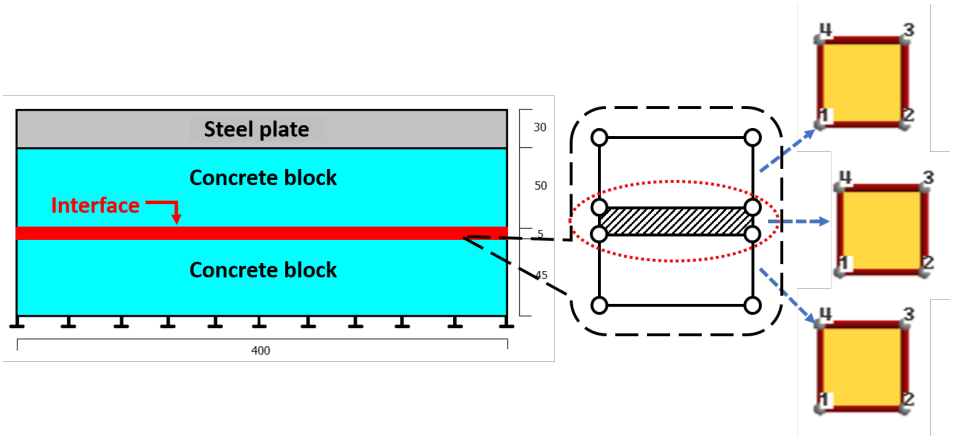

Figure 4.15: Schematization of small scale composite concrete model and finite element types used for numerical analysis (all dimensions are in mm) using ArtIM

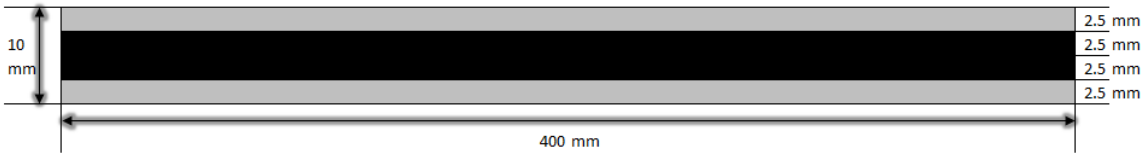

Figure 4.16: Interface detailing (straight element)

- The structure is made up of 2D elements in a 2D environment. Thickness of the elements is 300 mm;
- The steel plate is modelled as *plane stress elastic isotropic* elements with elastic modulus E = 210,000 N/mm^2 and Poisson's ratio = 0.3;
- The concrete block elements are modelled as *3D Non Linear Cementitious 2* elements, with exponential tension stiffening behavior, cube compressive strength of 50 MPa, Poisson's ratio = 0.2 and remaining properties defined as per Eurocode guidelines;
- The interface is modelled as *3D Non Linear Cementitious 2* elements, with exponential tension stiffening behavior, cube compressive strength of 12.5 MPa, Poisson's ratio = 0.2 and remaining properties defined as per Eurocode guidelines. To ensure localization of cracks in the interface layer, a weak material strength is chosen with a tensile strength of 0.5 MPa. Constant thickness of 5 mm is maintained throughout the length of the model;
- The mesh is generated using quadrilateral elements with an element size of 10 mm for steel and concrete elements and 5 mm for the artificial interface layer;
- The bottom edge of the substrate concrete layer is restrained in both x- and y-direction.
- Self-weight of the elements is disregarded in this analysis,
- Newton-Raphson solution method is used for the calculation of the numerical results

In the next sections, detailed discussion about the direct tension test (DTT) and shear load test (SLT) is performed by incorporating an explicit roughness to the model.

4.3.1. Direct Tension Test (DTT)

In this section, similar to the case with ATENA interface material model (IMM), a direct tension test is performed using the artificial interface layer (Figure 4.16). To ensure localization of cracks at the interface, lower strength concrete material properties are assigned to the interface element and are as shown in Figure 4.17. The tensile strength of the interface concrete layer corresponds to the weakest interface characteristics from the ATENA interface material, i.e, the smooth interface (section 4.2.1)[4]. Boundary conditions applied are similar to the ATENA IMM case. Figure 4.18 shows the mechanical and numerical models respectively, designed for the direct tension test (DTT).

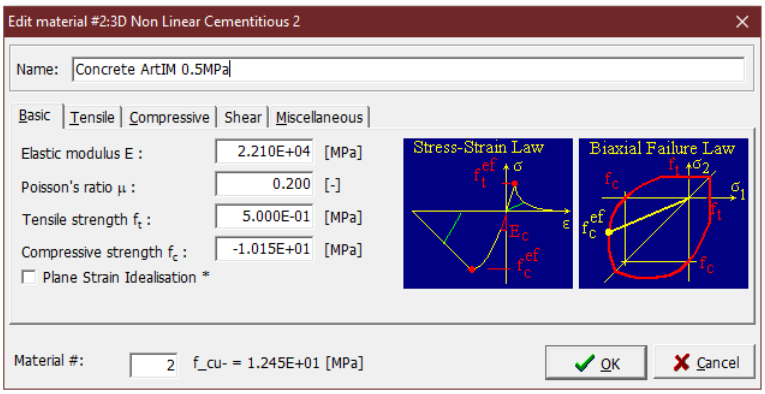

Figure 4.17: Interface element material properties

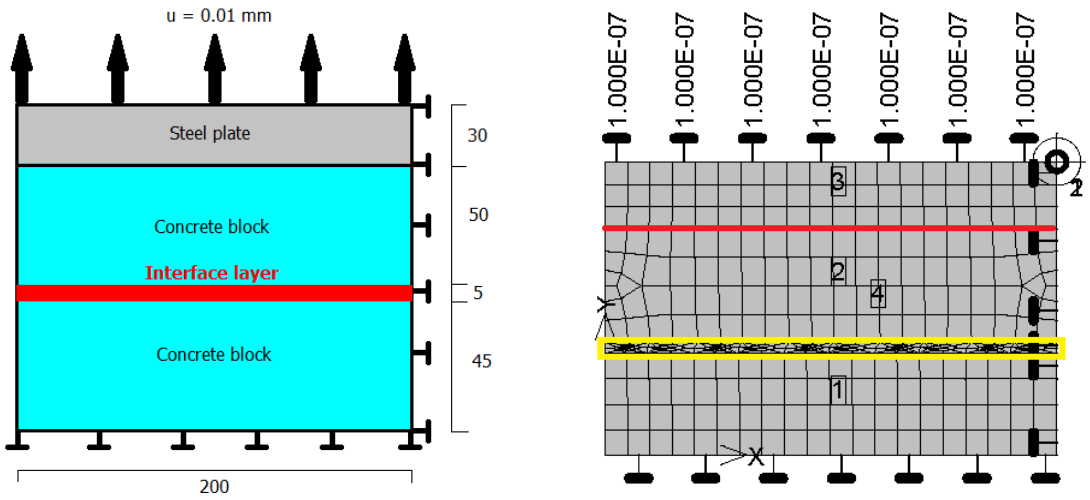

(a) Mechanical model (b) Numerical model

Figure 4.18: Mechanical and numerical model developed with ArtIM using symmetry
(All dimensions are in mm)

Figure 4.18b shows the numerical model used for the finite element analysis. The wide yellow section indicated in the figure is the artificial interface layer with a thickness of 5 mm. From the previous interface model it is evident that the two main parameters governing the shear strength of an interface, are cohesion and coefficient of friction. However, these parameters cannot be specifically defined for the artificial interface layer in this model. To ensure surface roughness, a modification of the interface layer is necessary in order to associate the effect of the roughness parameters. Therefore, an "explicit roughness" is incorporated instead

[4] Apart from the concrete strength class chosen for the analysis, an additional study is also performed with stronger material characteristics for the interface element attributing to the use of adhesive materials, for example, bonding agents. Results of this analysis are discussed in appendix A

of a straight interface element. This means that the interface layer is designed in a wave pattern such that a necessary roughness (wave amplitude) is purposely provided using the quadrilateral finite elements at the interface. This modification is made, keeping in mind the guidelines from Model code 2010 which distinguishes the roughness classes depending on the average roughness of the substrate concrete layer. Figure 4.19 shows the interface detailing incorporated for the *slightly rough* and *rough* substrate surface classes respectively. The explicit interface profile is distinguished as slightly rough and rough strictly based on the average roughness value along the interface mean line and not the physical property assigned to the interface layer. The use of symmetry is made to minimize the computation time as done in case of straight interface layer for a direct tension test. The numerical models designed for *slightly rough* and *rough* interface conditions are shown in Figure 4.20. However, for smooth interface a straight interface layer as shown in Figure 4.16 is used. Effect of explicit roughness depicting a smooth surface is investigated later into the chapter.

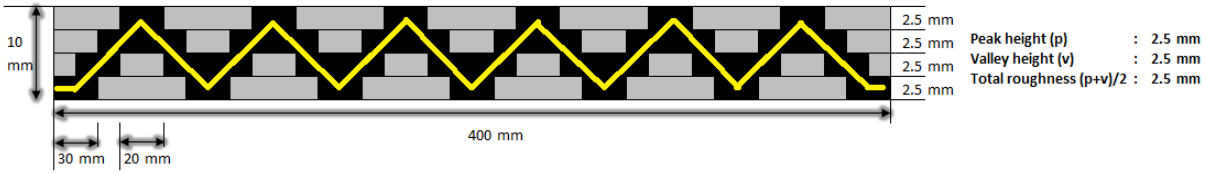

(a) Slightly rough interface

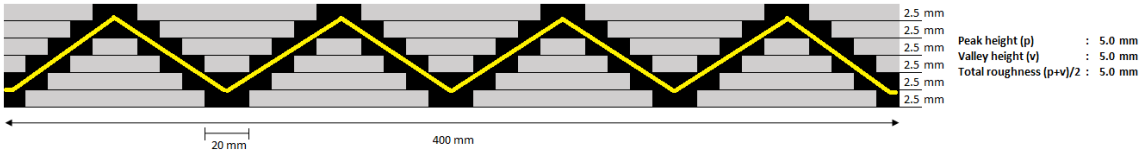

(b) Rough interface

Figure 4.19: Interface detailing for explicit roughness

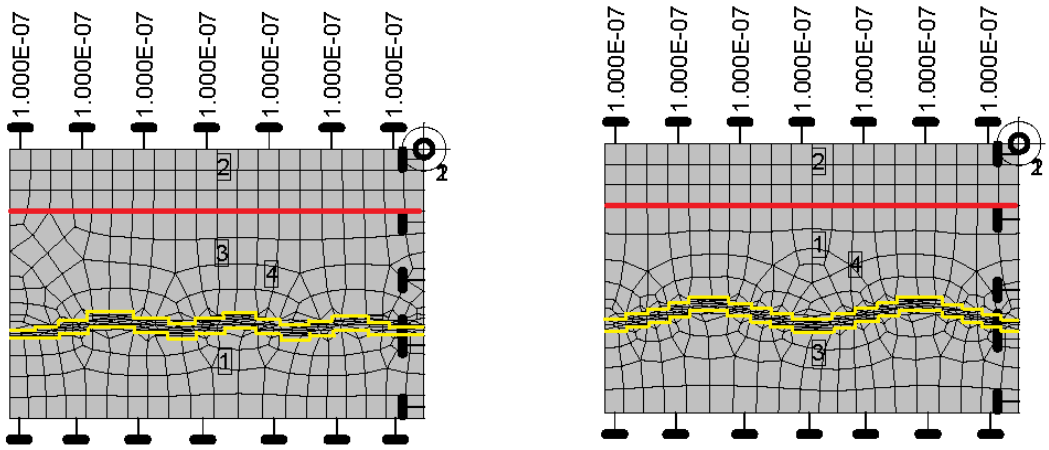

(a) Slightly rough interface

(b) Rough interface

Figure 4.20: Numerical models designed for slightly rough and rough interface conditions

The response of the composite model, to a direct tension test is discussed further. Crack distribution and normal stress (σ_{yy}) results are shown in figures below.

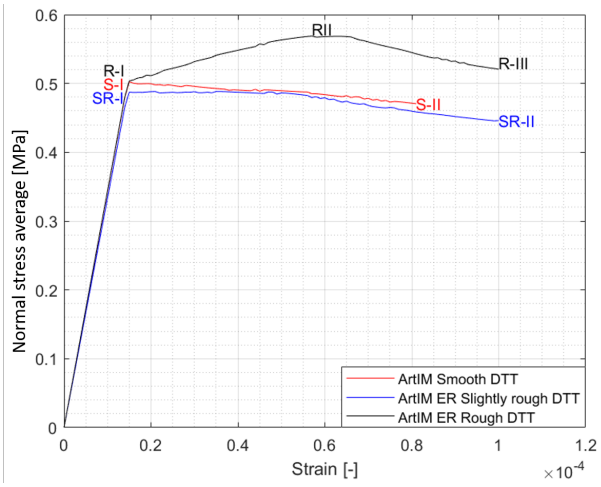

Figure 4.21: Normal stress - strain for different interface properties using ArtIM with explicit roughness

Figure 4.21, shows a comparison between the DTT responses, when explicit roughness is introduced for the interface elements. The model behaves linearly in the first phase of the analysis until the cracks appear at the interface elements. Once maximum tensile strength of the interface is attained, the curve changes path and goes in to the softening branch. However, in the case of rough interface (top-most curve in the Figure 4.21), concrete at the interface undergoes strain hardening until it attains peak strength and with further load increments shows softening behavior. This will be discussed in detail with a pictorial representation of the respective interface characteristics.

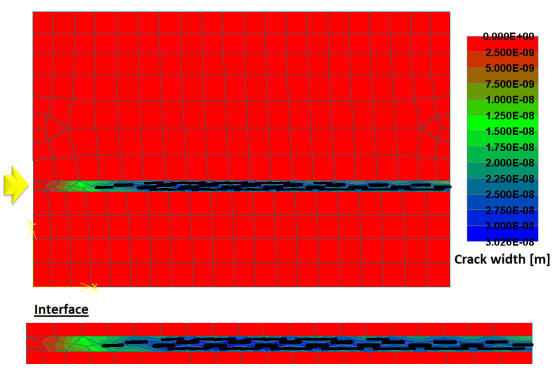

(a) Crack width at peak load (S-I)

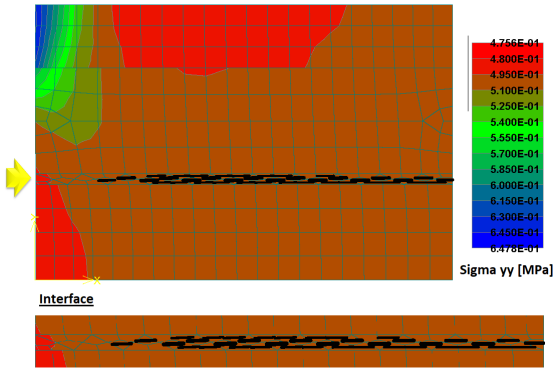

(b) Normal stress distribution at peak load (S-I)

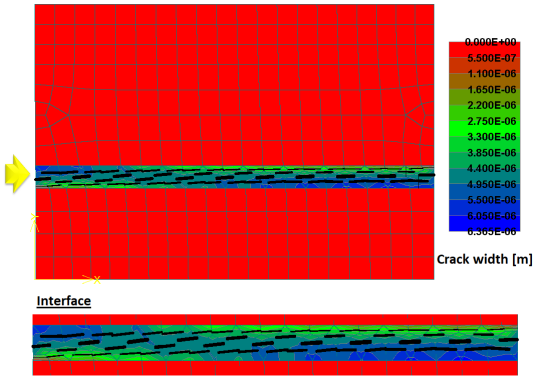

(c) Crack width at final load step (S-II)

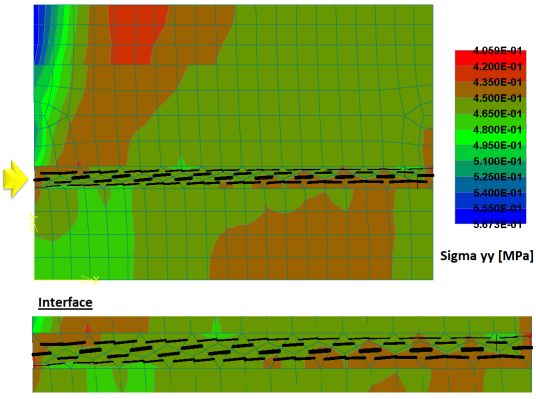

(d) Normal stress distribution at final load step (S-II)

Figure 4.22: Crack and normal stress distribution at smooth interface (Displacement Multiplier = 1000)

In Figure 4.22[5], the crack distribution and normal stress distribution in the composite model with smooth interface characteristics (straight interface element) is shown. Figures 4.22a - 4.22b, are the responses at the peak load step. The model (interface), attains maximum tensile strength at this point. The cracks are evenly distributed starting from the mid-plane axis of symmetry. As the tensile stress increases further, the cracks spread through the full length of the interface (Figures 4.22d - 4.22). Due to the straight shape of the interface elements, cracks propagate uniformly in the longitudinal direction of the model.

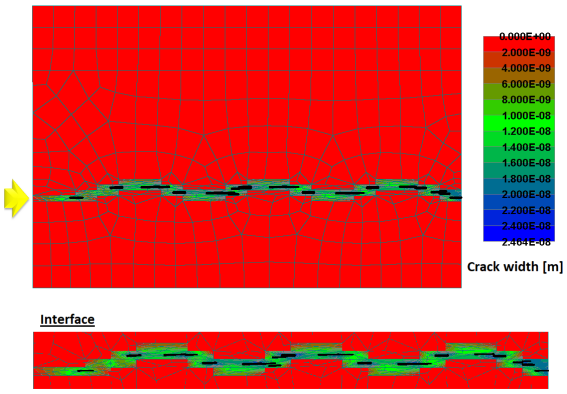

(a) Crack width at peak load (SR-I)

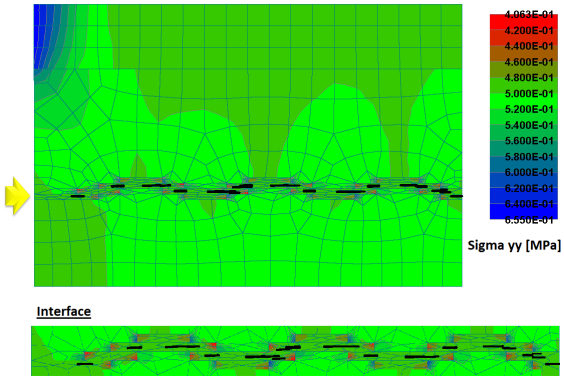

(b) Normal stress distribution at peak load (SR-I)

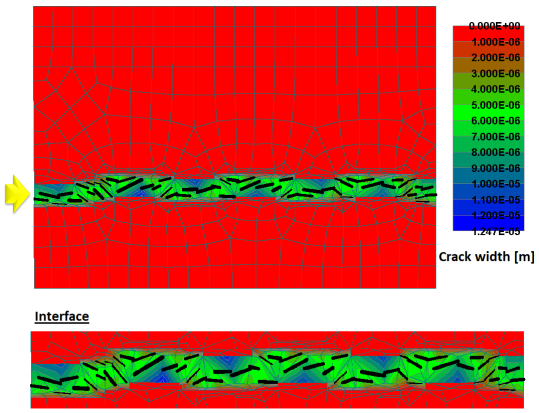

(c) Crack width at final load step (SR-II)

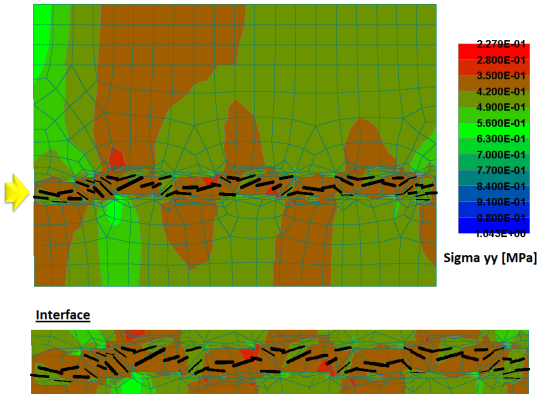

(d) Normal stress distribution at final load step (SR-II)

Figure 4.23: Crack and normal stress distribution at slightly rough interface (Displacement Multiplier = 1000)

In case of a slightly rough interface class (Figure 4.23), the behavior of the composite model is more or less similar to the previous case, despite of the explicit roughening of the interface elements. The consecutive peaks and valleys introduced in the interface layer, do not have sufficient heights to significantly affect the interface strength. Moreover, cracks propagate along the mean line of the interface elements (through the horizontal mid-plane between the peaks and valleys of explicitly rough interface element). Figures 4.23a - 4.23b show the crack and normal stress distribution at the peak load step. Whereas, at the end of the analysis, a minor concentration of tensile stresses can be observed near the respective peaks and valleys of the interface element. This indicates the influence of explicit roughness (peak and valleys) on the stress distribution in the model and that this can be controlled with appropriate regulation of the amplitude of the interface element.

[5] in the figures denote the location of the interface

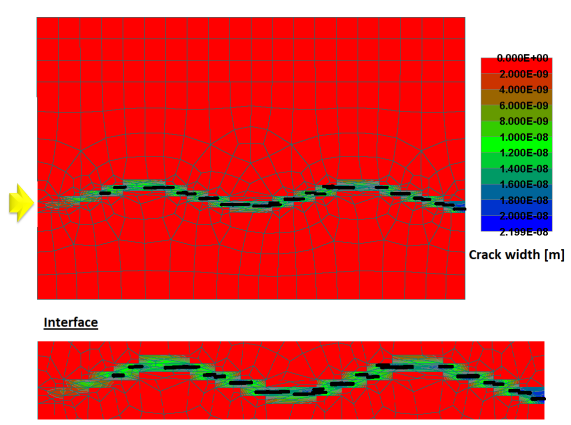

(a) Crack width at tensile strength level (R-I)

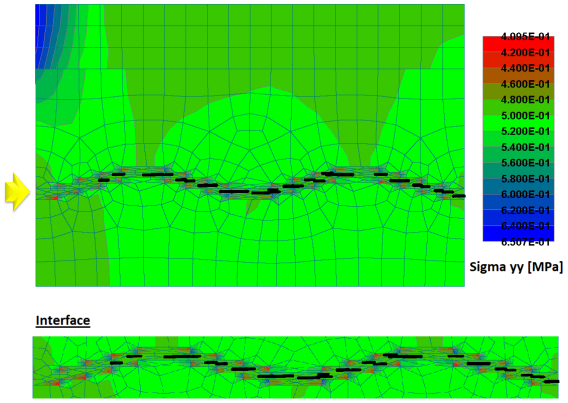

(b) Normal stress distribution at tensile strength level (R-I)

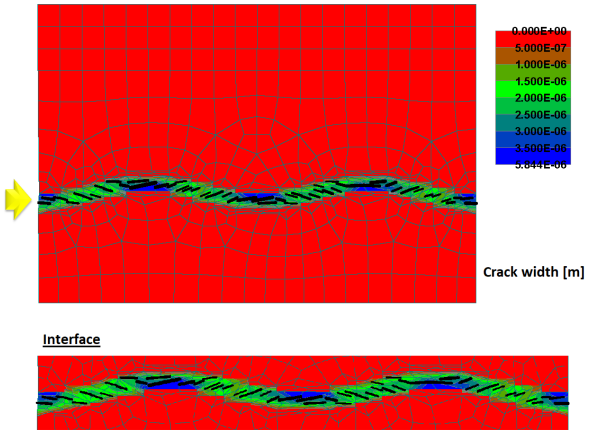

(c) Crack width at peak load (R-II)

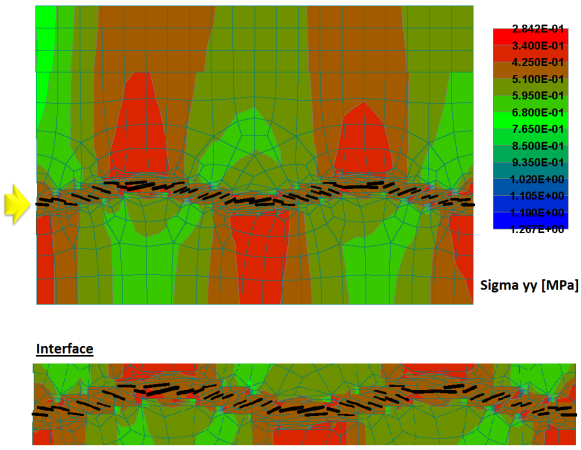

(d) Normal stress distribution at peak load (R-II)

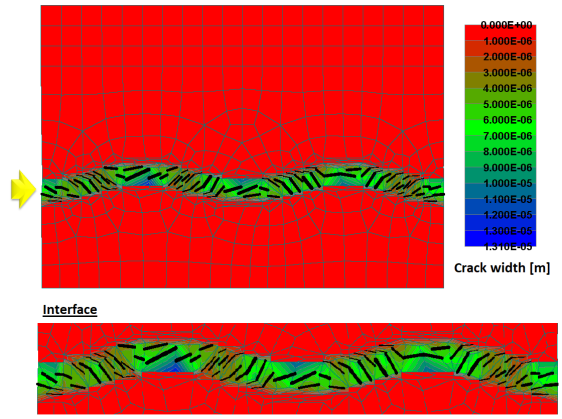

(e) Crack width at final load step (R-III)

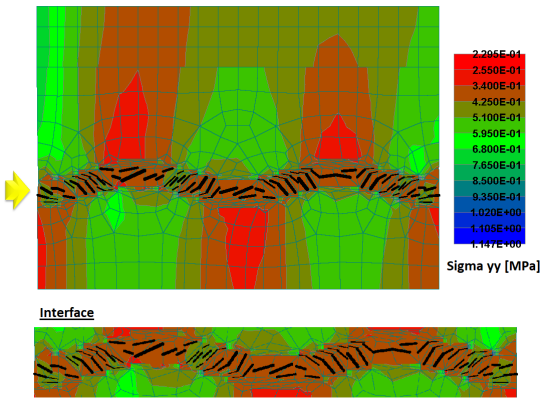

(f) Normal stress distribution at final load step (R-III)

Figure 4.24: Crack and normal stress distribution at rough interface (Displacement Multiplier = 1000)

Finally, Figure 4.24, shows crack and normal stress distribution when rough interface properties are assigned to the explicitly defined interface elements. Once the tensile strength of the interface elements is attained (Figures 4.24a - 4.24b), concrete in this layer undergoes strain hardening until peak strength of the material is achieved. The strain hardening mainly takes place due to concentration of tensile stresses near the peaks and valleys of the interface layer (Figure 4.24d). Since, it is considered to be a rough interface, the amplitude (height of the peaks and valleys measured from the mean line of interface) of the interface layer is high enough to cause this stress concentration. Moreover, the crack distribution in the interface layer is not

completely a straight line. It varies with the curvature of the interface, especially at the peak load (Figures 4.24c).

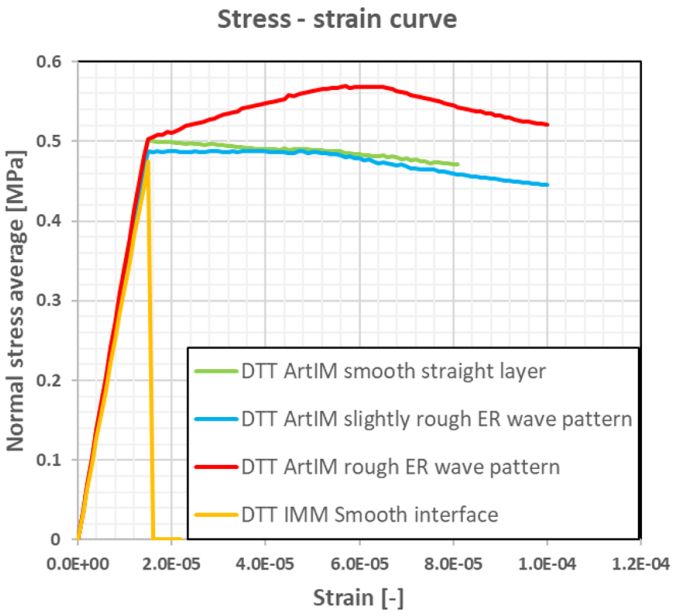

Figure 4.25: Comparison of DTT results between ATENA IMM and ArtIM

Figure 4.25, shows a direct comparison of results obtained from direct tension tests, using ATENA IMM and ArtIM. The ArtIM gives the model more ductility than in case of ATENA IMM, because softening law is not defined for the ATENA IMM. Since the artificial interface element has a very low tensile strength $0.5\ MPa$ (corresponding to the smooth surface class properties defined in ATENA IMM), the peak strength achieved by using ArtIM, is equal to the tensile strength of the smooth interface with ATENA IMM. The strain corresponding to the respective yield stress values is same for both interface models ($\approx 1.6 \times 10^{-5}$). In the next section response of the ArtIM is studied when shear loading is applied to the model.

4.3.2. Shear Load Test (SLT)

In this section, response of the artificial interface model is studied when the composite concrete model is subjected to lateral/shear loading. The boundary conditions enforced in the numerical model are identical to the case of ATENA IMM as discussed in section 4.2.2. The main difference in this case, is with the interface element used, and it has mesh size of 5 mm along-with the lines connecting the interface element to the adjacent concrete macro-elements. Furthermore, effects of various parameters pertaining to the strength of the interface element are studied in detail.

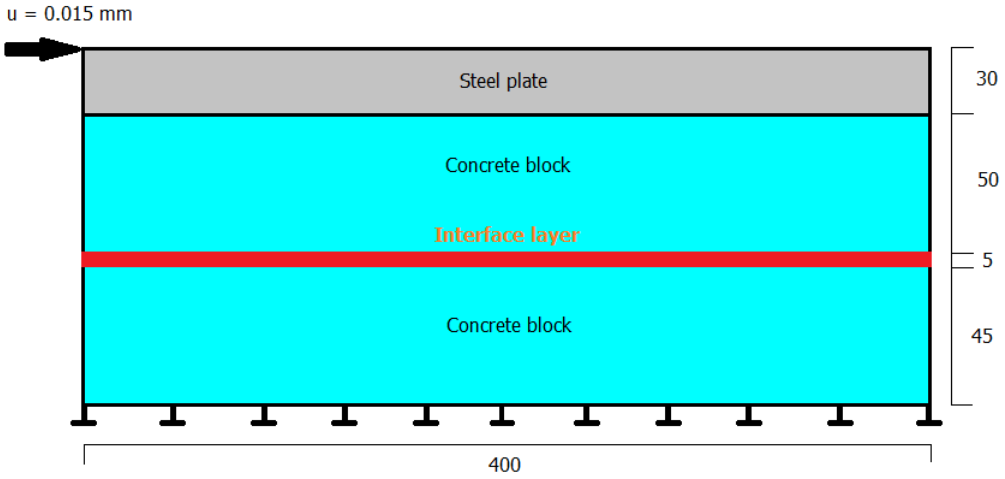

Figure 4.26: Mechanical model for shear load test using ArtIM

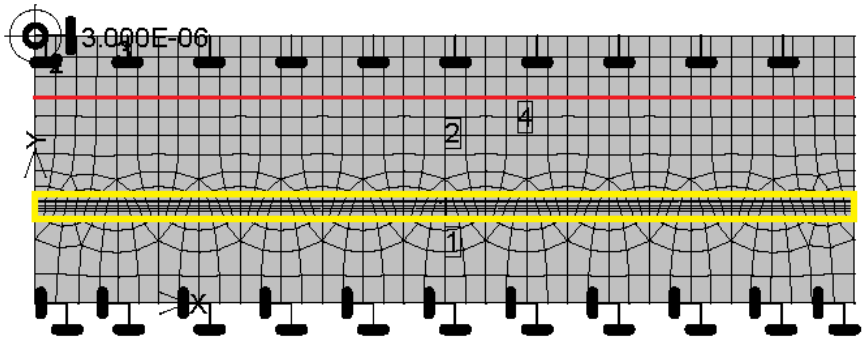

Figure 4.27: Numerical model for shear load test using ArtIM

Influence of explicit roughness at the interface element (without external compression)

As studied in section 4.2.2, like the influence of cohesion on the shear capacity, a similar parameter should be chosen, which will affect the shear capacity of the composite model when ArtIM is used. Moreover, a relation between the tensile and shear strength was also established earlier. For this purpose, the concrete class having the weakest tensile strength is chosen for the interface elements. This will also ensure localization of cracks at the interface. However, an additional study is also performed to check the behavior of the model, when relatively stronger concrete is used for the interface (pertaining to different kinds of bonding agents that can be applied as discussed in DTT) and the results are discussed in appendix A.

Unlike in the case of ATENA IMM, cohesion and friction coefficient parameters cannot be assigned for the artificial interface while using an ArtIM. Nevertheless, a distinction can be made by modifying the straight interface and introducing an explicit roughness, similar to the models undergoing direct tension in previous section. Interface detailing is same as designed for a DTT (4.19), but instead of a symmetric model (BCs

make the model asymmetric), full length specimen is tested in case of shear load test. Numerical models designed for the slightly rough and rough interface characteristics are shown in Figure 4.28[6]. Mesh size used for the analysis is same as used in DTT (10 mm for concrete and steel elements and 5 mm for interface elements).

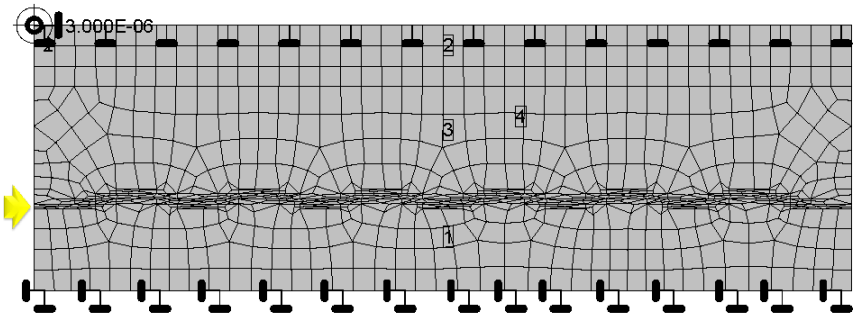

(a) Interface corresponding slightly rough interface

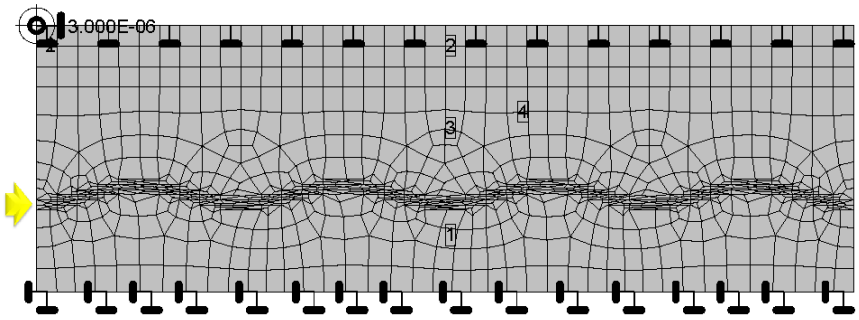

(b) Interface corresponding rough interface

Figure 4.28: Numerical models with explicit roughness at the interface elements

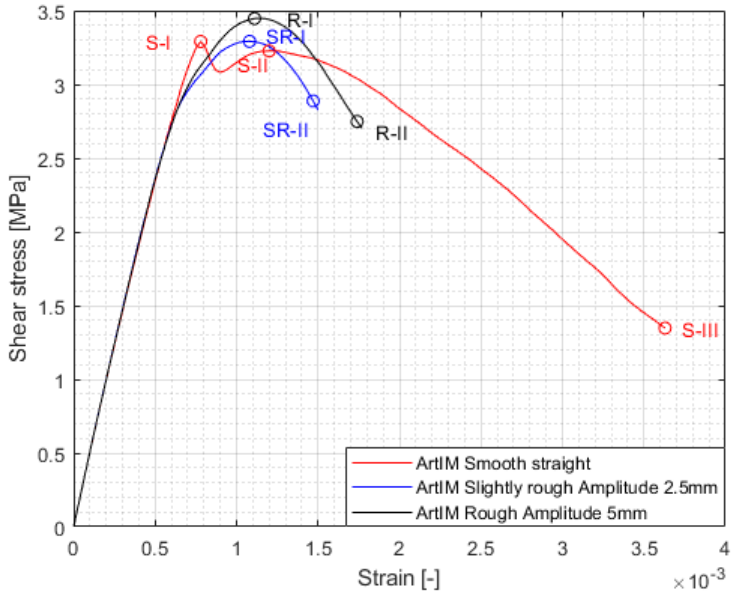

Figure 4.29: Shear stress - strain for different roughness conditions

6 in the figures denote the location of the interface

A shear load is applied to the model in the same way like in the DTT. External pre-compression is not present in this test. Response to the lateral loading for the respective interface cases are presented in Figure 4.29.

The graph (Figure 4.29), shows shear stress response of the composite model when the interface is modified by providing explicit roughness. The response of the models corresponds to brittle behavior (of the interface elements). There is a slight increase in the shear capacity with increase in the explicit roughness provided at the interface. Detailed discussion on the interface response is done further by comparing crack distribution at the interface.

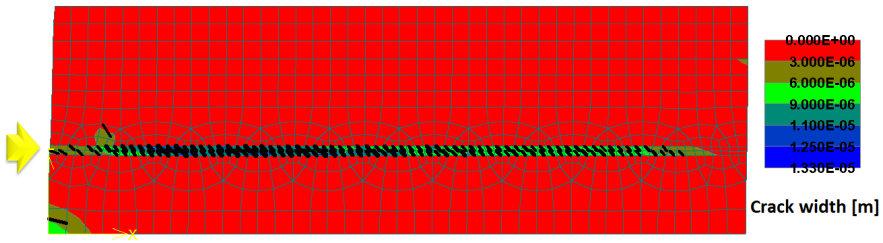

(a) Crack distribution at peak load step for smooth interface (S-I)

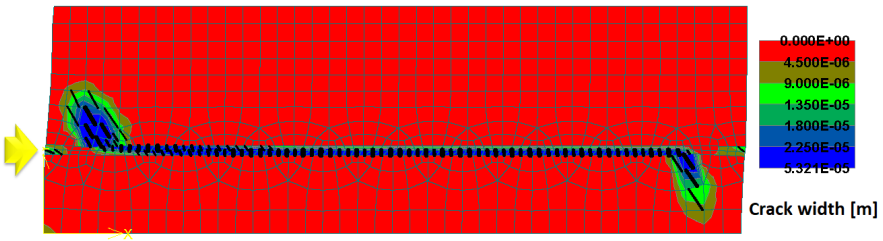

(b) Crack distribution at second peak load step for smooth interface (S-II)

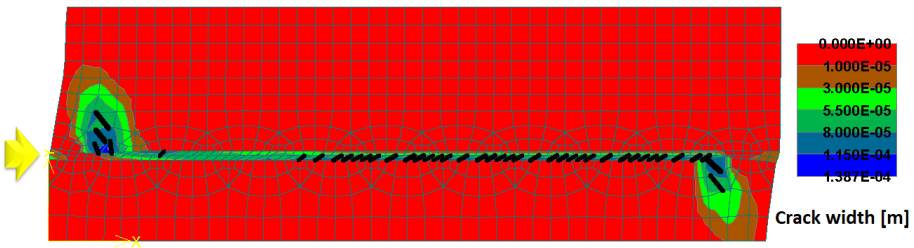

(c) Crack distribution at final load step for smooth interface (S-III)

Figure 4.30: Crack distribution when smoother interface (straight element) is modelled without external compression (Displacement Multiplier = 50)

The curve for smooth interface, drops after reaching the first peak strength value and on further load increment a small increase in the shear stress is observed leading to a subsequent reduction in strength. This can be explained with Figure 4.30a. In this figure it can be observed that, at the first peak shear stress, localization of cracks in the interface occurs. Once, the interface reaches its fully developed crack phase, with subsequent increase in the crack width, a diagonal major crack starts propagating towards the point of application of load and a dip in the shear stress is observed. Furthermore, as the diagonal crack width increases a second diagonal crack develops near the opposite edge of the model, again propagating from the interface towards the bottom fixed support. Figure 4.30b, shows this behavior at the second peak shear stress of the curve. Eventually, as the two diagonal cracks are fully developed the stress start decreasing thus showing softening behavior of concrete (Figure 4.30c). The diagonal cracking can be attributed to the strut-tie model in case of shear loading. As studied previously in ATENA IMM perfectly bonded condition (Figure 4.9d), when the composite model behaves as one homogeneous material, a major diagonal crack can be observed by connecting the weaker sections of the material, thus representing a strut-tie model. However, in this case, since the interface material cracks first, the diagonal cracks initiate from the interface level to the respective ends (point of application of load and bottom support).

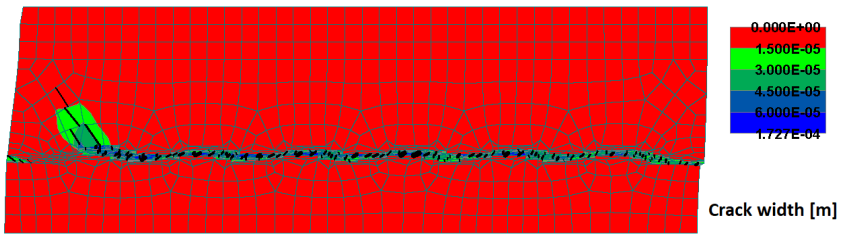

(a) Crack distribution at peak load step for slightly rough interface (SR-I)

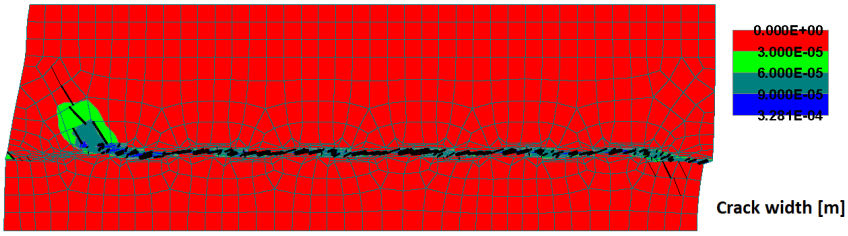

(b) Crack distribution at final load step for slightly rough interface (SR-II)

Figure 4.31: Crack distribution when slightly rough interface (sinusoidal pattern) is modelled without external compression (Displacement Multiplier = 100)

Figure 4.31, shows crack distribution in the composite material model when explicit roughness is incorporated (roughness corresponding to slightly rough surface characteristics with amplitude 2.5 mm) at the interface. As expected, cracks propagate predominantly in the interface elements. Due to the minor irregularity of geometry of the interface elements, the response is more or less similar to the case of smooth (straight) interface. Furthermore, at peak load step, since the interface is at fully developed crack stage, new cracks cannot develop at the interface and hence, a diagonal crack starts propagating from the interface to the point of application of load, similar to the case of smooth interface. However, in this case, cracks develop until the right-most end of the interface, thus, inducing very small cracks diagonally propagating towards bottom support. Hence, a second rise in the shear capacity is not observed here.

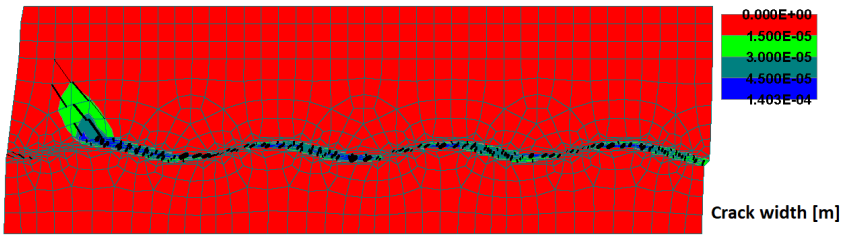

(a) Crack distribution at peak load step for rough interface (R-I)

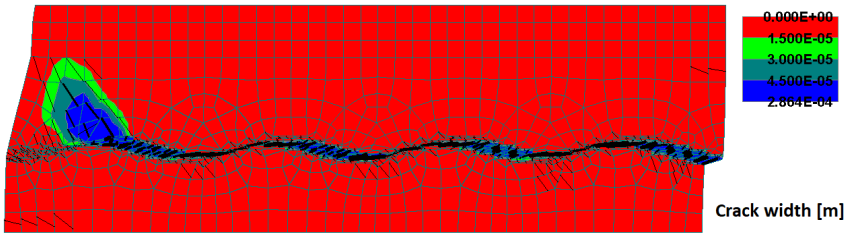

(b) Crack distribution at final load step for rough interface (R-II)

Figure 4.32: Crack distribution when rough interface (sinusoidal pattern) is modelled without external compression (Displacement Multiplier = 100)

Figure 4.32, shows crack profile in case of rough interface characteristics (amplitude equal to 5 mm) are

incorporated into the model. The amplitude of the roughness profile is double than in case of slightly rough interface. The crack propagation happens in the similar manner as in slightly rough interface condition. However, it is important to point out here that, with increasing amplitude of the roughness profile, cracking pattern in the interface becomes more prominent and the top concrete layer starts sliding over the substrate concrete layer. This also leads to a higher crack width of the major diagonal crack. In the next section effect of external compression is studied with the same set of interface models.

Influence of explicit roughness at the interface element (with external compression)

With the ATENA interface material model, the verification of friction coefficient was accomplished by comparing the slope of the plot (plotted using maximum normal and shear stress values) to the Mohr-Coulomb failure criteria. In the artificial interface model, since friction coefficient cannot be defined, the interface is designed in a way to replicate the effect of friction. For this the material properties of the interface layer are kept constant throughout the comparison. By changing the wavelength and amplitude of the interface wave pattern different roughness classes are simulated. Different pre-compressive stress levels are applied on the top edge of the steel plate of the composite model. The maximum pre-compressive stress applied on the model is of the magnitude 3.67 MPa, as in the case of ATENA IMM. Material properties are kept the same for this analysis as in case of shear load test. The maximum normal and shear stresses at the interface, obtained from the analyses are recorded in Table 4.3, for different interface characteristics. $\tan\alpha$ in the following table denotes slope of the line plotted using these maximum stress values pertaining to each roughness class.

Table 4.3: Maximum normal and shear stress values at the interface element for different load and roughness combinations (using ArtIM)

Interface type	**Interface layer Geometry**	**Precompression [MPa]**	σ_{max} **(x) [MPa]**	τ_{max} **(y) [MPa]**	$\tan\alpha$[7] **|-m$_\alpha$|**
Smooth	Straight element	0.000	-2.818	3.291	0.20
		3.670	-4.975	3.729	
	wave pattern	0.000	-3.328	3.392	0.56
		3.670	-4.908	4.280	
Slightly rough	wave pattern	0.000	-3.076	3.306	0.82
		3.670	-3.350	3.531	
Rough	wave pattern	0.000	-1.334	1.786	1.27
		3.670	-3.000	3.902	

Table 4.4: Maximum normal and shear stress values at the interface element for different load and roughness combinations (using ArtIM)

Interface type	**Model Code (friction coeff.)**	**ATENA IMM (friction coeff.)**	**ArtIM (slope of line-curve)**	**Interface layer Geometry**
	μ	$\tan\theta$ **|-m$_\theta$|**	$\tan\alpha$ **|-m$_\alpha$|**	**(ArtIM)**
Smooth	0.60	0.62	**0.20**	Straight element
			0.56	wave pattern
Slightly rough	0.90	0.89	0.82	wave pattern
Rough	1.30	**0.62**	1.27	wave pattern

Table 4.4, shows a direct comparison between slopes of the respective failure criteria lines. Second column

[7] α is the angle of Mohr-Coulomb failure criteria curve with the horizontal (i.e, the coefficient of friction); 'm$_\alpha$' is denoting the slope and not unit of length

of the table comprises of the values proposed by the Model Code 2010 (coefficient of friction μ). Third and the forth column show slopes of the curves obtained from the respective interface models, ATENA interface material model (IMM) and artificial interface model (ArtIM) respectively. Values from the Model Code and ATENA IMM show an increasing trend in the friction coefficient values with the subsequent increase in the roughness (i.e., from smooth to rough) except in case of rough interface in ATENA IMM. As explained earlier, in case of rough interface material failure is observed as opposed to interface failure. However, in case of artificial interface model (ArtIM), a smooth interface with elements arranged in a straight layer do not produce a slope close to the friction coefficient value from Model Code or ATENA IMM. To mitigate this problem and to enhance the value of slope using ArtIM, adjustments to the interface profile are made by providing a minor explicit roughness of lower amplitude than slightly rough and rough interface. Explicit roughness used for smooth interface to test the friction effect is shown in Figure 4.33. Furthermore, for slightly rough and rough interface type condition, the slope of the line obtained using ArtIM complies with the Model Code values as well as the ATENA IMM friction coefficient values. A similar rising trend is observed in the slope values with the subsequent increase in roughness.

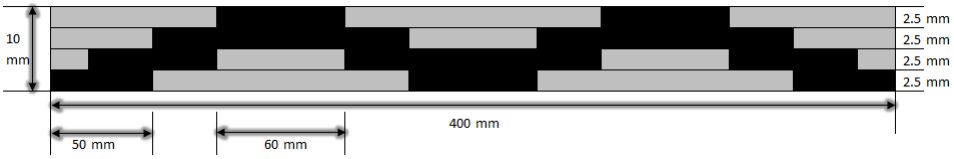

Figure 4.33: Interface detailing of explicit roughness provided to smooth interface characteristics

This shows that when the interface layer is modified with explicit roughness (interface elements in wave pattern), a friction effect similar to the ATENA interface material model can be achieved. Furthermore, an additional study is performed to test the roughness at the interface, by modifying wavelength of the wavy interface layer. Results of this study are discussed in detail in Appendix A. Important conclusion of this study is that, with a reduction in the wavelength (pertaining to the wave pattern of the interface layer), the post peak softening behavior becomes more and more brittle. Difference in the shear capacities for these respective wavelength models is not significant.

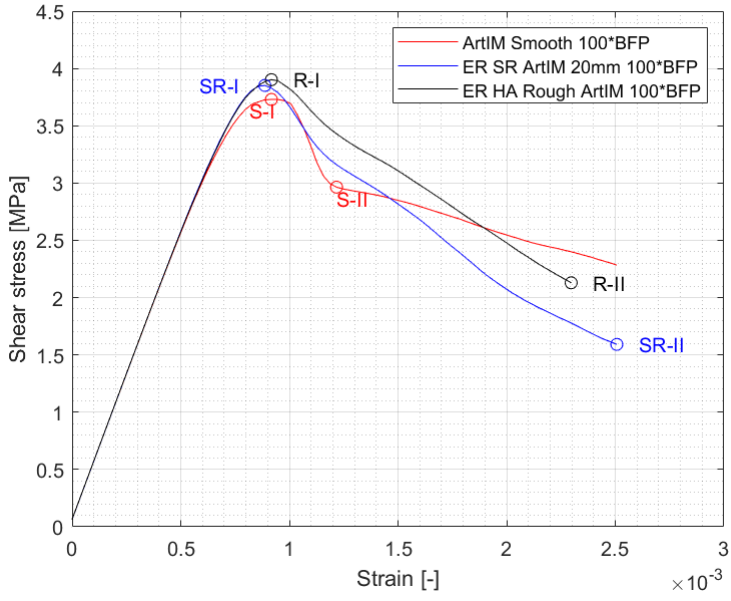

Figure 4.34: Shear stress - strain curve for different roughness conditions in presence of external pre-compressive stresses

Figure 4.34, shows comparison between shear stress vs. strain behavior for different roughness classes in presence of external pre-compressive stresses. The comparison is performed with same uniform pre-

compressive stress (3.67 MPa) acting on top edge of the steel plate. The strength achieved in all the models is comparable to each other. Strength varies by a very small magnitude. Nevertheless, rough interface produces highest strength among these roughness classes (Strength order: Rough > Slightly rough > Smooth). However, the post peak behavior varies significantly. Among the two models with explicit roughness at the interface, *slightly rough* and *rough* interfaces show similar material softening in the post-peak branch. Whereas, in case of smooth (straight) interface, post-peak response shows a certain deviation in the intermediate load step which will be discussed in detail with the crack distribution response.

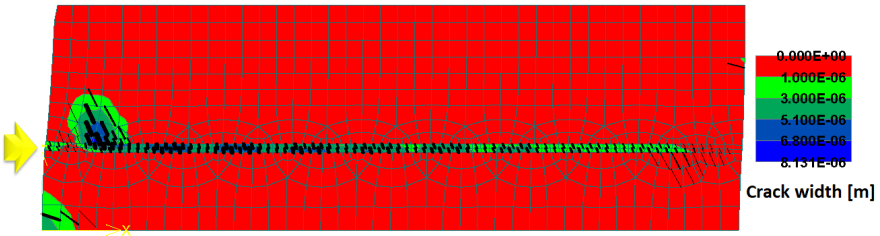

(a) Crack distribution at peak load step for smooth interface with pre-compression (S-I)

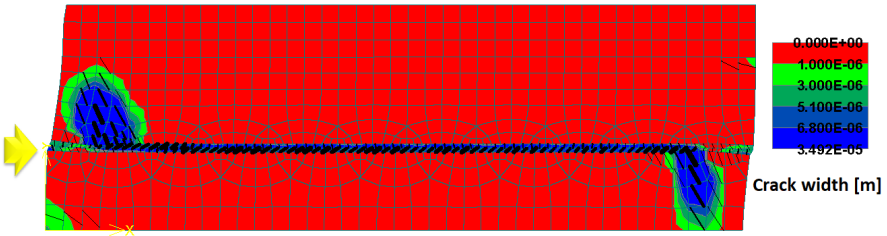

(b) Crack distribution at intermediate load step for smooth interface with pre-compression (S-II)

Figure 4.35: Crack distribution when smoother interface (straight element) is modelled with external compressive stresses (Displacement Multiplier = 100)

Figure 4.35, shows crack distribution in the model with smooth interface characteristics in presence of external compressive stresses perpendicular to the interface element. At peak load step (Figure 4.35a), cracks at the interface are localized similar to the case when no pre-compression is present. Moreover, a diagonal crack develops near the left edge of the model. On further increment of load, another major crack starts developing near the right edge of the model. When this crack reaches fully developed stage, the deviation in the softening branch is observed (S-II in Figure 4.34). After this load step, a constant softening of the material occurs until the end of analysis. This pattern is more or less similar to the case without external pre-compressive stresses.

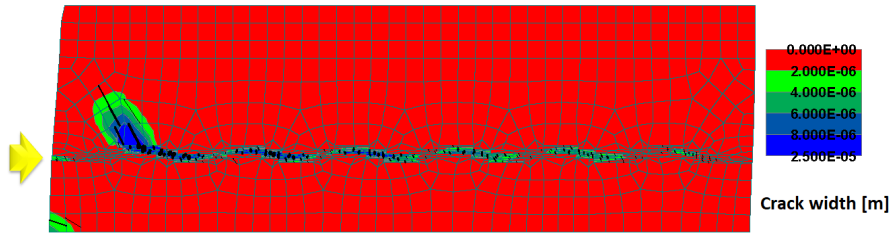

(a) Crack distribution at peak load step for slightly rough interface with pre-compression (SR-I) (Displacement Multiplier = 50)

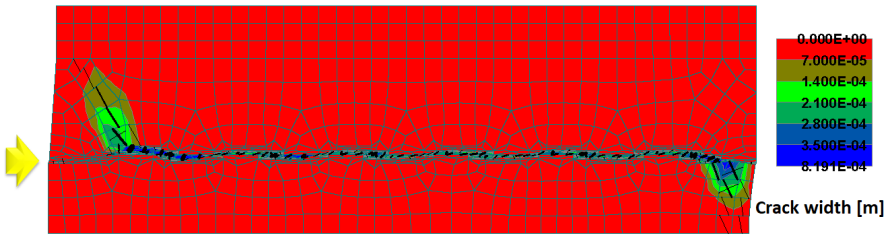

(b) Crack distribution at final load step for slightly rough interface with pre-compression (SR-II) (Displacement Multiplier = 50)

Figure 4.36: Crack distribution when slightly rough interface (straight element) is modelled with external compressive stresses

Figure 4.36, shows crack distribution when slightly rough interface is used with explicit roughness modification at the interface. At peak load (Figure 4.36a), crack distribution is similar to the smooth interface with localization at the interface level and a major diagonal crack propagating towards the point of application of load. However, at the final load step (Figure 4.36b), it can be observed that the second diagonal crack localization occurs almost near the right edge of the concrete specimen. This happens because the external compressive stresses induce crushing of the substrate concrete near the right edge. This effect can be attributed to an increase in friction between the two concrete layers, if interface is modelled using ATENA IMM. Moreover, there is no subsequent difference observed in the softening branch of the curve.

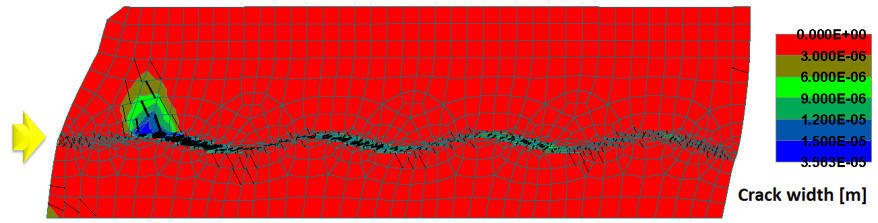

(a) Crack distribution at peak load step for rough interface with pre-compression (R-I) (Displacement Multiplier = 500)

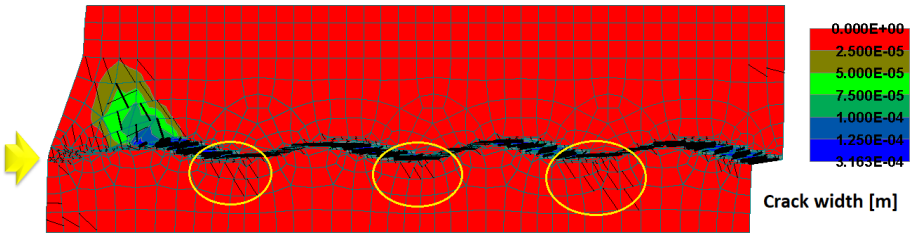

(b) Crack distribution at intermediate load step for rough interface with pre-compression (R-II) (Displacement Multiplier = 50)

Figure 4.37: Crack distribution when rough interface (straight element) is modelled with external compressive stresses

Figure 4.37, shows crack distribution when rough interface characteristics are assigned to the interface layer.

At peak load step (Figure 4.37a), the interface layer has already cracked and a diagonal major crack localizes near the left edge of the model. At this stage, the cracks in the interface layer are in fully developed state and the interface begins to slide in the direction of application of load. Furthermore, with the increment of lateral loading, due to crushing of concrete near the contact area between the overlay and substrate concrete layers (specially near the valleys of the roughness profile), minor cracks are developed in the substrate concrete element (areas marked with yellow circles in Figure 4.37b). Again, this effect is analogous to the friction acting between the two concrete layers.

Furthermore, an additional study is performed to understand the influence of different boundary conditions on the small scale bond model. Detailed analysis is presented in Appendix A. Important conclusion of this additional study is that, with the reduction in lever arm (distance between point of lateral load application and interface level), initial stiffness of the composite concrete model also reduces. However, the post-peak response (softening behavior) is similar to the boundary conditions used in this section.

4.4. Discussion

In this chapter, verification of the two interface models was performed. The ATENA interface material model is able to simulate the direct tension test and shear load test on a small scale bond model. It can be concluded from the stress strain curves that, the boundary conditions assigned and parametric values provided to the model, reliably estimate the tensile and shear strength of the composite concrete specimen. The roughness parameters, such as the tensile strength and cohesion are verified for their respective parametric values for the different roughness classes defined in the chapter. Coefficient of friction is verified in the presence of external pre-compressive stress. Interface failure is observed in case of smooth and slightly rough interfaces and thus, the Mohr-Coulomb failure criteria is satisfied in these cases. Whereas, for a rough interface, material failure of the composite concrete model is observed since, the external compressive stress induces higher friction resistance at the interface resulting in a subsequent increase in the shear capacity.

As an alternative to the ATENA interface material model (IMM), an artificial interface model (ArtIM) is developed in which a third material element is designed between the two adjacent concrete elements acting as an artificial interface layer. Explicit roughness is incorporated by designing the interface in a wave pattern with different combinations of wavelengths and amplitudes. The different configurations chosen for this purpose are verified by the roughness criteria defined in Model Code 2010. This artificial interface is assigned lower strength concrete material properties in order to ensure localisation of cracks at the interface. The tensile strength obtained from the direct tension test is the same as in the case of ATENA IMM, since the material properties assigned to the interface element are in accordance with the parametric value range chosen for the ATENA IMM. As the amplitude of the wavy artificial interface increases, stress concentration at the peaks and valleys also increases. This results in strain hardening of the concrete near these higher amplitude regions. Thus, a more ductile behavior is exhibited by the model undergoing direct tension test.

Material properties are kept constant for the artificial interface layer in the shear load test. By using the artificial interface model (ArtIM), shear capacity obtained for the composite concrete specimen is significantly higher than in case of ATENA IMM. This is valid, if tensile strength of the interface is kept constant for both the interface modelling techniques. This increase in shear capacity can be attributed to the thickness and compressive strength of the interface elements in ArtIM.

Verification of the friction parameter is carried out using the ArtIM. For this, an external pre-compressive stress is applied before loading the model laterally. The external stress, increases the friction resistance, ultimately increasing the shear capacity. Since, a distinct friction coefficient parameter cannot be assigned to the artificial model, this effect is generated by incorporating an explicit roughness to the interface. An artificial interface element (shape similar to saw-tooth model) is tested for the effect of friction in this model. Using the guidelines of Model Code 2010 and roughness parameter *'R'* the respective wavelengths and amplitudes are chosen for the given classification of surface roughness (i.e., smooth, slightly rough and rough interface). At first a straight line model, depicting a smooth interface, is loaded with pre-compression and lateral loading. Due to the absence of explicit roughness effect of friction is not observed which is evident from the value of slope obtained for smooth surface in case of straight element geometry. However, as a modification, an explicit roughness with a certain wavelength and lower amplitude is incorporated in place of the straight interface element. This interface profile provides satisfactory slope of the curve (curve

is plotted using the maximum normal and shear stress values at the interface elements) that corresponds to the ATENA IMM and Model Code friction coefficient values. Moreover, slope obtained using the slightly rough and rough interface profiles agrees with the ATENA IMM and Model Code guidelines for respective roughness classes. An increasing trend is observed in all the friction coefficient values obtained by ATENA IMM and ArtIM similar to the Model Code guidelines, with increasing roughness.

Two additional studies are performed in this chapter. First study focuses on the influence of different boundary conditions on the small scale bond model by using the artificial interface model. Lateral loading is applied at the middle of the top concrete layer by simultaneously providing a lateral support to the bottom concrete on the opposite edge. With a reduced lever arm between the point of application of load and the interface level, decrease in the initial stiffness is observed followed by a similar post peak softening behavior like with the use of previously mentioned boundary conditions. Second study focuses on the influence of different values of wavelength of the artificial interface element. Interface block-elements with different lengths are used to achieve the variation in wavelength. From this test, it can be concluded that, as the wavelength of the artificial interface reduces, a more brittle behavior is expected from the composite model. Nevertheless, difference in the shear strength is not very significant.

In this chapter, even though the two interface models are verified successfully, it is necessary to validate these numerical models. This validation will be performed in the next two chapters using two different experimental test setups. First validation is performed by using the experimental findings obtained by T. Paulay, R. Park and M. H. Phillips [1]. This involves numerical modelling on a bond model with slightly larger dimensions than the small scale model used for the verification. A numerical analysis using both the aforementioned interface models is performed on this composite concrete specimen. Second validation is performed on a structural level. A case study regarding the Eindhoven car park garage failure is studied by simulating tests related to this research with the help of reports provided by TNO [2] and Adviesbureau ir. J. G. Hageman B.V [3]. An attempt is made to produce a numerical model depicting the same interface failure using both the interface models.

5

Validation of numerical models

Two interface models, ATENA interface material model (IMM) and artificial interface model (ArtIM), are verified in the previous chapter using numerical analysis. However, the correctness of these numerical models can only be justified, if the results obtained are in accordance with experimental results. To achieve this validation, experimental results obtained from the work carried out by T. Paulay, R. Park and M. H. Phillips is used. These researchers performed experiments on a similar kind of bond model by varying interface properties between two concrete layers. However, the substrate and overlay concrete blocks in their experiments have slightly higher dimensions than those considered in the previous chapter. They also used reinforcement crossing the interface to study the influence of shear connectors at the interface and their effect on shear capacity. To study the interface parameters in detail, first a basic validation of the numerical results obtained in Chapter 4 is performed.

5.1. Numerical model detailing and experimental set-up

The geometry of the model and reinforcement detailing used in the experiments are shown in Figure 5.1. Interface is denoted by dotted lines.

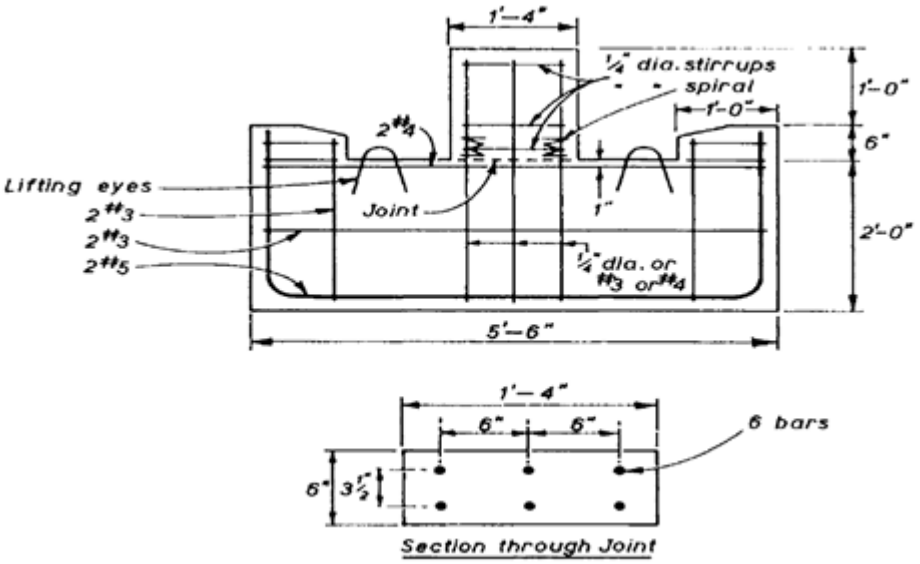

Figure 5.1: Mechanical model used for the experiment [1]

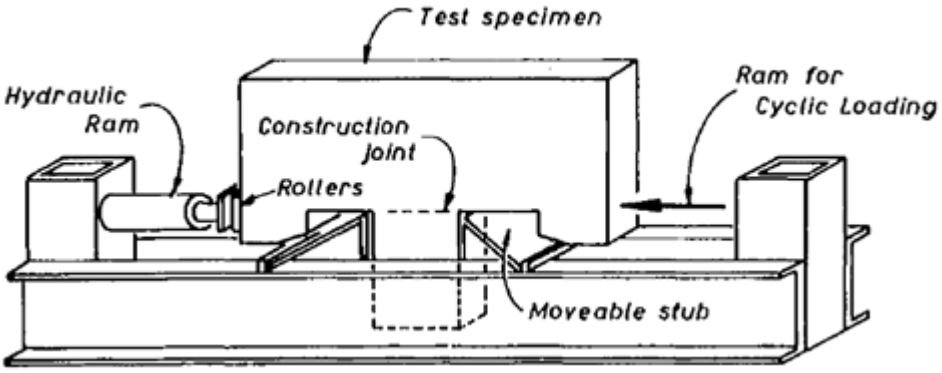

Figure 5.2: Test setup

Figure 5.2, shows the test setup used to perform the experiments. The specimen is placed upside down such that, the wider section is free to move in the horizontal direction whereas, the narrower section is fixed between the two movable stubs placed on 2 steel C-sections.

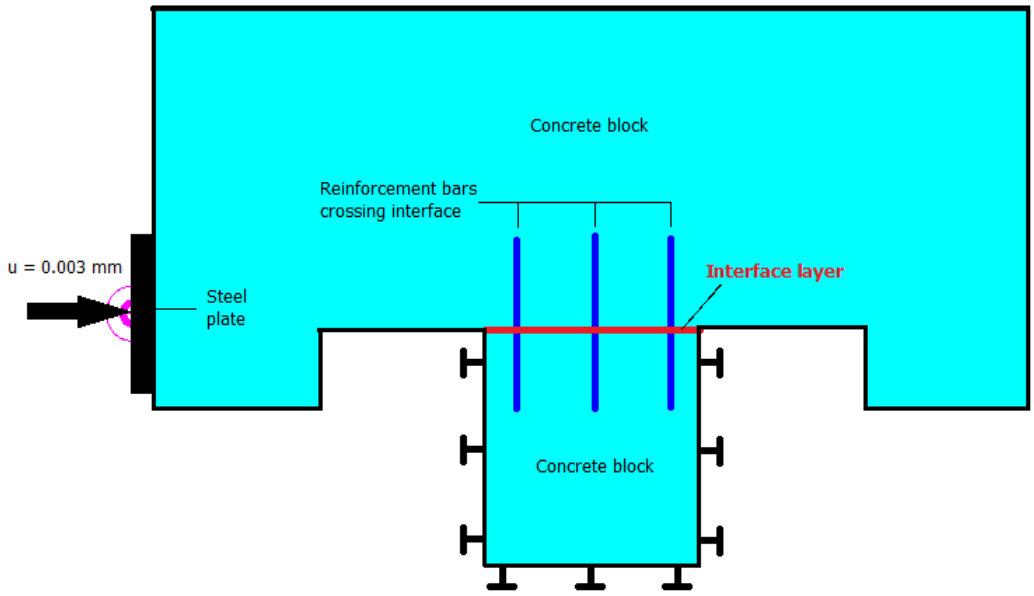

Figure 5.3: Mechanical model used for simulation and numerical analysis

Figure 5.3 shows the mechanical model of the test setup created for the analysis. To replicate the constraints from the experimental setup into the numerical model, the narrower section of the specimen is supported from all three sides such that the wider/top section (Figure 5.3) is free to move in the horizontal/x-direction.

To simulate this model using ATENA, a numerical model as shown in Figure 5.4 is proposed. The reinforcement detailing in the numerical model is kept as accurate as possible. However, main attention is given to the reinforcement bars crossing the interface. A small test is simulated to decide the length of reinforcement bars crossing the interface. Detailed analysis of this test is presented in appendix B. The analysis of this test concludes, that with an anchorage length of 100 mm ($\approx 5\phi$), results obtained are similar to those with full length (equal to height of experimental model) of the RF bars. Main reason for this is the bond between the steel and concrete. Since, perfect bond is assumed in this validation there is no difference in the results obtained. Hence, in the numerical model, the RF bars crossing the interface have a total length equal to 200 mm (100 mm on both sides of the interface). The yellow line in the numerical model is the interface in consideration.

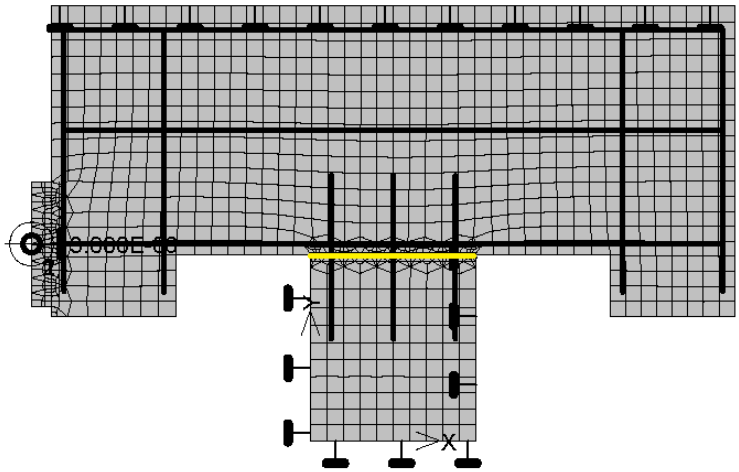

Figure 5.4: Numerical model used for analysis showing mesh refinement

The aim of this validation study is to check the accuracy of interface material model (IMM) and artificial interface model (ArtIM) by comparing the results with an experimental study. Hence, the tests simulated hereafter, correspond to the tests performed by T. Paulay, R. Park and M. H. Phillips [1]. Similar to the verification, validation of the model is also performed by using the previously described interface models; ATENA Interface Material Model (IMM) and Artificial Interface Model (ArtIM).

5.2. ATENA Interface Material Model (IMM)

The experimental results show a direct comparison between models with different surface roughness. In addition to the concrete-concrete interaction, reinforcement bars crossing the interface also influence the shear capacity of a composite concrete specimen. However, for the validation only the concrete-concrete interaction is necessary. For this reason the effect of reinforcement bars (or dowel action) needs to be subtracted from the final response. Hence, in the experimental results, the load - slip response shown for different surface roughness classes is obtained by subtracting the effect of dowel action from the combined response for each model. To obtain response of dowel action, first a '*no bond*' interface condition is incorporated in the model.

5.2.1. No Bond condition

The first test simulated corresponds to '*no bond*' condition at the interface with RF bars crossing through the interface. The reinforcement ratio is kept identical to that used in the experiments ($\rho = 0.69\%$). 1-D discrete reinforcement (RF) bar elements are used to model the RF bars crossing the interface. Interface material properties and RF properties used for this analysis are given in Figures 5.5 - 5.6. To replicate a *no bond* condition, strength of the interface needs to be very low and hence, these specific properties are chosen.

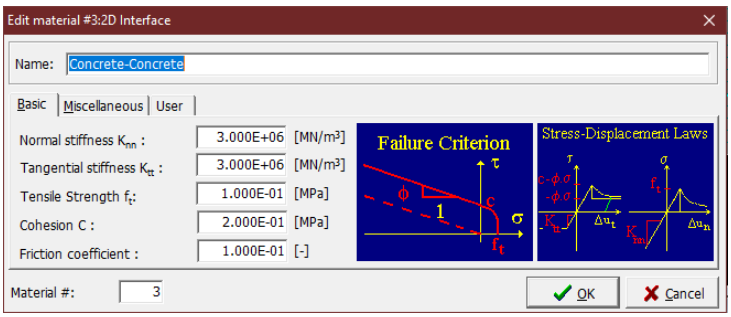

Figure 5.5: Interface properties used for the analysis (No Bond condition)

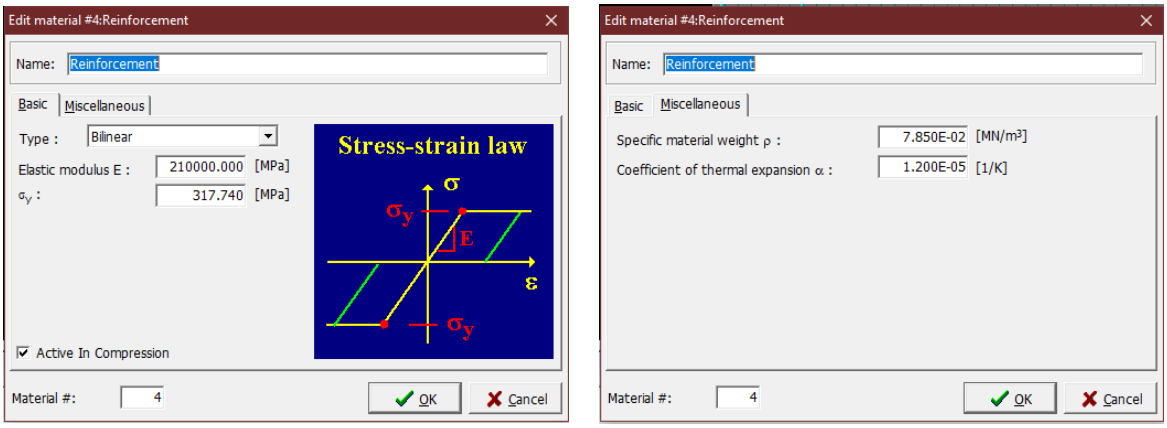

(a) Basic properties (b) Miscellaneous properties

Figure 5.6: Reinforcement detailing used for the analysis (No Bond condition)

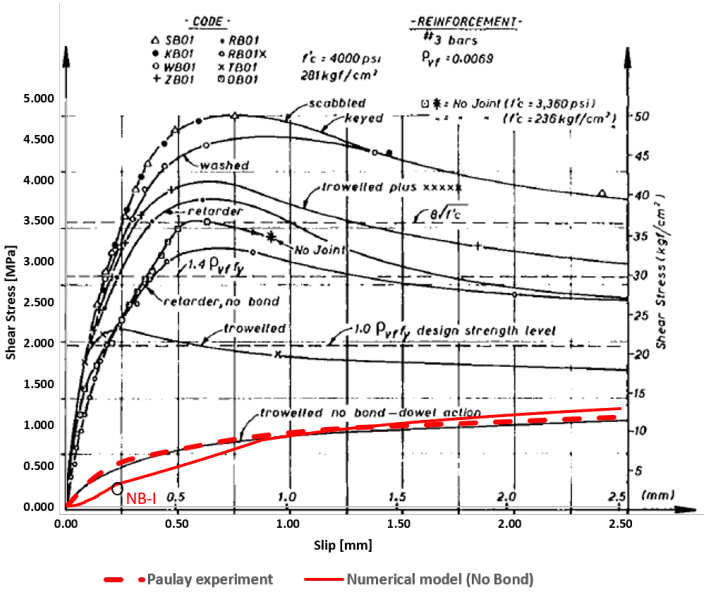

Figure 5.7: Shear stress - slip comparison between numerical model and experimental results [1] (No Bond condition)

The nature of graph shown in Figure 5.7, for the numerical model (solid red curve) resembles the trend of the experimental results (dotted red curve). However, in the initial part of the curve, stiffness of the numerical model is slightly lower than the experimental model. This reduced stiffness value only considers the axial stiffness of the reinforcement bars and not the bending and shear stiffness values. This problem will be discussed in this chapter in the last section. At a slip of about 1.5 mm, the numerical model has shear strength almost equivalent to the experimental model. Furthermore, the results obtained from the numerical analysis, at higher slip values, agree with the experimental findings.

Figure 5.8, shows the crack distribution at the interface as well as the axial stress distribution in the reinforcement bar elements for a *no bond* condition. Cracks develop near the reinforcement bars, since there is not much interaction between the adjacent concrete elements (because of the *no bond* condition). The maximum crack width is observed at the interface level near the RF bars placed at the middle. Cracks near the edges of the substrate concrete layer are very small in magnitude and only develop near the concrete-RF bond. Moreover, the RF bar in the middle yields first than the remaining two bars near the re-entrant corners.

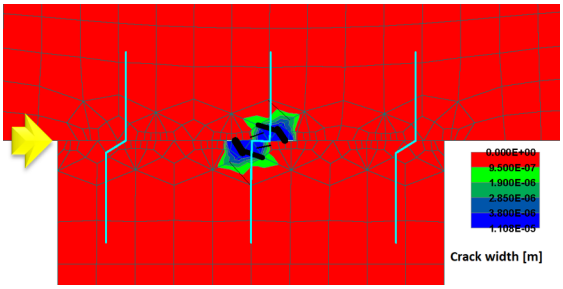

(a) Crack distribution near interface [m]

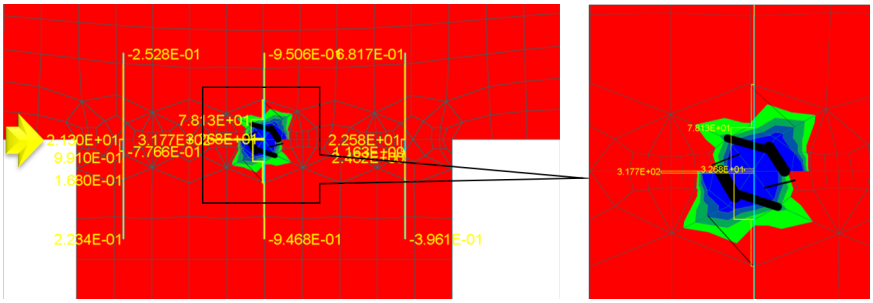

(b) Reinforcement stress distribution (σ_{xx}) [MPa]

Figure 5.8: Crack and RF axial stress distribution near the interface (No Bond condition) (NB-I)

In the next sections, interface properties are varied by changing the parameters using both the interface models; ATENA Interface Material Model (IMM) and Artificial Interface Model (ArtIM). The effect of concrete-concrete interface is studied by subtracting the results of '*no bond*' conditions from the respective load - slip responses of the different interface conditions, since the no bond condition yields only the response of reinforcement bars (dowel action).

5.2.2. Rough Interface condition

In this section, the influence of rough interface characteristics are validated with the experimental results. Different surface preparation techniques are used in the experiment to create variation of roughness. Similarly, different parameters are varied in the ATENA IMM, to have a good resemblance with the experimental techniques.

First, the same roughness characteristics are assigned to the interface as prescribed by the Model Code 2010 similar to the previous chapter. Eventually, different combinations of tensile strength, cohesion and friction coefficient are also tested. Material properties are given in Table 5.1. Each roughness parameter class is analyzed one by one. Discussion is made on every model once all the results are presented.

Table 5.1: Interface material parameters used to represent different surface roughness classes

Interface properties	**Unit**	**Parameter 1**	**Parameter 2**	**Parameter 3**	**Parameter 4**
Tensile strength (f_t)	MPa	1.50	1.50	2.00	3.00
Cohesion (c)	MPa	3.00	3.00	4.00	6.00
Coefficient of friction (μ)	-	1.30	2.60	2.60	2.60

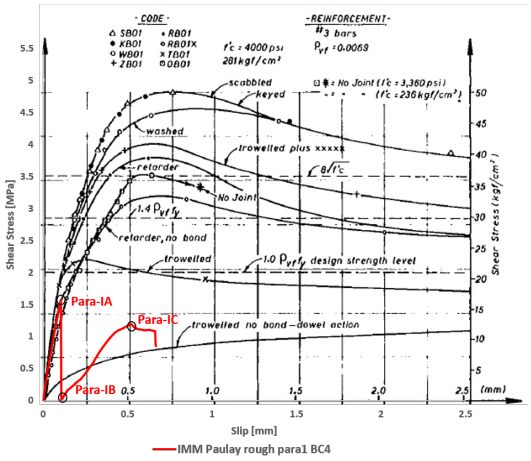

(a) Interface parameter 1

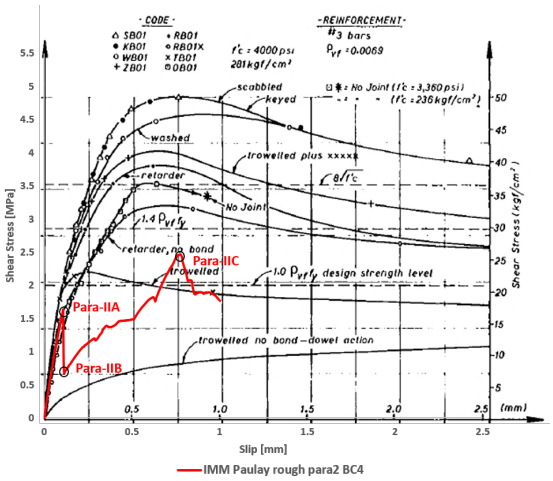

(b) Interface parameter 2

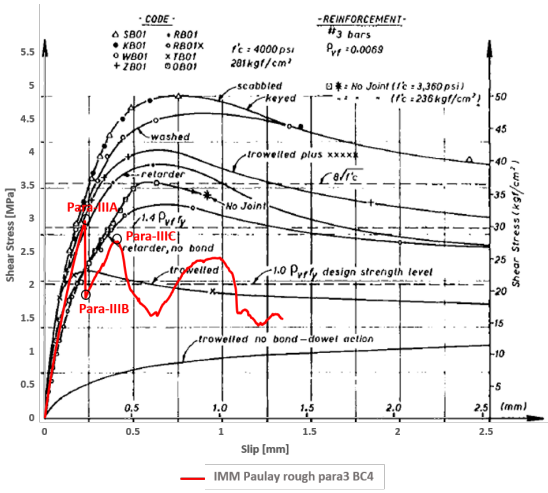

(c) Interface parameter 3

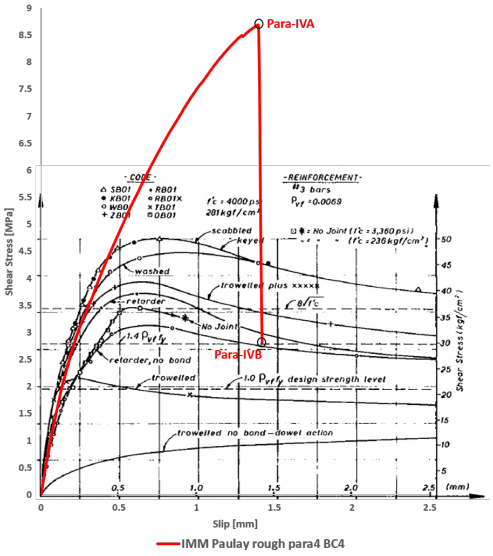

(d) Interface parameter 4

Figure 5.9: Shear stress - slip comparison between experimental and numerical results for rough interface condition usin IMM

PARAMETER 1

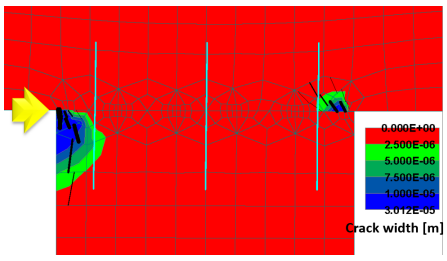

(a) Crack distribution near interface [m]

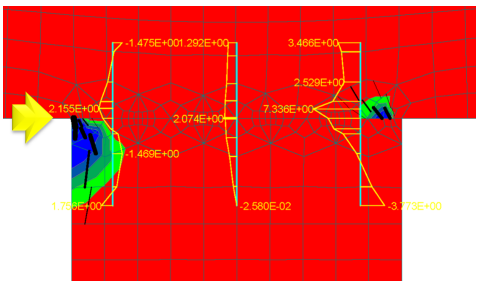

(b) Reinforcement stress distribution (σ_{xx}) [MPa]

Figure 5.10: Crack and RF axial stress distribution at first peak load step (rough parameter-1) (ParaBC4-IA)

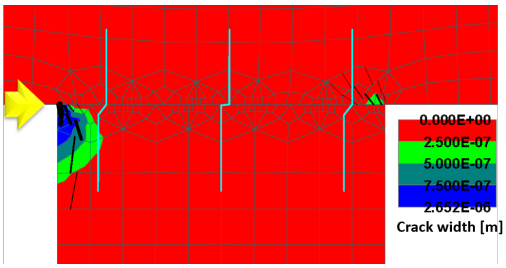

(a) Crack distribution near interface [m]

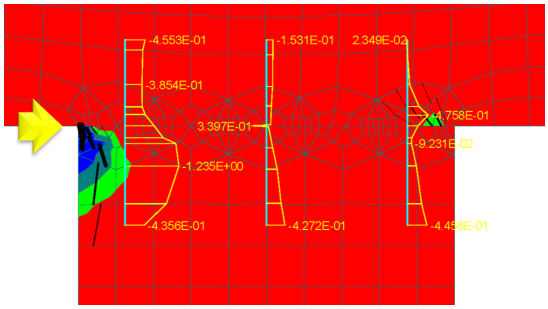

(b) Reinforcement stress distribution (σ_{xx}) [MPa]

Figure 5.11: Crack and RF axial stress distribution at next load step after peak (rough parameter-1) (ParaBC4-IB)

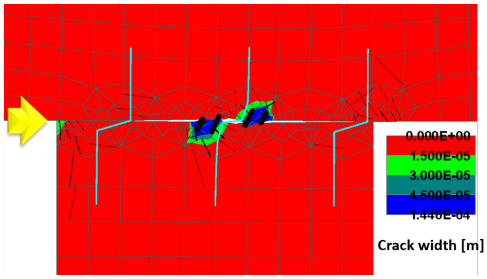

(a) Crack distribution near interface [m]

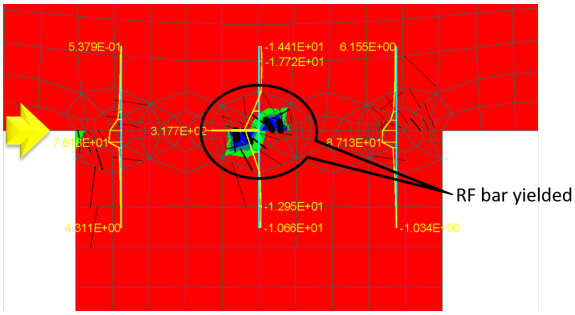

(b) Reinforcement stress distribution (σ_{xx}) [MPa]

Figure 5.12: Crack and RF axial stress distribution at second peak load step (rough parameter-1) (ParaBC4-IC)

Figure 5.9, shows the comparison between numerical and experimental results pertaining to different roughness conditions. Figures 5.10 - 5.12 show evolution of the crack distribution in case of parameter 1 roughness condition. These parameters are chosen as per the Model Code guidelines and the response of the bond model is observed. Minor cracks initiate near the re-entrant corners of the specimen due to high stress concentration. However, with further load increment the interface fails and stress in concrete drops to zero. Hereafter the load is carried by the reinforcement (RF) bars. Hence, crack width near the middle RF bar increases and the bars undergo bending. RF bars in the middle attain their yield strength before the bars near the edges. Due to the combined stiffness of concrete and RF bars, stresses develop in the adjacent concrete elements and the rise in stress values is observed from the graph in Figure 5.9a.

PARAMETER 2

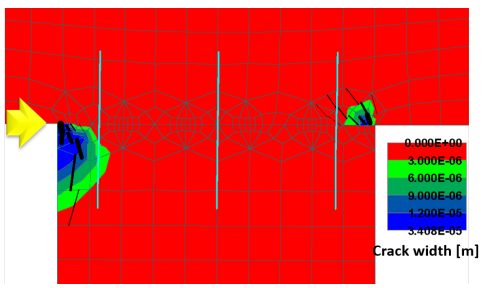

(a) Crack distribution near interface [m]

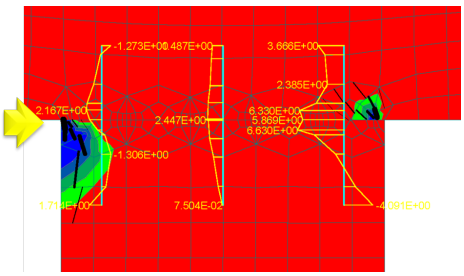

(b) Reinforcement stress distribution (σ_{xx}) [MPa]

Figure 5.13: Crack and RF axial stress distribution at first peak load step (rough parameter-2) (ParaBC4-IIA)

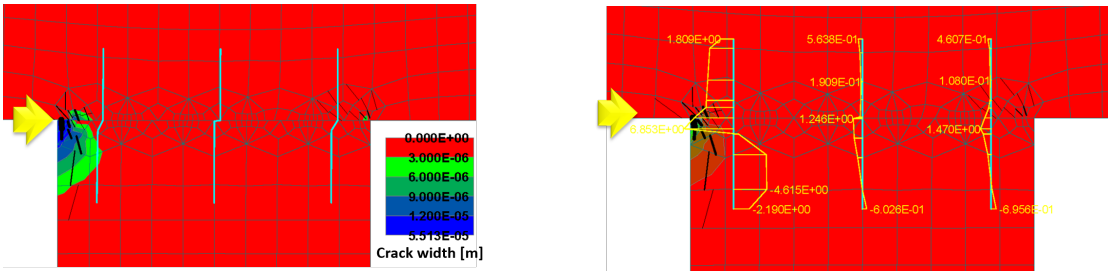

(a) Crack distribution near interface [m] (b) Reinforcement stress distribution (σ_{xx}) [MPa]

Figure 5.14: Crack and RF axial stress distribution at next load step after peak (rough parameter-2) (ParaBC4-IIB)

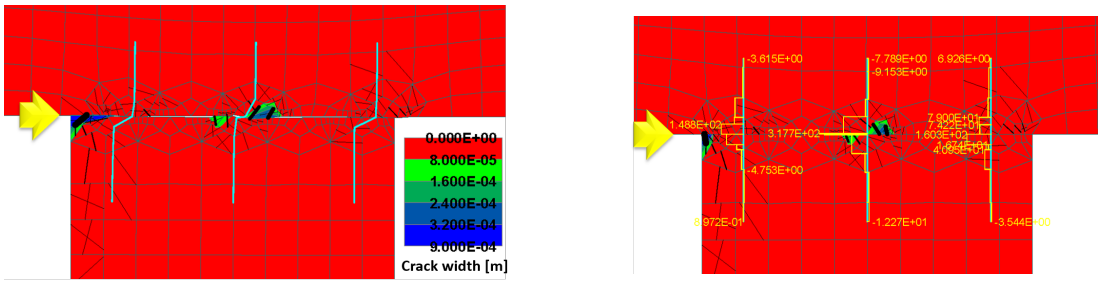

(a) Crack distribution near interface [m] (b) Reinforcement stress distribution (σ_{xx}) [MPa]

Figure 5.15: Crack and RF axial stress distribution at second peak load step (rough parameter-2) (ParaBC4-IIC)

Figures 5.13 - 5.15 show evolution of the crack distribution in case of parameter 2 roughness condition. In this case, the coefficient of friction obtained in the experiment is double the value considered in the previous case. Due to the increment in friction coefficient, shear stress does not drop to zero after the interface failure but drops to a value corresponding to dry friction at the interface ($\sigma\mu$, where σ is the self-weight of the top concrete element). Eventually the stresses again increase with further load increment (Figure 5.9b) similar to the previous case. A more ductile behavior is observed, in the post-peak response of the model.

PARAMETER 3

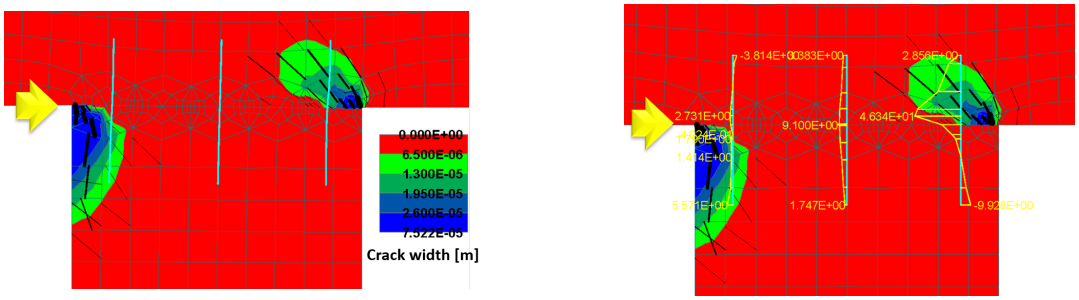

(a) Crack distribution near interface [m] (b) Reinforcement stress distribution (σ_{xx}) [MPa]

Figure 5.16: Crack and RF axial stress distribution at first peak load step (rough parameter-3) (ParaBC4-IIIA)

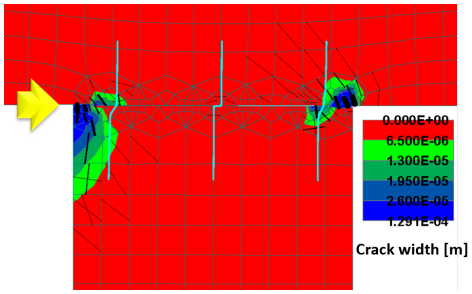

(a) Crack distribution near interface [m]

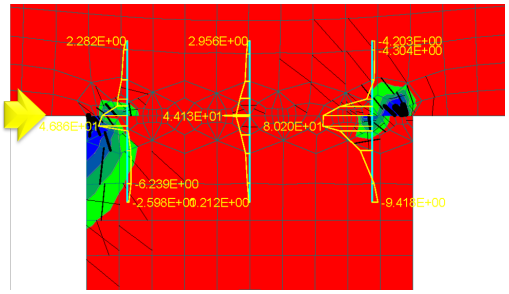

(b) Reinforcement stress distribution (σ_{xx}) [MPa]

Figure 5.17: Crack and RF axial stress distribution at next load step after peak (rough parameter-3) (ParaBC4-IIIB)

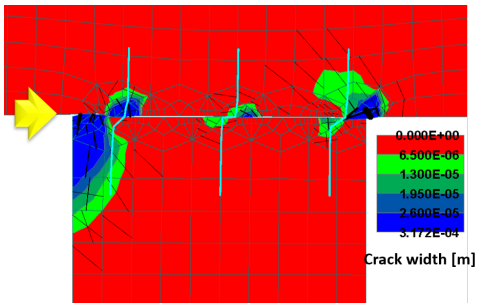

(a) Crack distribution near interface [m]

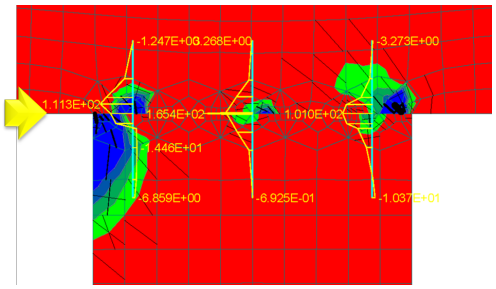

(b) Reinforcement stress distribution (σ_{xx}) [MPa]

Figure 5.18: Crack and RF axial stress distribution at second peak load step (rough parameter-3) (ParaBC4-IIIC)

Figures 5.16 - 5.18 show evolution of the crack distribution in case of parameter 3 roughness condition. In this case, the tensile strength and cohesion at the interface are increased to understand the influence of these parameters on the shear strength of the interface. However, the tensile strength of the interface is close to that of the adjacent concrete elements. Due to this the interface strength increases in relation to the adjoining concrete elements and diagonal cracks start developing in the top and bottom concrete elements. With further load increment, the interface fails and the stress in the concrete drops. A subsequent rise in the stress value is observed in the post-peak response of the curve in Figure 5.9c.

PARAMETER 4

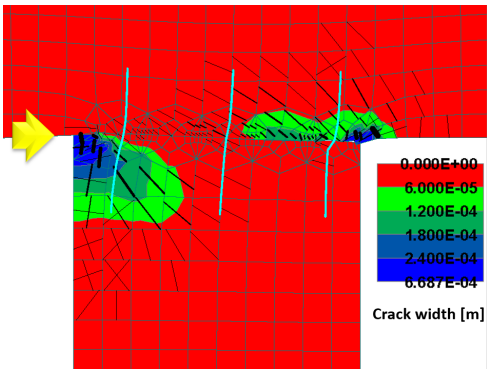

(a) Crack distribution near interface [m]

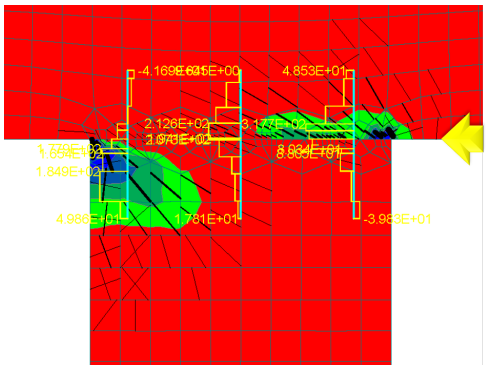

(b) Reinforcement stress distribution (σ_{xx}) [MPa]

Figure 5.19: Crack and RF axial stress distribution at peak load step (rough parameter-4) (ParaBC4-IVA)

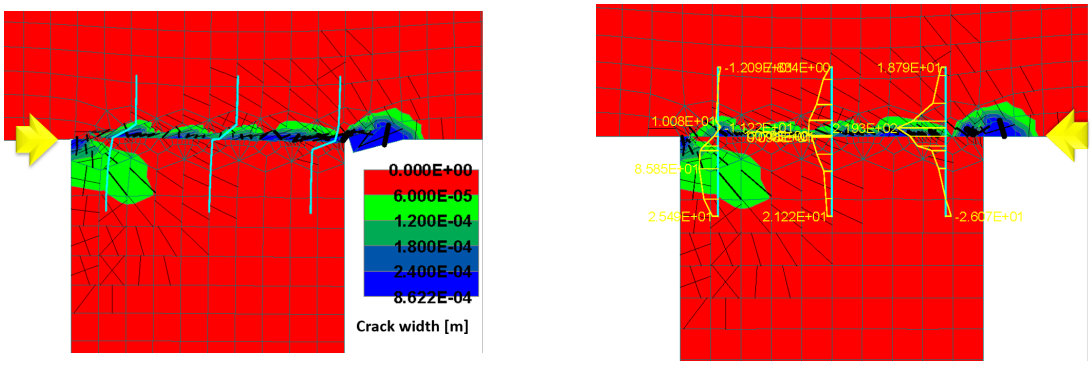

(a) Crack distribution near interface [m]

(b) Reinforcement stress distribution (σ_{xx}) [MPa]

Figure 5.20: Crack and RF axial stress distribution at last load step exhibiting significant stress drop (rough parameter-4) (ParaBC4-IVB)

Figures 5.19 - 5.20 show evolution of the crack distribution in case of parameter 4 roughness condition. In this case the tensile strength of the interface is higher than the adjacent concrete elements. This means that, the concrete material will fail even before the interface reaches its strength. This case corresponds to a perfect bond situation between the two concrete elements. Interface is very strong and hence, cracks develop in the concrete elements in a diagonal fashion. From Figure 5.9d, it can be observed that the shear capacity of the model is very high as compared to the previous cases and also than the experimental results. Eventually, brittle failure of the concrete material occurs and a sudden drop in the stress value is observed. Stress in the RF bars is induced due to the displacement of the top concrete layer after disintegrating near the interface level.

Discussion

A discussion about the results presented earlier is done in this section. Only rough interface is used in the numerical models for the validation because, results available from the experiment only correspond to rough surface condition. A *no bond* condition is tested in the beginning in order to identify the contribution of dowel action in the shear transfer between the two concrete elements. Once the dowel action contribution is obtained then, it can be subtracted from the shear capacity of remaining roughness models to obtain only the concrete-concrete interaction.

Unlike in the small scale bond model from Chapter 4, there are two re-entrant corners present at the two ends of the interface in the model. Due to this singularity, cracks initiate near these nodes on account of high stress concentration, in the beginning of the analysis. However, these cracks have very low crack widths and hence do not cause any significant stress re-distribution. The interface is still activated due to the lateral loading and stress at this layer keeps on increasing until it reaches its shear strength (first peak). As soon as the peak stress is attained, the interface fails and the reinforcement bars crossing the interface have a sudden stress increment.

With a subsequent rise in cohesion at the interface, an increase in the shear capacity is observed. After attaining the first peak strength, failure at interface occurs with a sudden drop in stress. This brittle behavior is expected from the model on account of the default softening evolution law present in ATENA. Since, any specific softening law is not defined in the model, the curve follows the same trend as described in the verification of small scale bond model. Furthermore, as the lateral load increases, the stress starts increasing because of the combined stiffness of the concrete and reinforcement bars crossing the interface. Thus, a second peak strength is achieved on account of the concrete strength of the adjacent macro-elements.

In the last parameter 4 case, the tensile strength is higher than the adjacent concrete elements. This means the concrete elements will fail even before the interface attains its maximum strength. Due to this strong interface condition, diagonal cracks from the re-entrant corners propagate further into the concrete elements. This results in a very high shear strength of the composite model which is evident from the stress-strain diagram (Figure 5.9d).

The cracking pattern observed in all these above cases, especially at the re-entrant corners is compared to the models mentioned by Schlangen in his thesis work [25]. He studied various fracture processes in concrete using experimental and numerical analyses.

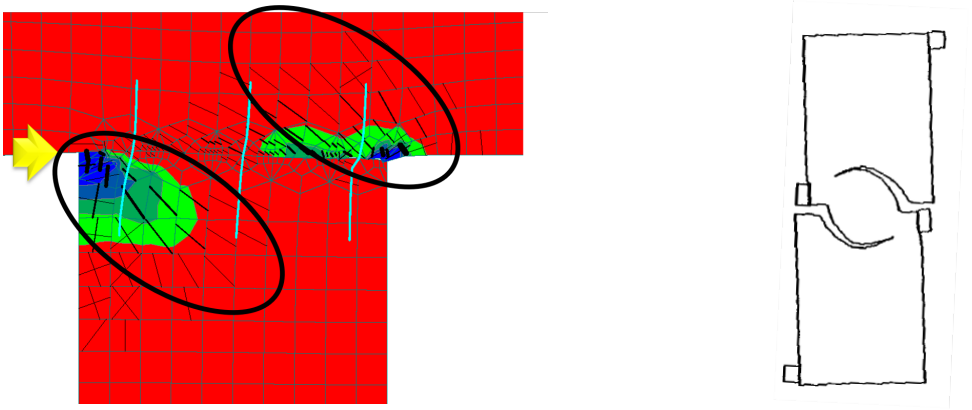

(a) Crack pattern in numerical model (parameter 4 condition)

(b) Crack pattern in double-edge-notched beam simulated by Swartz and Taha [25]

Figure 5.21: Crack pattern from numerical model and experimental observation by Swartz and Taha

While comparing his numerical results with different experimental findings, Schlangen came across a research that was performed by Swartz and Taha, in which they explain the influence of boundary conditions on the cracking pattern of a laterally loaded concrete specimen. A double-edge-notched beam was loaded in shear and the cracking pattern observed had most similarities with the experimental results obtained by Schlangen. Cracks initiated at both ends of the beam near the notches. On further loading, a curvature in the cracks was observed as shown in the Figure 5.21b. Similarly, in all the cases inspected in this chapter, cracks initiate near the re-entrant corners of the composite concrete model. Re-entrant corners have the same effect as notches in a beam and generate singularity as a result of which high stress concentration is observed in the initial stage of analysis. Furthermore, a curvature of these cracks can be observed in the figures above. For non-rigid bond cases as the bond strength at the interface reaches its ultimate capacity (for parameter 1, 2 and 3 conditions), the interface cracks and top concrete layer moves in the direction of lateral loading. However, in case of a very strong/rigid bond (parameter 4 condition) this cracking pattern is clearly visible in Figure 5.21a. In the next section, the artificial interface model (ArtIM) is used instead of ATENA IMM and same tests are carried out keeping the boundary conditions constant.

5.3. Artificial Interface Model (ArtIM)

Influence of explicit roughness on the shear capacity of a composite model is studied in the previous chapter. Although different configurations of the interface layer were considered in the parametric analyses, the material strength of the interface element was always kept constant. As evident from the research on a small scale rectangular bond model, difference in the shear capacities using various wavelengths and amplitudes (pertaining to the interface layer wave pattern) at the interface, was quite insignificant. Hence, in this section, influence of different material strength classes is studied for the similar explicit roughness as considered in the previous chapter. Results of the tests are compared with IMM models, from the preceding section and a direct comparison with the experimental results is also presented.

The variation of material properties used for the interface layer, corresponds to the tensile strength assigned to the interface in the preceding section. However, from verification of the artificial interface model in Chapter 4, it is evident that the ratio between shear strength and tensile strength is significantly higher than in case of ATENA IMM. This means that for a certain tensile strength a very high shear strength is achieved if ArtIM is used to model the interface. Taking this into consideration, the material properties chosen for the analysis are as given in Figure 5.1. Hereafter, the results are presented for the different material properties using the artificial interface model. The contribution of dowel action is considered same as in the ATENA interface material model.

5.3.1. High strength interface material condition (using explicit roughness)

In this section, variation in the interface material class is tested for its influence on the shear capacity. Material properties are varied corresponding to the tensile strength of the interface element, as modelled in previous sections using ATENA IMM. Basic material properties used here for the analyses are given in Figure 5.22.

Properties	CC 0.5		CC 1.5		CC 3.0	
Elastic modulus E :	2.210E+04	[MPa]	2.675E+04	[MPa]	3.325E+04	[MPa]
Poisson's ratio μ :	0.200	[-]	0.200	[-]	0.200	[-]
Tensile strength f_t :	5.000E-01	[MPa]	1.500E+00	[MPa]	3.000E+00	[MPa]
Compressive strength f_c :	-1.015E+01	[MPa]	-1.918E+01	[MPa]	-3.962E+01	[MPa]
Compressive strength cyl f_cu :	1.245E+01	[MPa]	2.352E+01	[MPa]	4.859E+01	[MPa]

Figure 5.22: Basic material properties used for the analysis (stronger interface material)

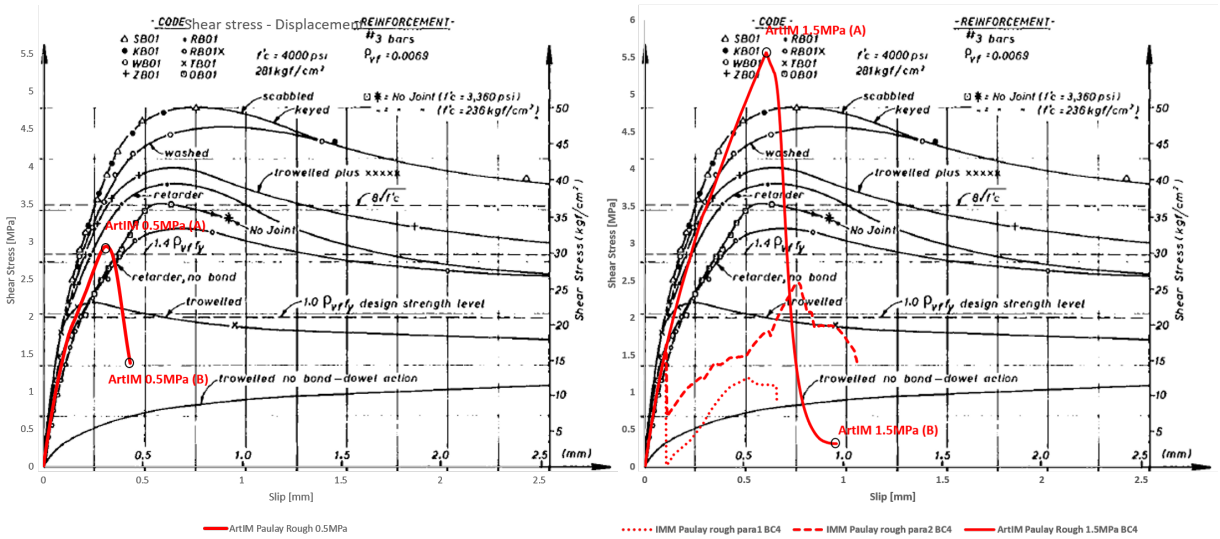

(a) CC 0.5

(b) CC 1.5

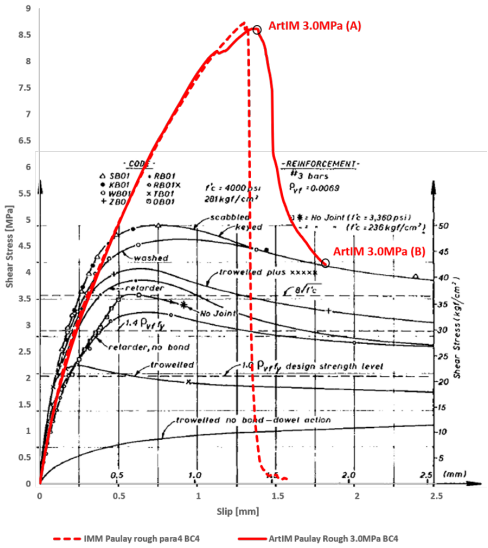

(c) CC 3.0

Figure 5.23: Shear stress - slip comparison between experimental and numerical results for rough interface condition using artificial interface model (ArtIM)

CC 0.5

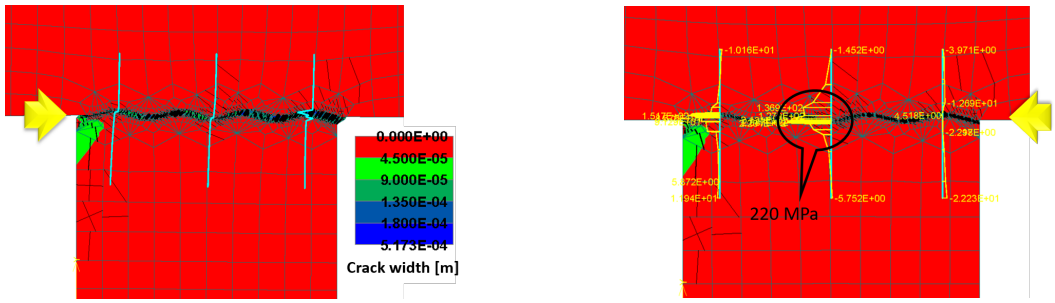

(a) Crack distribution near interface [m]

(b) Reinforcement stress distribution (σ_{xx}) [MPa]

Figure 5.24: Crack and RF axial stress distribution at peak load step (CC0.5) (ArtIM 0.5MPa (A))

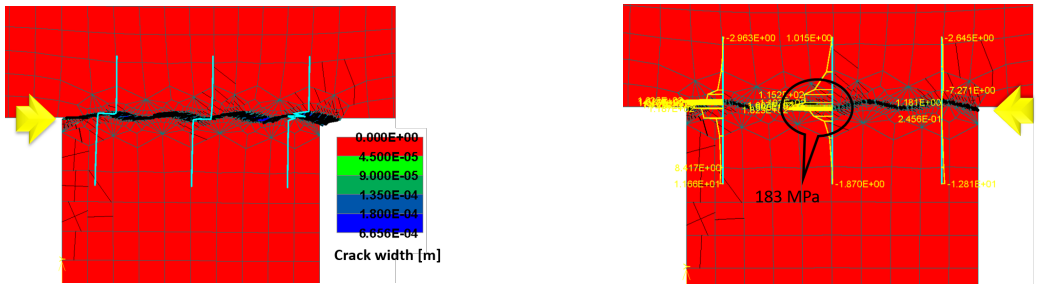

(a) Crack distribution near interface [m]

(b) Reinforcement stress distribution (σ_{xx}) [MPa]

Figure 5.25: Crack and RF axial stress distribution at final load step (CC0.5) (ArtIM 0.5MPa (B))

Figure 5.23, shows the shear stress - strain response in different roughness conditions and a direct comparison between the ATENA IMM results and experimental observations. As expected from the results obtained in verification of the bond model, shear strength of a low strength material is very high with respect to the tensile strength of the material. Unlike in case of ATENA IMM, a brittle response is observed while using ArtIM irrespective of the material strength. Figures 5.24 - 5.25 show the evolution of crack pattern at the interface layer. Although, localisation of cracks is observed at the interface, stress in concrete does not drop to zero magnitude after peak strength has been attained. Concrete at the interface layer undergoes softening and only a certain part of the stress is carried by the reinforcement (RF) bars. The RF bars are well within their yield limit and deform elastically.

CC 1.5

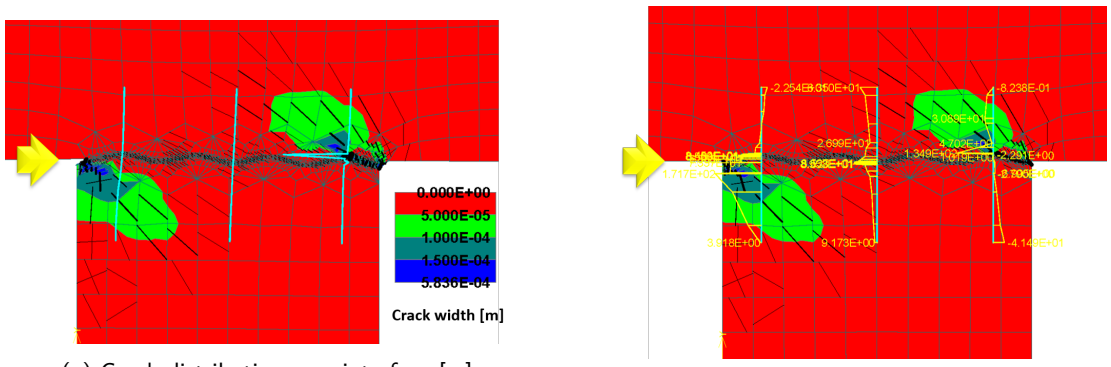

(a) Crack distribution near interface [m]

(b) Reinforcement stress distribution (σ_{xx}) [MPa]

Figure 5.26: Crack and RF axial stress distribution at next load step after peak (CC1.5) (ArtIM 1.5MPa (A))

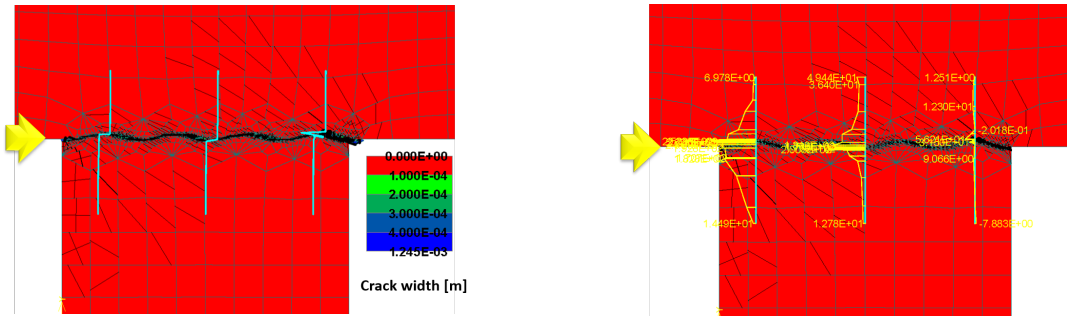

(a) Crack distribution near interface [m]

(b) Reinforcement stress distribution (σ_{xx}) [MPa]

Figure 5.27: Crack and RF axial stress distribution at second peak load step (CC1.5) (ArtIM 1.5MPa (B))

A direct comparison between the two interface models is clearly shown in Figure 5.23b. In this case, the tensile strength assigned is same for the interface in ATENA IMM and material property in ArtIM. There is a significant difference in the shear capacities obtained by both the interface models. This can be mainly attributed to the ratio between shear strength and tensile strength for the respective interface models. Since, shear capacity, in case of ArtIM, entirely depends on the material characteristics, this value is very high as compared to the case of ATENA IMM, where shear capacity mainly depends on the cohesion parameter of the interface model. Moreover, after attaining maximum stress, a brittle response is exhibited by the model unlike the ATENA IMM results. Localisation of cracks is observed in the initial stage of the analysis with subsequent diagonal cracking developing overtime into the adjacent concrete elements. Interface is relatively very strong in this case as compared to the lower strength material interface condition and hence, response of the model becomes analogous to a perfect bond condition.

CC 3.0

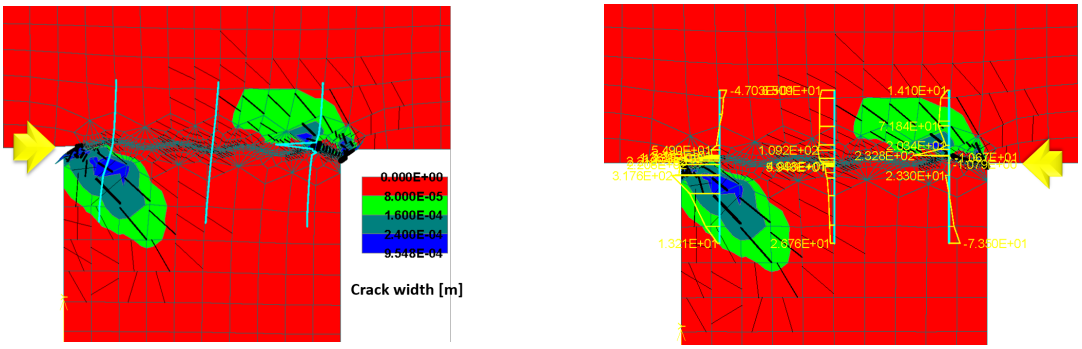

(a) Crack distribution near interface [m]

(b) Reinforcement stress distribution (σ_{xx}) [MPa]

Figure 5.28: Crack and RF axial stress distribution at next load step after peak (CC3.0) (ArtIM 3.0MPa (A))

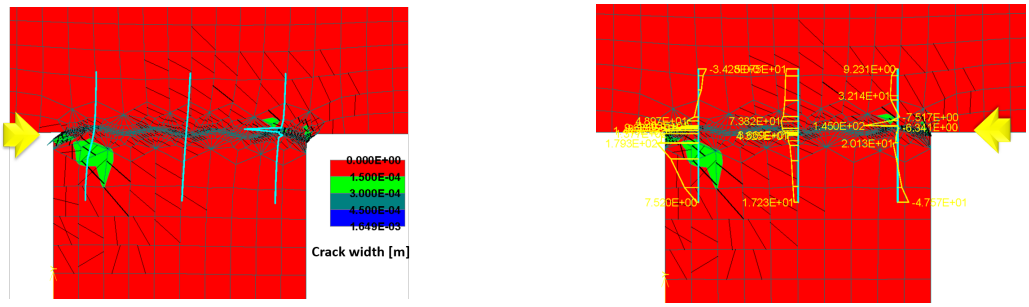

(a) Crack distribution near interface [m]

(b) Reinforcement stress distribution (σ_{xx}) [MPa]

Figure 5.29: Crack and RF axial stress distribution at second peak load step (CC3.0) (ArtIM 3.0MPa (B))

In case of a high strength material at the interface (CC 3.0, $f_t = 3.0MPa$), bond strength becomes very strong and the model exhibits a response similar to that of a perfectly bonded condition. The maximum shear strength obtained using both interface models is same in this case, since, in both the cases brittle material failure of the adjacent concrete elements is observed. Diagonal cracks are clearly visible in the adjacent concrete elements in Figures 5.28 - 5.29.

Discussion

A discussion about the ArtIM and its influence on the shear capacity of the composite concrete model is done hereafter. A similar observation regarding the crack pattern is noticed during the initial stages of the analyses, irrespective of the material strength of the interface element. The cracks always initiate at the re-entrant corners similar to the ATENA IMM condition as explained in the previous section. On increasing the load further, localization of cracks in the interface element is observed in the models with relatively weaker

(than the adjacent concrete macro-elements) interface element strength (*CC 0.5* and *CC 1.5*). However, the shear capacities obtained for these models are much higher than in case of ATENA IMM. The artificial interface layer exhibits a very high shear strength which is also evident from the verification of a small scale bond model. Required shear capacity can be achieved using this interface model but a brittle response of the composite model will be exhibited. Unlike in the previous cases, when stresses in the interface elements drop to zero and the RF bars bear the stresses in the post-cracking stage, in this case, on account of a stronger interface element, the RF bars never attain their respective yield strength.

After these analyses comparison of the cracking patterns should be made between the numerical and experimental results. Following figures show cracking pattern at the interface level as observed in the experiments. Detailed pictures for each roughness scenario are not available hence, only the two patterns are compared.

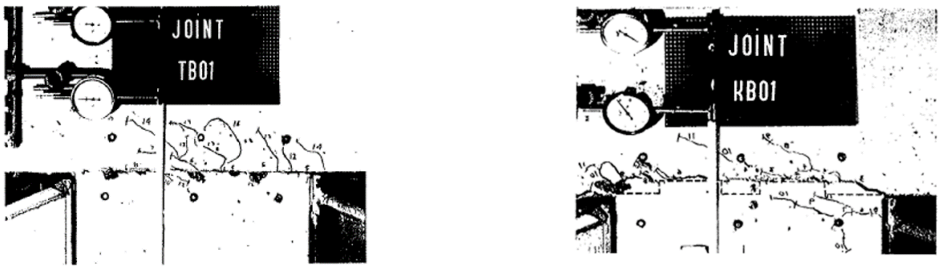

(a) Trowelled bonded joint (b) Keyed joint

Figure 5.30: Failure planes along a (a) trowelled bonded joint and (b) keyed joint of experiment performed by T. Paulay, R. Park and M. H. Phillips [1]

Figure 5.30a shows the failure plane at the interface level where the two concrete elements are bonded by a trowelled joint. This resembles the ATENA interface material model (IMM) and can be compared to the results presented earlier. Whereas, Figure 5.30b, shows the failure plane in case the two concrete elements are bonded by a keyed joint. This resembles with the artificial interface model (ArtIM), where an explicit roughness is incorporated at the interface level instead of just roughening the surface of the substrate concrete element. In both the figures the crack pattern observed initiates at the re-entrant corners and the curvature of the cracks is the same (Figure 5.21b) as explained by Schlangen in his paper [25].

In case of *no bond* condition, it was observed that the initial stiffness of the load displacement curve was lower than the experimental results. The reason behind this is the 1-D discrete reinforcement bar model used in ATENA to design steel reinforcement. This model only considers the axial stiffness of the bars without considering the contribution from bending and shear stiffness. To mitigate this problem influence of reinforcement bars crossing the interface is studied in detail, in the next section, with different reinforcement modelling techniques.

5.4. Influence of different reinforcement modelling techniques

Sometimes, mechanical devices such as reinforcement bars are used at the interface level to connect the two adjacent concrete elements. Apart from concrete-concrete interaction, the shear capacity of a composite model also depends on the resistance provided by these reinforcement bars crossing the interface. In this section the composite concrete layers are connected with shear connectors and then shear load test is simulated on the model to understand the influence of shear connectors. A bi-linear material type is assigned to the reinforcement bars in the ATENA model.

The dowel action phenomenon studied in section 5.2.1, cannot be apprehended completely just with the use of 1-D discrete reinforcement bar elements. This is because these elements only have an axial stiffness and hence, bending and shear component of the connectors cannot be studied using this default model. An attempt is made to design the RF bars using different techniques to have a holistic view about the dowel action phenomenon and its influence on the bond strength at the interface level.

Various techniques are undertaken to design the shear connectors in order to obtain best representation of actual experimental results. Some of the techniques use the 1-D discrete RF bar elements to model the RF bars but with some altercations to make use of the bending and shear stiffness. However, another one of the four techniques to be discussed make use of a macro-element to model the RF bar with dimensions equal to the area of the actual RF bars used in the experiment. Loading and boundary conditions are similar to the previous cases of shear load tests when shear connectors are not present. The following Figures 5.31 show the numerical models used for analysis of different reinforcement modeling to understand the dowel action phenomenon.

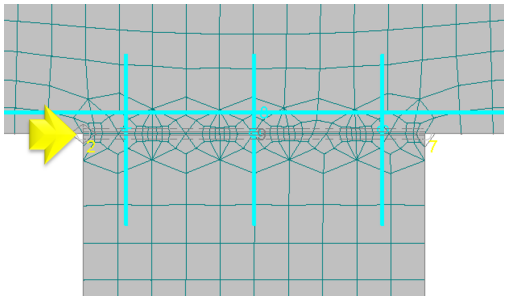

(a) 1-D discrete reinforcement bar element

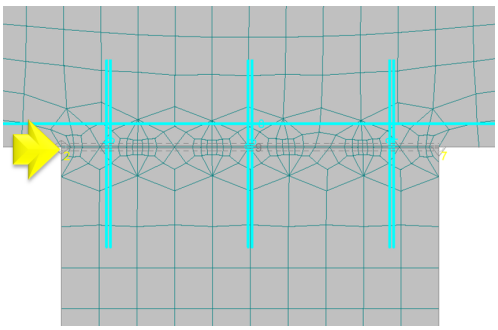

(b) 1-D two discrete reinforcement bar elements

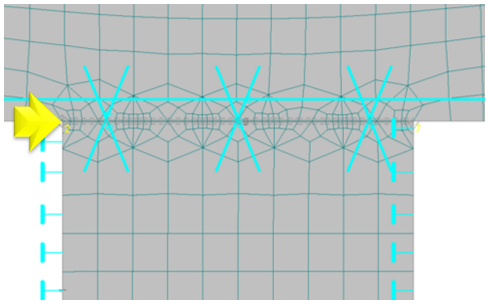

(c) 1-D discrete reinforcement bar elements crossing each other

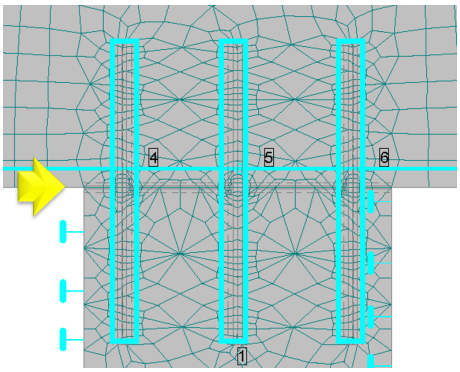

(d) Macro-elements assigned steel properties

Figure 5.31: Numerical models showing different techniques to model reinforcement bars

The ATENA IMM interface model is used for this study and the parameters assigned to the interface correspond to that of a *no bond* condition like in the previous sections. This is done in order to activate the stresses in the reinforcement bars as soon as the lateral loading is applied. Thus, only the contribution of the RF bars, and not the concrete-concrete interaction, is recorded. The reinforcement ratio is kept constant in all the models ($\rho = 0.69\%$) (equal to the reinforcement ratio of the experimental set-up discussed previously). Hereafter, a comparison between four different reinforcement models is shown, where 3 models use the 1-D discrete reinforcement bar elements to design the reinforcement. Whereas, a macro-element is used to design reinforcement in the fourth model. The geometry of the reinforcement bars used in the following models are as shown below.

A 1-D one discrete reinforcement bar element
1 bar area ($A_s = \frac{\pi}{4}9.5^2 = 71\ mm^2$); Interface area ($A_{cint} = 61800\ mm^2$) - $\rho = 6 \times A_s / A_{cint} = 0.69\%$

B 1-D two discrete reinforcement bar elements
1 bar area ($A_{s1} = A_s/2 = \frac{\pi}{8}9.5^2 = 36\ mm^2$); Interface area ($A_{cint} = 61800\ mm^2$) - $\rho = 12 \times A_{s1} / A_{cint} = 0.69\%$

C 1-D discrete reinforcement bar elements crossing each other
1 bar area ($A_s = \frac{\pi}{4}9.5^2 = 71\ mm^2$); Interface area ($A_{cint} = 61800\ mm^2$) - $\rho = 6 \times A_s / A_{cint} = 0.69\%$

D Macro-element assigned with steel properties and cross-section according to the reinforcement ratio

1 bar area ($A_{s2} \approx 2 \cdot A_s = 12 \times 12 = 144\ mm^2$); Interface area ($A_{cint} = 61800\ mm^2$) - $\rho = 3 \times A_{s2}/A_{cint} = 0.69\%$

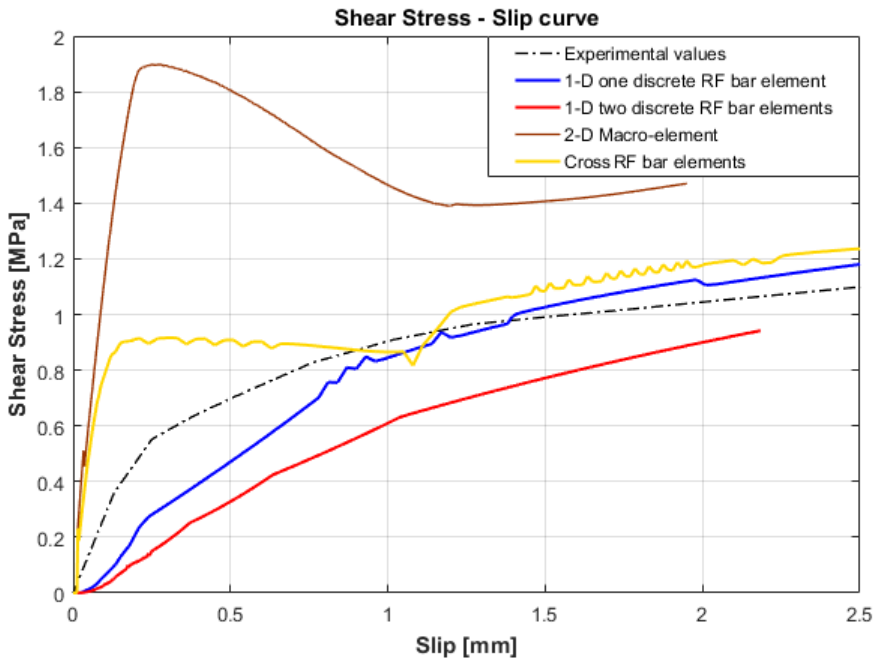

Figure 5.32: Shear stress - slip comparison between different RF modelling techniques and experimental results

The black dotted curve corresponds to the experimental *no bond* condition of the model. All the results obtained with different RF modelling techniques are compared with this curve.

The blue curve corresponds to the 1-D discrete reinforcement bar element as used in the previous sections, when *no bond* condition of the interface is analysed in detail. A decent estimation of the shear capacity is obtained when only 1 bar element is used to model one RF bar with the main difference in the initial stiffness of the curve. Only axial stiffness of the RF bars is accounted for with this modelling technique.

The bottom-most curve in Figure 5.32, shows the shear stress - slip behavior of the numerical model when RF bars are modelled using 2 RF bar elements of half of the area of the original RF bar. These two bars are placed at the geometric centers of the two halves of one bar when one RF bar is divided in two equal parts (as shown in Figure 5.33). Shear and bending stiffness is accounted for in this case, since concrete between these 2 bar elements, contributes to the stiffness of the bars. However, the combination of these two bar elements with concrete in between, underestimate the shear capacity of the entire model. Distance between these two RF bar elements is crucial for the bond strength at the interface level.

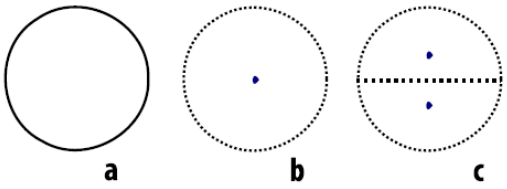

Figure 5.33: Cross-section of reinforcement bar divided in two equal parts to account for bending and shear stiffness

A cross pattern of RF bars is used to model the RF at the interface, and the stress - slip behavior is shown with a yellow curve in the Figure 5.32. The shear capacity certainly resembles the experimental nature of the model. The main difference is between the initial stiffness of the curve. A relatively higher stiffness is observed in the initial stage pertaining to the shear and bending stiffness. Although, the cross RF bar

pattern overestimates the stiffness, this can be adjusted by varying the inclination of the RF bar elements in the model. This cross pattern effect of the RF bars gives a very accurate estimation of the actual shear capacity of the real life composite specimen.

The upper-most curve is the stress - slip behavior when RF is modelled using a steel macro-element. This gives a very high stiffness to the RF bars. The same reflects from the curve as well, since the initial stiffness exhibited by the curve is the highest of all cases. Moreover, the shear capacity of the composite specimen is strongly overestimated.

Out of all these techniques, the stiffness and overall stress - slip response is accurately estimated when RF bars are modelled in cross pattern across the interface. However, to improve the response even further, a variation of the cross pattern technique is studied. In this variation study, angle between the RF bar and the interface (horizontal) is increased (from 67.4° – 80.5°) and the response is analysed. Numerical model for this variation is shown in Figure 5.34.

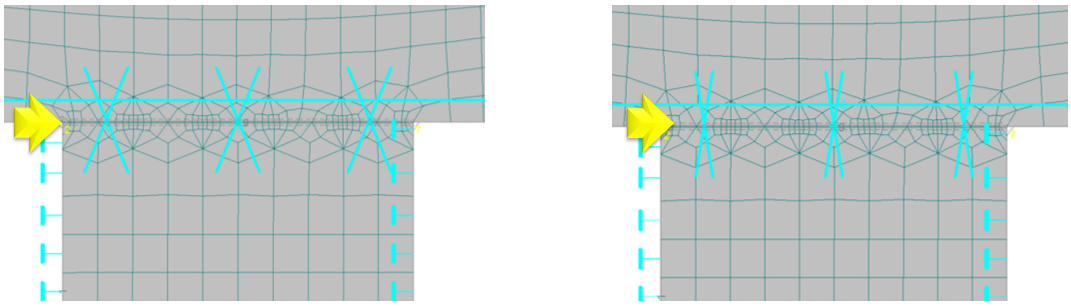

(a) Original cross bars crossing the interface (b) Inclination of cross bars changed

Figure 5.34: Numerical models showing variation in inclination of crossbars crossing the interface

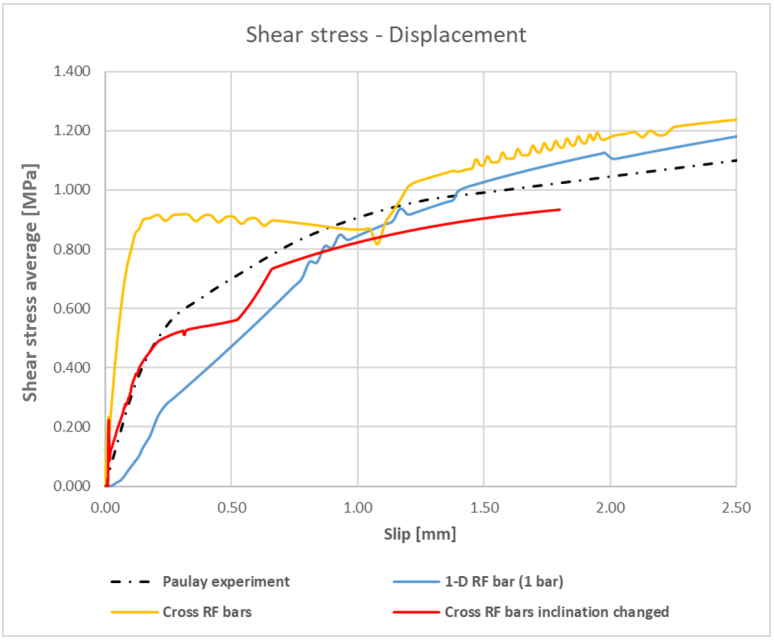

Figure 5.35: Sear stress - slip response of two different RF orientations corresponding to cross bars crossing the interface

Responses of the two variations adopted to model reinforcement (RF) bars in cross pattern are shown in Figure 5.35 along-with the experimental results, for *no bond* condition at the interface. As the inclination of the bars with the horizontal (interface) increases (the orientation of bars becomes similar to 1-D bars perpendicular to the interface), the initial stiffness of the composite concrete specimen decreases thus, complying with the initial stage of the experimental curve. However, there is a gradual dip in the shear stress

after the first crack develops at the interface level. With further increment in loading, shear stress rises due to concrete-concrete interaction pertaining to the complex geometry near the connection between concrete and RF bars. Eventually with an increase in the slip at the interface, a conservative stress-strain behavior is obtained corresponding to the experimental results. Thus, by varying the inclination of RF bars, crossing the interface, a good estimation of the shear response can be predicted by using cross-pattern technique to model the RF bars.

However, variation of inclination angle between RF bars and interface layer studied in this section does not promise the validity to implement the same in a generic sense. The magnitude of this inclination will vary for different roughness characteristics. Nevertheless, comparison in this section shows that the technique adopted to model RF bars in a cross-pattern can be helpful in considering the bending and shear stiffness contribution of the reinforcement bars crossing the interface. Further research is required to address the inconsistency in shear stress development using cross-pattern RF bars.

In the next chapter, validation of the numerical models using both ATENA IMM and ArtIM is performed on a structural level. For this a case study from Eindhoven about a car park garage collapse is selected. Failure of a weak interface bond strength of the top floor slab led to the collapse of one part of the entire structure. An attempt is made to simulate tests related to this research with the help of reports provided by TNO [2] and Adviesbureau ir. J. G. Hageman B.V [3].

6

Validation of numerical models with a structural test

6.1. In general

In the previous chapter, the numerical model was validated by comparing the results with a bond model from the experiment carried out by T. Paulay. However, the model tested in the experiments was still a small scale. To incorporate the phenomenon of interface strength on a structural level, a second validation is required. For this validation, case study of Eindhoven airport car parking garage is studied. On 27^{th} May, 2017, a car parking garage near Eindhoven airport collapsed due to weak connection between the prefabricated slab and the in-situ concrete poured over it. In this case, interface between the slabs was crucial and hence this case study is chosen for validation of the numerical model on structural level.

Figure 6.1 shows the experimental setup of the model, constructed in a laboratory with a four-point bending load combination.

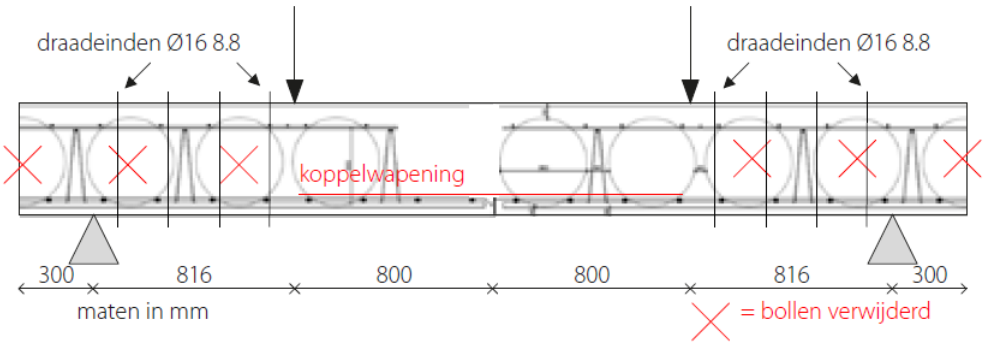

Figure 6.1: Experimental setup simplified from the structural model

The setup is made of two prefabricated bubbledeck slab placed side by side with insitu concrete poured over it to make the connection. The balls marked with red cross in the figure mean that they are not included in the experimental setup. However, while designing a numerical model all the balls are omitted from the model since, the stress transfer through these plastic balls is insignificant. There is an added limitation of ATENA 2D that does not allow modelling of such a shape for numerical analysis. A coupling reinforcement is provided in the middle section of the specimen above the connection of the two bubbledeck slabs. Material properties used for the setup are provided in Tables 6.1 - 6.3.

Table 6.1: Concrete material properties

Structural element		Bubble-deck slab	In-situ slab	Unit
Material type		3D Non Linear Cementitous 2	3D Non Linear Cementitous 2	
Elastic Modulus	E	36280	34080	MPa
Poisson's ratio	μ	0.2	0.2	-
Tensile strength	f_t	3.80	3.21	MPa
Compressive strength	f_c	53	43	MPa
Crack model		Fixed	Fixed	

Table 6.2: Steel bolts/reinforcement material properties

Structural element		Reinforcement	Steel bolts	Unit
Material type		Bilinear	Bilinear with hardening	
Elastic Modulus	E	210	200	GPa
Yield strength	σ_y	500	640	MPa
Maximum strength	σ_t	-	800	MPa

Table 6.3: concrete-concrete interface properties

Structural element		Concrete-concrete	Unit
Material type		2D Interface	
Normal stiffness	K_{nn}	3×10^6	MN/m^3
Tangential stiffness	K_{tt}	3×10^6	MN/m^3
Tensile strength	f_t	0.15	MPa
Cohesion	c	0.30	MPa
Friction coefficient	μ	0.60	-

Numerical model used for the analysis is shown in Figure 6.2 for unreinforced and fully reinforced model. Mesh sizes used for the analysis are, 35 mm for the bubbledeck slab, 70 mm for the in-situ concrete slab and 20 mm for the steel plates. A four point bending test is simulated on this numerical model. A small 6 mm wide notch is present at the connection of the two bubble-deck slabs near the bottom fibre. Since, it is a very long specimen, use of symmetry can be done to reduce the computation time. For this, results obtained from both full length model and symmetric model are compared to the experimental results to verify the use of symmetry. Numerical model using symmetry is shown in Figure 6.3.

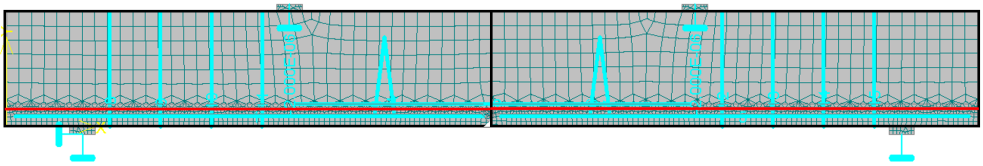

(a) Partially reinforced model (no shear reinforcement in the flexural span)

Figure 6.2: Full length numerical model of Eindhoven case study

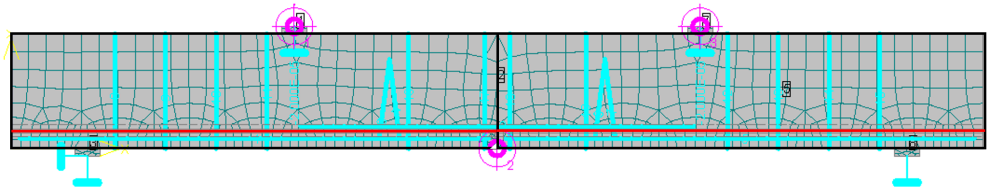

(b) fully reinforced model (shear reinforcement crossing the interface in the flexural span)

Figure 6.2: Full length numerical model of Eindhoven case study

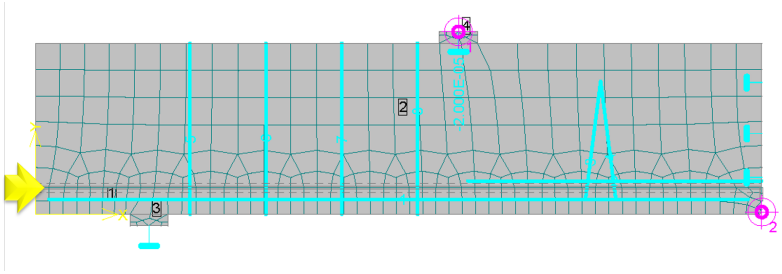

(a) Partially reinforced model (no shear reinforcement in the flexural span)

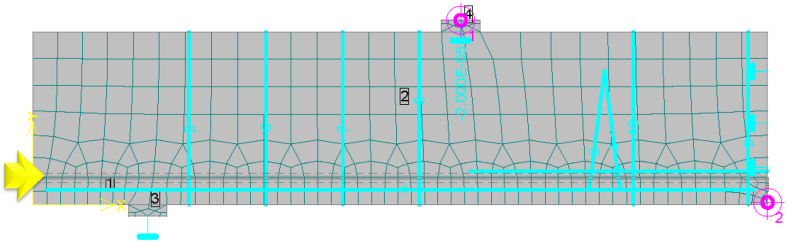

(b) fully reinforced model (shear reinforcement crossing the interface in the flexural span)

Figure 6.3: Symmetric numerical model of Eindhoven case study

Results of the analysis are presented hereafter with a direct comparison between the full length and symmetric models.

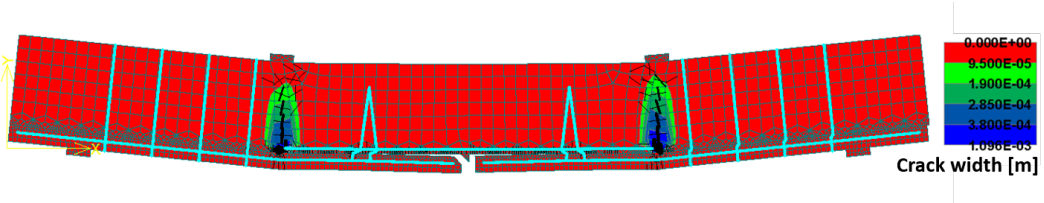

(a) Crack pattern in partially reinforced model (no shear reinforcement in the flexural span)

Figure 6.4: Crack distribution in full length numerical model of Eindhoven case study

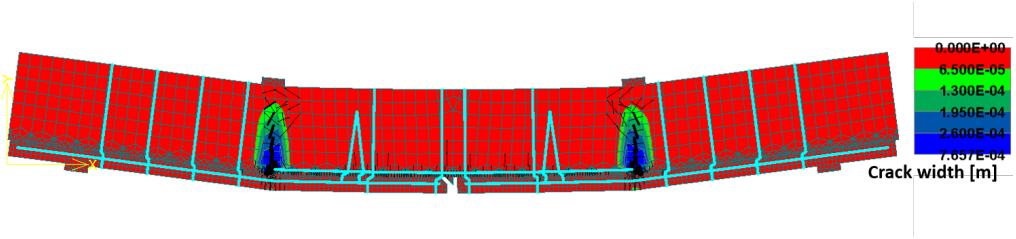

(b) Crack pattern in fully reinforced model (shear reinforcement crossing the interface in the flexural span)

Figure 6.4: Crack distribution in full length numerical model of Eindhoven case study

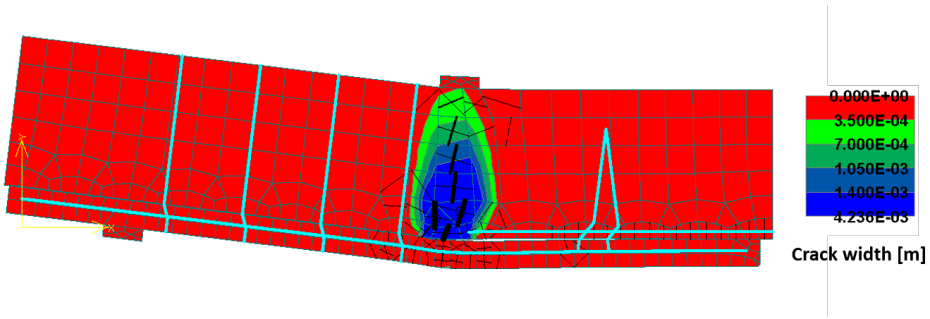

(a) Crack pattern in partially reinforced model (no shear reinforcement in the flexural span)

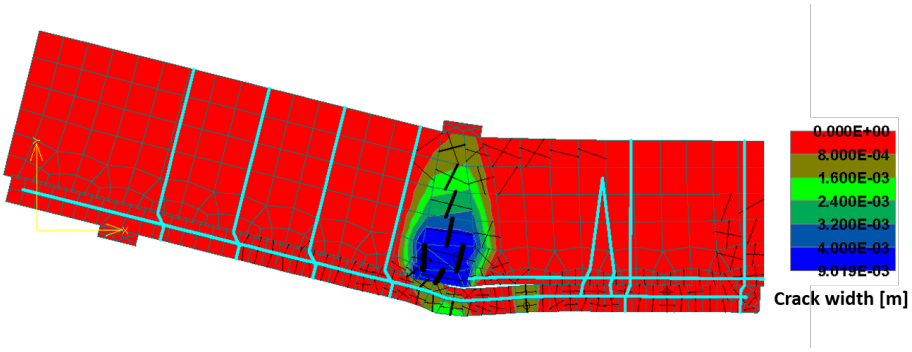

(b) Crack pattern in fully reinforced model (shear reinforcement crossing the interface in the flexural span)

Figure 6.5: Symmetric numerical model of Eindhoven case study

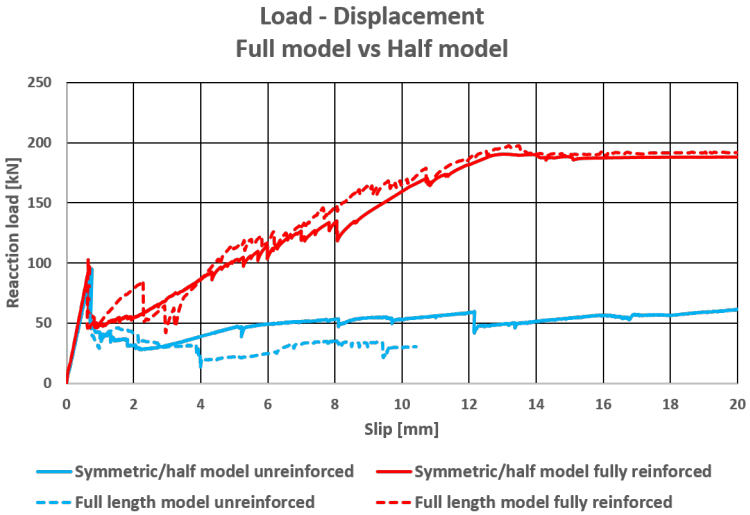

Figure 6.6: Load - displacement comparison between full length and symmetric models

Figure 6.6, shows a direct comparison between a full length model and a symmetric model undergoing bending in an unreinforced and fully reinforced model. The initial stiffness for all cases is exactly same with a sudden stress drop once the interface fails. There are some differences in the post-peak response for the full length model and a symmetric model. However, these differences occur as a result of certain computation error which can be neglected. For most of the post-peak behavior, a ductile response is exhibited by all the models. Moreover, the crack distribution in the symmetric model resembles to that of the full length model. Hence, it is safe to assume that a symmetric model will behave in a similar manner as a full length specimen. Henceforth, all the numerical analyses will be performed on a symmetric model with appropriate boundary conditions. Similar to the verification and first validation of the bond models, even the structural model will be tested using both interface models.

6.2. ATENA Interface Material Model (IMM)

For a validation of the numerical model, results of the analysis are now compared with the experimental findings using ATENA interface material model (IMM). Figure 6.7 shows the load displacement curves for the numerical model and the experimental set up. Numerical models used for the analysis are the same as shown in Figure 6.3.

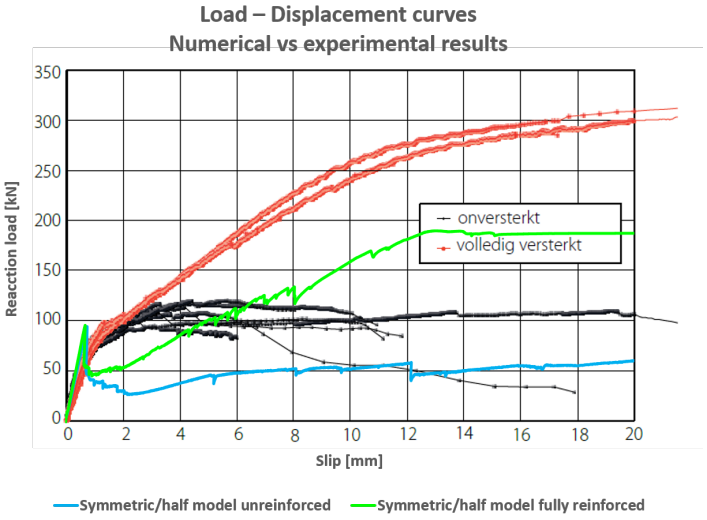

Figure 6.7: Load - displacement comparison between numerical and experimental results

Initial stiffness obtained from the numerical analysis is slightly higher than the experimental stiffness. Nevertheless, a good estimation of the first peak load carrying capacity is obtained from the numerical analysis using ATENA IMM (Load ≈ 100 kN). On attaining the maximum interface strength, a sudden drop in the curve is observed pertaining to the default softening behavior as explained in the verification and validated again with a bond model. The ATENA IMM in a structural model exhibits same post softening response as the experimental load displacement curve. However, the difference in the load values in the post peak branch of the curve can be explained by the softening evolution law present in the ATENA software, which exhibits a brittle response right after the first peak load is achieved. This is valid in both cases tested with the numerical analysis for unreinforced and fully reinforced specimen. Figure 6.8 shows the crack pattern at the interface and the subsequent propagation in the top in-situ concrete slab for both experimental and numerical analysis.

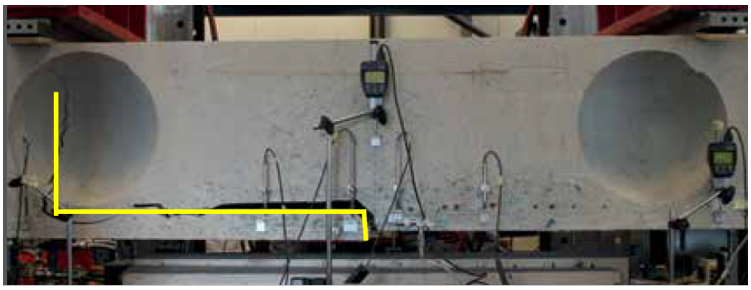

(a) Experimental crack pattern

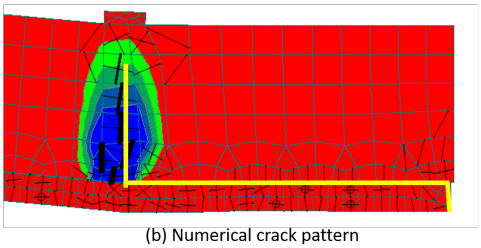

(b) Numerical crack pattern

Figure 6.8: Crack pattern in (a) experiment and (b) numerical model

The yellow lines in both the figures denote the cracked surface. First crack initiates at the notch near the bottom fibre of the bubble-deck slab. It propagates through the interface between the bubble-deck slab and the cast in-situ concrete slab. Eventually, a vertical crack propagates to the top concrete slab at the end of the coupling reinforcement (RF) bars. Coupling RF bars are shown clearly in Figure 6.1 which end at the first ball of the bubble-deck slab.

6.2.1. Mesh sensitivity analysis

Meshing is an important aspect of numerical modelling and it is crucial to select the right mesh size to obtain satisfactory results. In the analysis with ATENA, first a very fine mesh was tested (≈ 10-15mm) but unfortunately the analysis could not proceed further than 2-3 mm of slip distance. There is a limitation of ATENA 2D software that any file beyond 2Gb computation memory cannot run the analysis further this limit. To overcome this problem a mesh sensitivity analysis is performed in order to validate the choice of mesh size used for the analyses in previous section.

Different mesh sizes are chosen for the bubble-deck slab, 20 mm, 35 mm and 50 mm. Mesh size for the in-situ concrete slab is kept higher than the bubble-deck slab since, thickness of this layer is much higher than the bottom slab. Mesh sizes chosen for the in-situ concrete slab vary approximately in the same ratio, 50 mm, 70 mm and 100 mm respectively. Boundary conditions are kept constant throughout the mesh sensitivity analysis. Figure 6.9 shows the load-displacement curves for the respective mesh sizes along-with the crack distribution at the end of each analysis.

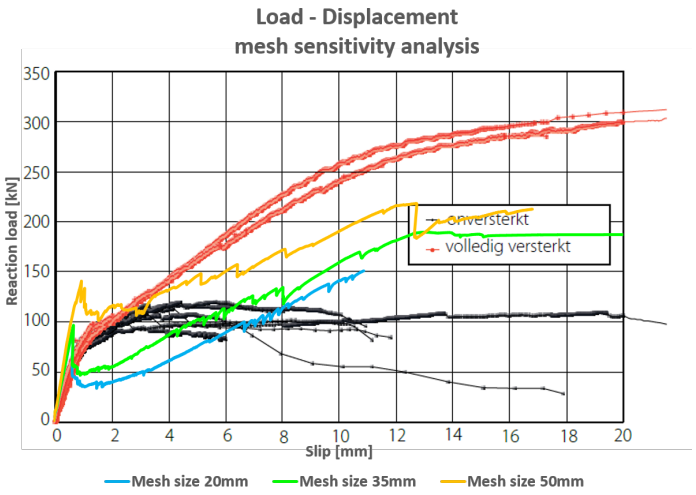

Figure 6.9: Load displacement curves for numerical models with different mesh sizes

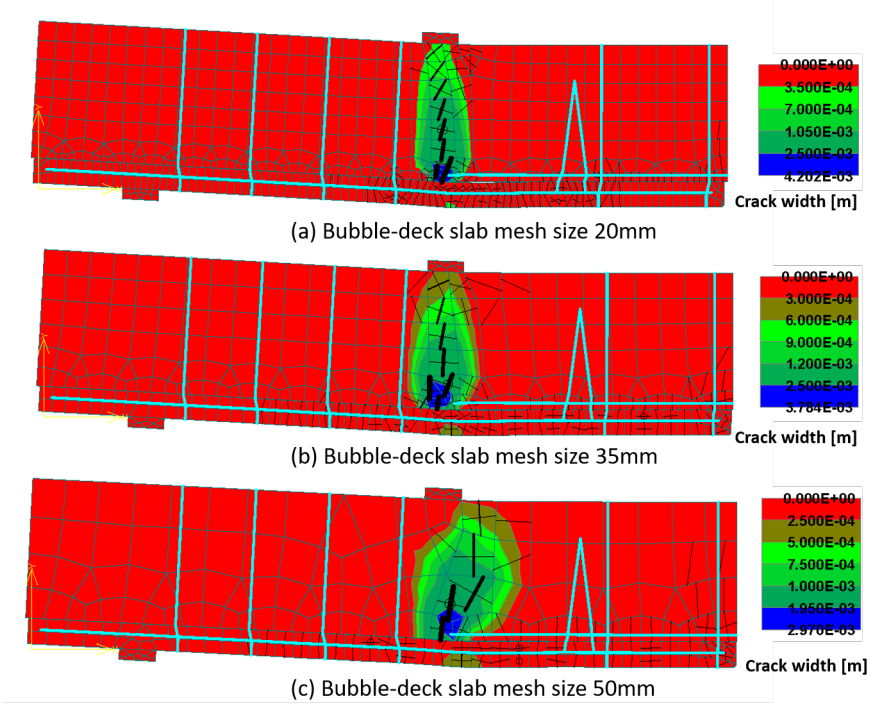

Figure 6.10: Crack distribution in structural model using different mesh sizes (a) 20mm, (b) 35mm and (c) 50mm of bubble-deck slab

Simulations for 20mm mesh size stopped at a displacement value of about 10.5mm without finishing the analysis. It is considered that accuracy of the results increases with a finer mesh. However, in this case results corresponding to 35mm mesh size are also quite satisfactory since, there is not much difference between the values obtained from these two mesh sizes. Moreover, a complete analysis can be performed using 35mm mesh size for the bubble-deck slab. If the mesh size is increased further up to 50mm, an overestimation of the first peak load as well the overall load carrying capacity is exhibited by the model. This is not good for the model on account of safety of the structure. Thus, the mesh size of 35mm for the bubble-deck slab is considered optimum for the numerical analysis on account of the significant mesh dependency.

In the next section influence of the artificial interface model is studied on the structural model.

6.3. Artificial Interface Model (ArtIM)

Estimation of the load carrying capacity of the model is carried out quite successfully using ATENA IMM. However, influence of ArtIM on the structural model is necessary in order to validate the use of this interface model. The interface between the bubble-deck slab and the cast in-situ slab has properties corresponding to a very smooth interface. Thus, a straight element layer is assumed as an artificial interface in this case. Considering that ratio between shear strength and tensile strength is significantly higher than '2', very weak concrete material properties are assigned to the interface. Tensile strength of the interface material is 0.15 MPa and thickness is 5mm. Figure 6.11 shows the numerical model used for the analysis.

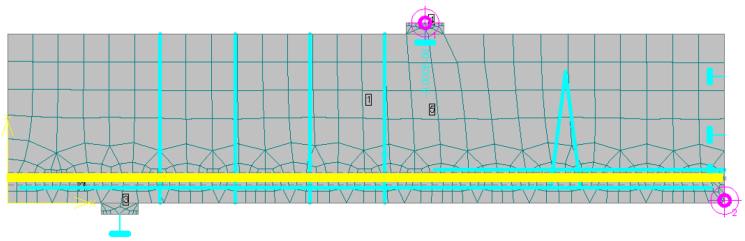

Figure 6.11: Symmetric numerical model of Eindhoven case study using ArtIM

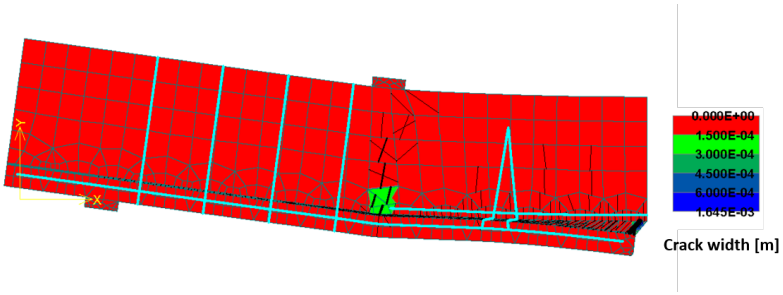

Figure 6.12: Crack distribution in structural model using ArtIM

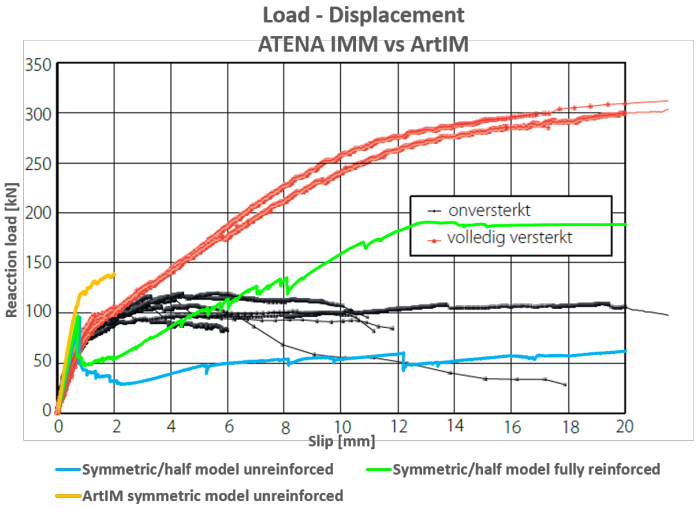

Figure 6.13: Load - displacement curve comparison between ArtIM, ATENA IMM and experimental results

From the load - displacement curve in Figure 6.13, it is clear that the shear strength in case of ArtIM is very high. In fact, the load carrying capacity of the partially reinforced model using ArtIM is higher than

the fully reinforced model using IMM. However, important observation in this case is the response of the numerical model once first peak load is attained. A stress drop cannot be observed unlike in case of IMM, thus, complying with the experimental response in the post peak branch. Furthermore, the number of finite elements in the interface layer is very high thus making the computation very difficult and time consuming. If mesh size is to be increased in order to make the computation run quicker, then compatibility between the adjacent finite elements will be lost near the interface layer.

Figure 6.12, shows the crack distribution in the structural model using ArtIM. Crack width at the end of coupling reinforcement bars is limited due to the artificial interface layer. Due to the overestimation of the load carrying capacity of the model, use of ArtIM for structural model is not advisable.

7

Conclusions and recommendations

The aim of this research was to investigate whether ATENA software reliably predicts the interface behavior using the standard finite elements available in the software. For this purpose, two different techniques are adopted to model the interface between adjacent concrete elements. The models used for the analysis are, the ATENA interface material model (IMM) which uses *2D line 4 node interface elements* with zero length to represent the interface and an artificial interface model (ArtIM) which uses *2D linear quadrilateral 4-noded material elements* to create an artificial interface layer. Characterisation of the roughness parameters in each of these models is performed with utmost detailing and influence of these roughness parameters as well as reinforcement bars crossing the interface are studied from composite concrete bond tests and structural test. Verification of both the interface modelling techniques is performed successfully. The eventual comparison of experimental and numerical results led to a validation of the models and their practical usability in estimating shear capacity of composite concrete bond models and load bearing capacity in structural tests.

7.1. Conclusions

7.1.1. ATENA Interface Material Model (IMM)

- ATENA IMM was able to simulate direct tension test and shear load test successfully on a small scale bond model. The response appears to be more brittle because of the absence of softening law to the interface model. Characteristics of the bond between the adjacent concrete elements are changed as per the different roughness criteria

- According to convention and from the work of various researchers such as Randl and Zanotti [4], Peyerl and Steiner [5], bond strength of the interface in shear should be approximately twice the bond strength in tension. The ATENA IMM exhibits a similar ratio (1.6 - 2.4) between the shear strength and tensile strength in the small scale bond model.

- Shear capacity of the interface increases with the increasing cohesion and tensile strength of the interface and is of the similar magnitude as the cohesion value inputted in the model. Similarly, friction coefficient inputted for the respective roughness classes, follows the Mohr-Coulomb failure criteria. A successful check is established for the input parameters.

- In a no bond/very smooth interface condition IMM is able to accurately estimate the dowel action contribution. However, the initial stiffness could not be reliably predicted because the 1-D reinforcement bar element only takes into account the axial stiffness of the bar whereas, bending and shear stiffness are neglected. While estimating the concrete-concrete interaction, only the initial stiffness obtained from the numerical analysis complied with the experimental bond test. Once the interface fails, IMM fails to rightly predict the shear response of the model by exhibiting a brittle response.

- In case of a structural model, a very smooth interface is assigned between the bubble-deck slab and the case in-situ concrete slab. From the comparison between load-displacement curves obtained from experiment and numerical modelling, a good estimate of the first peak load carrying capacity

is achieved. However, once the interface elements attain their tensile strength, a sudden stress drop is observed which does not comply with the experimental results and eventually a conservative shear response is predicted by IMM. Crack distribution obtained from the numerical analysis complies to the crack pattern obtained in the experimental test findings.

- Moreover, there is a huge mesh dependency while simulating a structural interface failure case using IMM.

7.1.2. Artificial Interface Model (ArtIM)

- In the artificial interface model (ArtIM), an artificial layer is introduced between the two concrete elements that acts as an interface. To replicate different roughness classes, an explicit roughness or a modified surface profile is provided to the interface layer. Lower strength concrete material properties are assigned in case of small scale bond models. The direct tension test exhibits same tensile strength of the interface as in case of IMM. Moreover, a ductile response is observed as opposed to the brittle nature while using IMM.

- An overestimation of shear strength is predicted by using ArtIM while simulating a shear load test on a small scale bond model. Thus, ratio between the shear strength and tensile strength increases significantly when material elements are used to create an artificial interface layer.

- Explicit roughness provided to the interface layer (artificial interface created in wave pattern) in ArtIM is able to simulate the effect of friction. This is done because a friction coefficient cannot be defined specifically for ArtIM.

- By increasing material strength of the artificial interface layer, shear strength of the composite concrete specimen is significantly overestimated. This result does not comply with the experimental observation for interface strength in shear. Moreover, shear strength predicted using ArtIM is significantly higher than that estimated using the IMM.

- Shear strength of the artificial interface layer depends on the concrete compressive strength and tensile strength assigned to the material elements representing the artificial interface layer. However, for IMM, cohesion provided to the interface elements is mainly responsible for the shear bond strength. The degree of increment of these parameters cannot be assumed to be the same, i.e, if cohesion in IMM is doubled the shear strength is also approximately doubled however, if tensile strength of material elements in ArtIM is doubled shear strength exhibited by the composite concrete specimen increases significantly. Hence, use of the artificial interface model (ArtIM) should not be done to calculate the shear strength of the composite bond model on account of its strength overestimation.

- In case of structural validation, similar response like in the case of experimental bond model test is exhibited by using ArtIM. Since, in this scenario, the shear strength of the interface is very important in order to transfer stresses, a significant overestimation of the load carrying capacity of the model is noticed. Even with very weak material properties, load carrying capacity of a partially reinforced structural model is estimated to be significantly higher than the fully reinforced case of IMM. However, an important observation while using ArtIM is that the first stress drop exhibited by IMM after first crack initiation cannot be observed here. This stress drop is not observed in the experimental results as well.

- Due to a very high number of finite elements in the interface layer, computation of the model using ArtIM is very difficult and time consuming. If mesh size of the elements is increased, then there is a possibility that the model will become incompatible. Hence, use of artificial interface model is not advisable to simulate the interface behavior.

Modelling of the reinforcement (RF) crossing the interface is also studied. While using 1-D RF bar elements perpendicular to the interface, the initial stiffness of the load-displacement curve is underestimated and does not comply with the experimental results. This is because the 1-D RF bar element only considers the axial stiffness of the bar and the shear and bending stiffness contributions are neglected. To overcome this limitation, different RF modelling techniques are tested. Out of all the different approaches implemented, RF bars modelled in cross pattern give a good estimation of initial stiffness for the dowel action contribution in

shear stress transfer. By varying the angle between the RF bar and the interface, stiffness of the composite model can be adjusted. The optimum angle between the RF bars and horizontal (interface layer) should be maintained close to 90°. In this project, only one model is tested for RF modelling hence, further research should be done to understand this technique in more detail.

According to the numerical analysis performed in this research, both the techniques used to model an interface do not predict the interface behavior perfectly under the prescribed roughness characteristics. While using ATENA IMM, once the interface fails, stress redistribution occurs due to which the post-peak behavior does not comply with the experimental results. On the other hand, in ArtIM very few parameters can be defined to the interface layer which are not sufficient to replicate the different roughness characteristics for an interface. Ratio between the shear strength and tensile strength of the interface is very high in case of ArtIM which does not comply with experimental findings of Randl and Zanotti [4], Peyerl and Steiner [5].

After studying the two techniques implemented to create an interface on bond level and structural level, it can be concluded that, the ATENA interface material model (IMM) using *2D line 4-node interface elements* and an artificial interface model using *2D linear quadrilateral 4-node material elements* do not predict the interface behavior reliably with the finite element analysis in ATENA.

7.2. Recommendations

Recommendation pertaining to this research and future prospective research topic are stated in this section

- The effect of creep and shrinkage is not accounted in this research while considering the bond between concrete cast at different times.
- Detailed research should be done in case of reinforcement modelling techniques, relation between angle of inclination of reinforcement bars with the interface should be obtained.
- Any other finite element software should be tested in order to study interface behavior considering the test cases of this report

A

Verification of model

While designing the artificial interface element, an additional study with respect to the material properties of the interface was performed. The concrete strength class chosen for the interface element is varied according to the tensile strength of the interface model as considered in the Table **??** of ATENA IMM. The increase in the tensile strength and subsequently the strength of this interface layer can be attributed to the different bonding agents (epoxy resin, synthetic resin or super strong concrete bonding adhesives) used in real life, between two concrete layers. The material properties used for this analysis are given in Table A.1. Direct Tension Test (DTT) and Shear Load test (SLT) are performed on the model with interface having different material strength properties. Results are discussed below.

Table A.1: Input parameters in numerical model for different roughness classes using ArtIM

Parameters	**Symbol**	**Units**	**Smooth Interface**	**Slightly Rough Int.**	**Rough Interface**
			??	**??**	**??**
Material properties					
Cube compressive strength	$f_{c,cube}$	[MPa]	50	50	50
Interface material properties					
Cube compressive strength	$f_{c,cube}$	[MPa]	12.45	17.27	23.52
Cylinder compressive strength	$f_{c,cyl}$	[MPa]	10.15	14.09	19.18
Tensile strength	f_t	[MPa]	0.50	1.00	1.50
Young's modulus	E_{cm}	[MPa]	22100	24381	26747

A.1. Direct Tension Test (DTT)

A DTT is conducted for different concrete strength class for the interface by using the ArtIM. In the report, results of the interface with properties corresponding to a tensile strength of $0.5\ MPa$ are compared in order to ensure localization of cracks at the interface. Whereas, an additional study is performed using two more higher strength concrete classes (tensile strengths: $1.0\ MPa$ ($f_{c,cube} = 17.27\ MPa$), $1.5\ MPa$ ($f_{c,cube} = 23.52\ MPa$)) assigned to the interface elements.

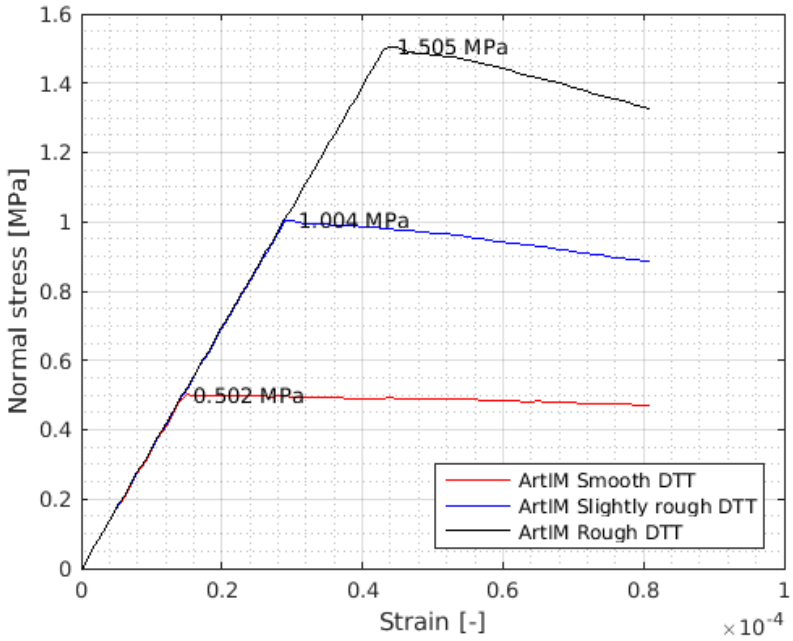

Figure A.1: Stress - strain curve for models with different interface material strength using ArtIM

The peak normal stress achieved in each case, corresponds to the tensile strength of the respective concrete strength class used for the interface elements. Important observation in this case is about the post-peak response of the model. The composite model exhibits ductile behavior once the interface has cracked. On the contrary, in case of ATENA IMM, an immediate drop in the interface stresses was observed, pertaining to the breaking up of the interface layer (when non-rigid bond properties are applied to the interface). In this case, since, the interface element is assigned the properties of a concrete material (possibly, corresponding to a concrete adhesive bonding agent), a post-peaking softening curve is obtained.

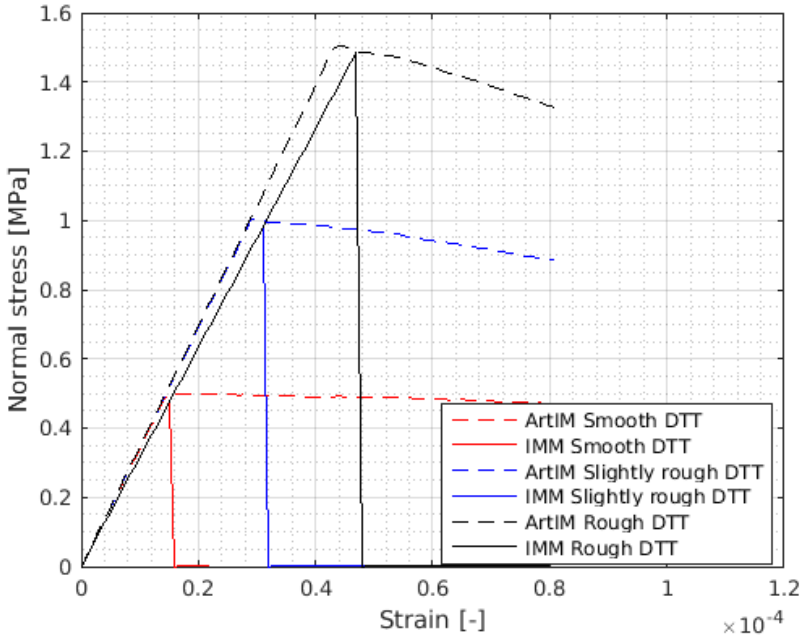

Figure A.2: Normal stress - strain comparison between ATENA IMM and ArtIM with different roughness classes

Figure A.2, shows the comparison between normal stress - strain behavior when ATENA IMM and ArtIM are used respectively. The maximum tensile strength for the ArtIM, depends on the tensile strength of the interface element. Similarly, for ATENA IMM, the interface parameters assigned at the interface of the composite model, vary as per the classification of the roughness classes (Model Code 2010).

A.2. Shear Load Test (SLT)

Similar to the DTT, a shear loading test is conducted using a straight interface element. Higher concrete strength values for the interface are tested in order to understand the influence of material strength. Results of the tests are shown below.

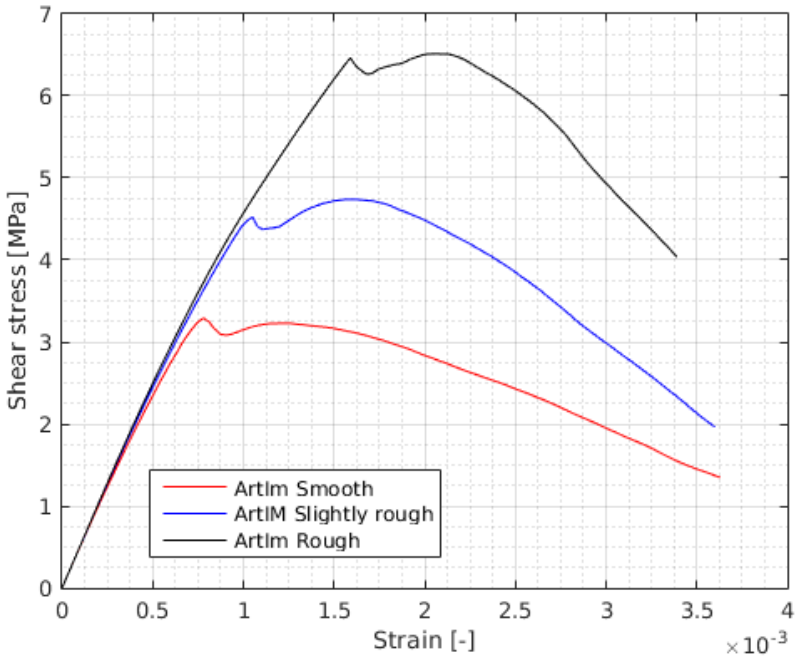

Figure A.3: Shear stress - strain curve for different interface material properties

From Figure A.3, a clear distinction is observed between the three cases considered for the models. The lower-most curve corresponds to the smooth surface roughness class and has tensile strength of $0.5\ MPa$. Whereas, the upper-most has a material strength corresponding to rough surface characteristics in ATENA IMM, with a tensile strength of $1.5\ MPa$.

From the graph, it can be observed that all the three curves, after attaining their first peak value, drop to a small extent and then again rise until a second peak value is achieved. After the second peak, a constant drop in the curve is observed, pertaining to the fully developed cracks in the interface element and thus, denoting softening of concrete in this branch. For smooth and slightly rough interfaces, the first peak is reached on the onset of cracking of the interface. Whereas, for rough interface characteristics, after the development of cracks near the bottom edge, diagonal cracks can be observed in the material near the interface. This means that, for relatively weaker interface elements, cracks appearing at the interface element imply an interface failure (interface material failure). Whereas, a material failure is observed in the composite model with relatively stronger interface element.

Due to the initial cracking at the interface, a drop in the shear stress is observed as a result of redistribution of stresses. However, on further increment of load, shear stresses increase with relatively lesser stiffness than in the initial stage of the analysis. Once, all the cracks are fully developed at the interface element (for smooth and slightly rough interfaces) diagonal cracks develop near the edges of the concrete element starting from the weaker sections of the interface. Whereas, for rough interface model, this state is reached when diagonal cracks near one of the edges of the material, influence the cracking at the interface element. Fully developed

cracks appear when the model approaches its maximum shear capacity (second peak). Furthermore, at peak load, second big diagonal crack develops near the opposite edge of the model again propagating from the weaker sections of the interface element. Thus, a softening behavior is observed in the post peak branch of the graph indicating reduction of the shear strength of the composite concrete model.

Variation of wavelength for the artificial interface layer with explicit roughness

In this section, an effort is made to understand the influence of wavelength of the interface layer on the shear capacity. Similar to the previous section, the interface layer is modelled in a wave pattern but here, with different wavelengths (repetitiveness of the wave pattern). For this purpose, size of one interface block-element (small blue-marked element in Figure A.4 with dimensions $n \times 2.5\ mm^2$) is varied to incorporate the change in wavelength. n is the length of one element and has values equal to 60, 30 and 20 mm respectively (Figures A.5d, A.5f and A.5h). The wavelength of the interface layer (like the wavelength of a wave profile) decreases with subsequent reduction of the interface block-element size. It might seem that the roughness in all these different cases is identical, however this is not the case. If the interface of the model is divided into 5 equal sampling lengths, then roughness is calculated by the maximum peak and valley heights in these respective sampling lengths (lengths separated by green dotted lines in Figure A.4). This phenomenon is clearly explained by Santos and Julio in their research on roughness quantification methods for concrete surfaces [26].

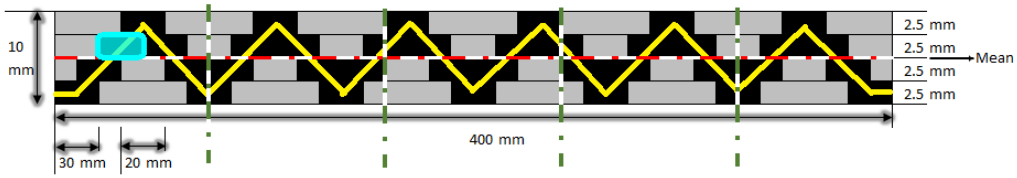

Figure A.4: Division of length into five equal sampling lengths to calculate roughness

The mechanical models used for the analyses and the interface detailing are given in Figure A.5. The numerical model is shown in Figure A.6. The mesh size used in the numerical model is $10\ mm$ for the concrete macro-elements as well as for the steel plate on top and $5\ mm$ for the interface elements. The interface detailing is such that the block-elements in black color constitute the actual interface. Weaker material properties are assigned to these block-elements to ensure localization of cracks in the interface layer, between the two concrete layers. The dimensions of the elements are also shown in the figures for better understanding.

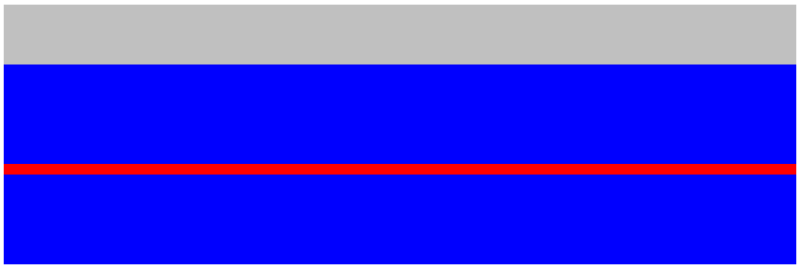

(a) Mechanical model with straight interface element

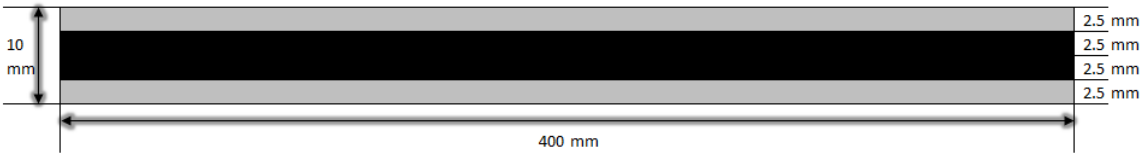

(b) Interface detailing (straight element)

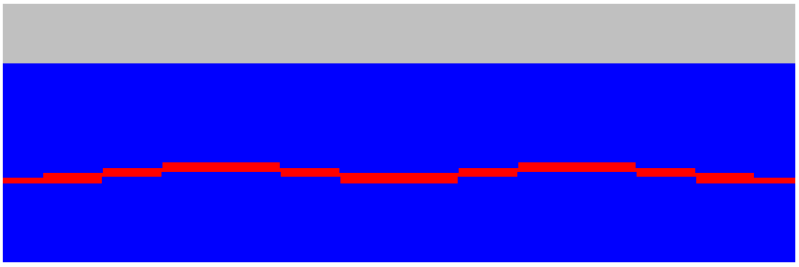

(c) Mechanical model with sinusoidal interface element (element size=60mm)

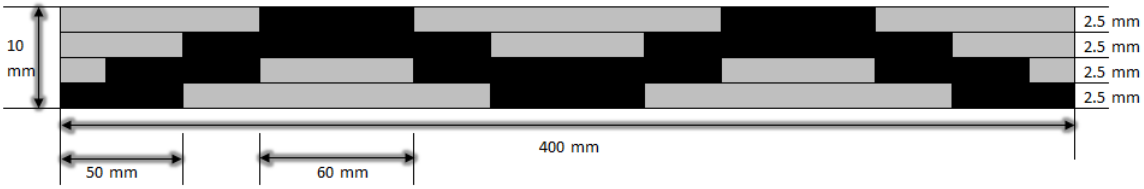

(d) Interface detailing (sinusoidal element 60mm)

Figure A.5: Mechanical models and interface detailing for layered interface elements

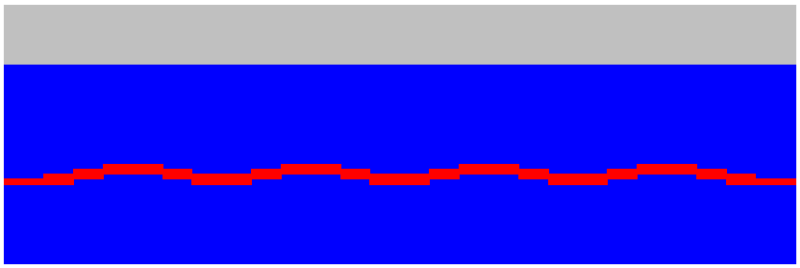

(e) Mechanical model with sinusoidal interface element (element size=30mm)

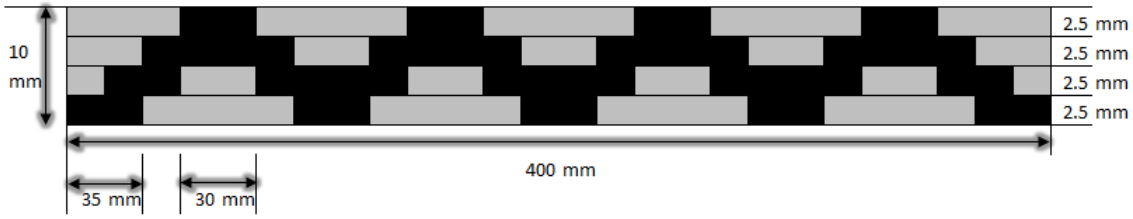

(f) Interface detailing (sinusoidal element 30mm)

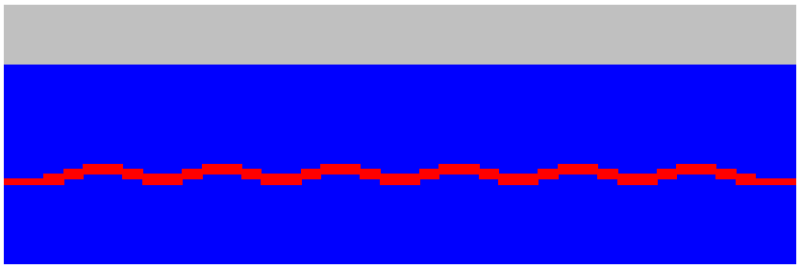

(g) Mechanical model with sinusoidal interface element (element size=20mm)

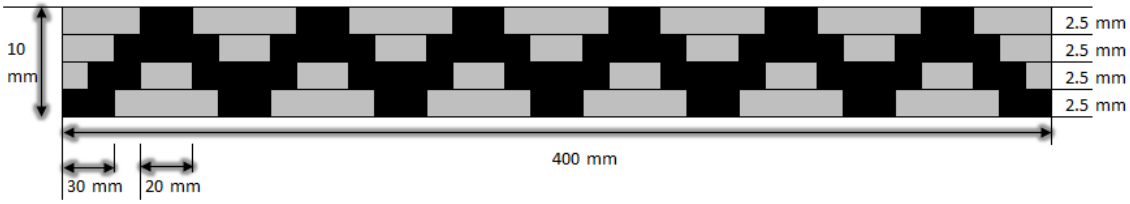

(h) Interface detailing (sinusoidal element 20mm)

Figure A.5: Mechanical models and interface detailing for layered interface elements

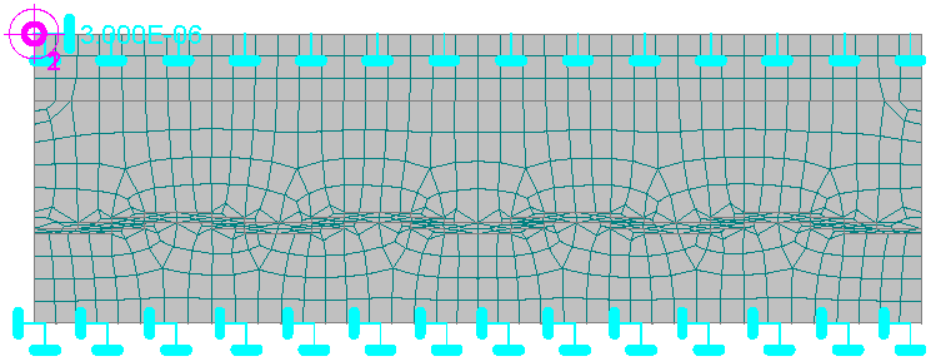

Figure A.6: Numerical model used for modified interface layering ($30mm$ interface element size)

The interface is divided into small layers of 2.5 mm thickness each. The grey-colored regions are part of the adjacent concrete macro-elements and have the same material properties as those concrete elements. The cube compressive strengths assigned to the interface layer is 12.45 MPa ($f_t = 0.5\ MPa$) (corresponding to a weaker/smooth interface).

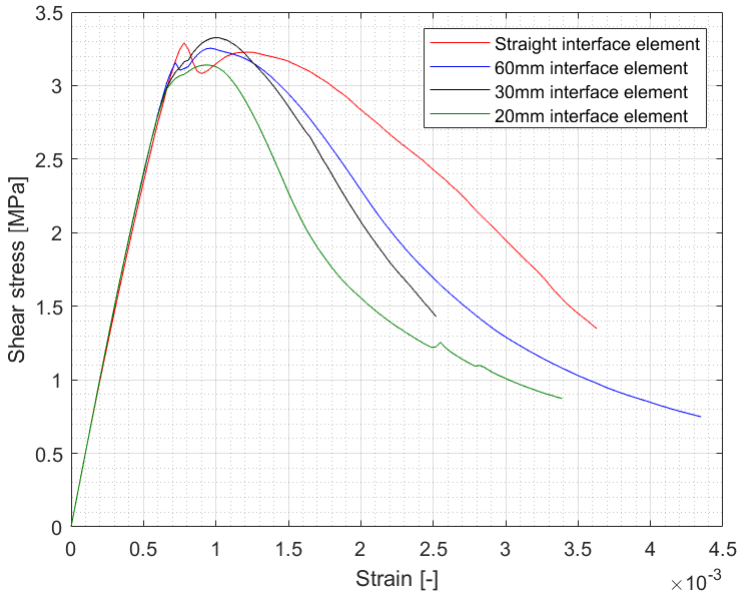

Figure A.7: Shear stress - strain curves with different interface element sizes

Figure A.7, shows the shear stress - strain behavior of the composite concrete models when different interface detailing is incorporated. The maximum shear capacities for all the different interface designs are more or less same. However, important factor here is the post-peak response of these models. Model with a straight interface layer shows higher ductility than the models with wavy interface. Moreover, the ductility decreases as wavelength of the artificial interface elements is reduced. This behavior can be attributed to the orientation of weak points in the interface layer. This means that, in a straight line-interface, although the weak points are distributed randomly, but the transfer of stress between the elements make the entire assembly more ductile than in the case of explicitly rough interface.

Influence of Boundary conditions

The boundary conditions used so far are chosen according to the manual details of ATENA engineering software package. However, there can be many different combinations possible for boundary conditions to test the shear capacity of the interface. Hence, an additional test is performed using different boundary conditions (BC2), details of which are shown in the mechanical model (Figure A.8). In this model, the top and bottom layers are fixed in vertical direction, to ensure failure at the interface. Lateral loading is applied to the top concrete element through a steel plate and support in horizontal direction is provided to the bottom concrete element on the opposite edge of the model.

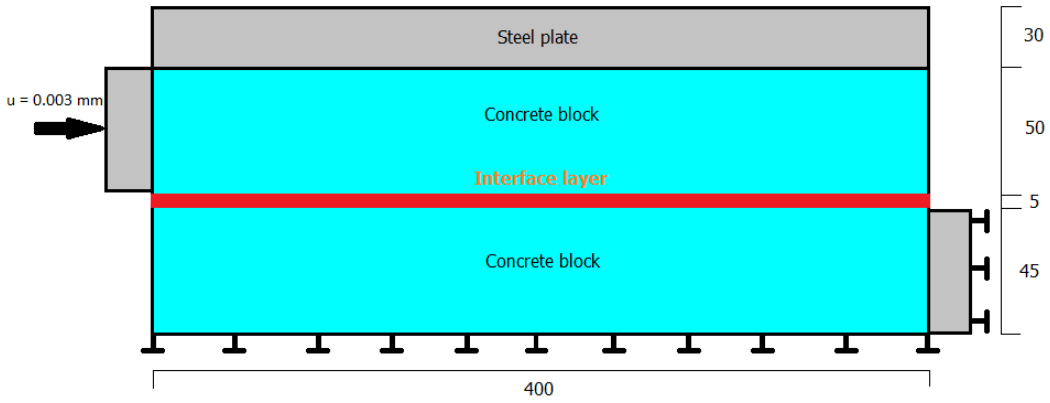

Figure A.8: Mechanical model for different boundary conditions (BC2)

The interface layer shown in the above figure is varied in the same manner as in the previous shear test model; straight layer (for smooth surface class) and wave pattern with two different amplitudes (for slightly rough and rough surface classes). The material property used for these interface layers is same as before, corresponding to a weaker concrete class ($f_t = 0.5\ MPa$).

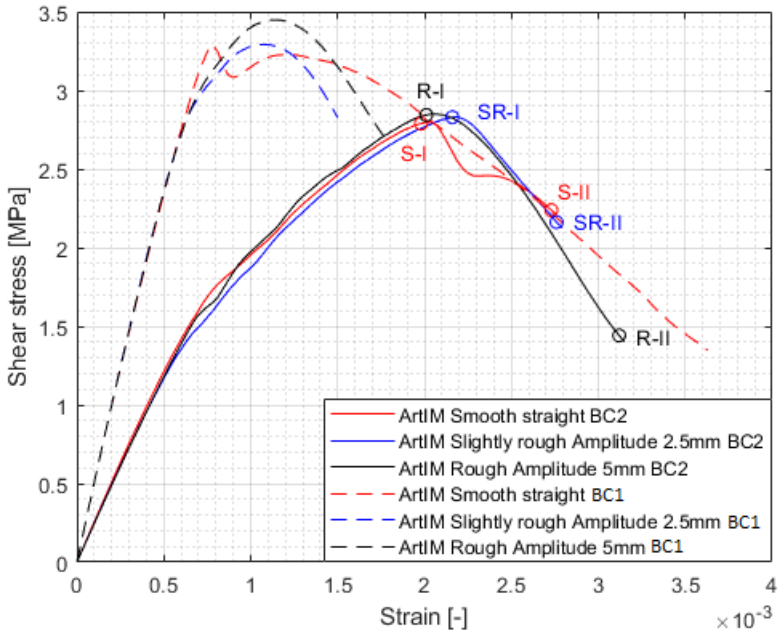

Figure A.9: Shear stress - strain comparison between old and new boundary conditions

Figure A.9, shows a direct comparison in the stress - strain curve between the two boundary conditions (old and new). The dotted curves represent old boundary conditions (BC1) and the solid line curves represent new boundary conditions (BC2). The trend of both the curves is in correspondence with each other. However, the initial stiffness of the model when loading is applied directly to the concrete layer from the side (BC2 case) is much lower than the case when, load is applied to the top steel plate by using the old boundary conditions (BC1 case). Moreover, use of BC2 underestimates the shear capacities of the respective models. The shear response does not vary significantly for the different roughness classes when new boundary conditions are used. Crack distribution in the respective models is displayed hereafter.

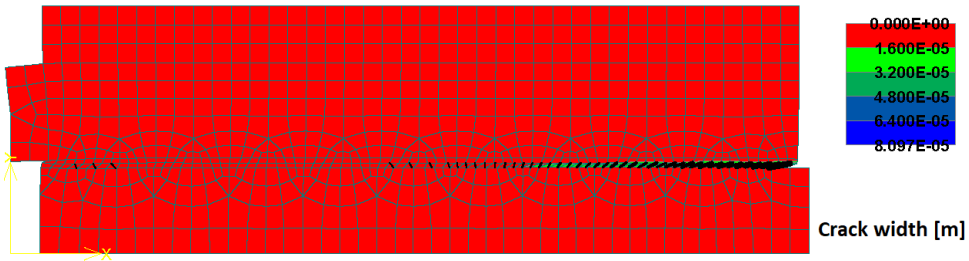

(a) At peak load step (S-I)

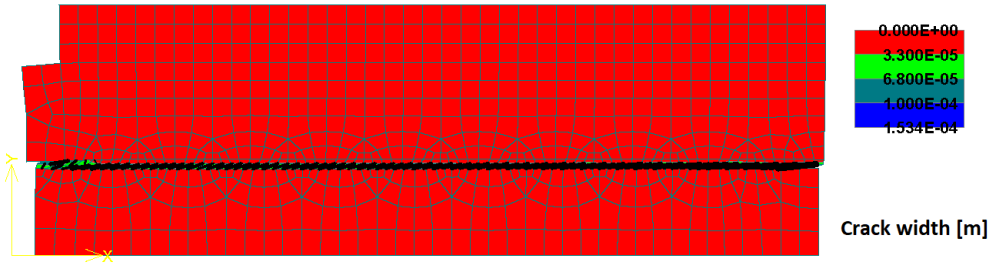

(b) At final load step (S-II)

Figure A.10: Crack distribution when smooth interface (straight element) is modelled using BC2 (Displacement Multiplier = 100)

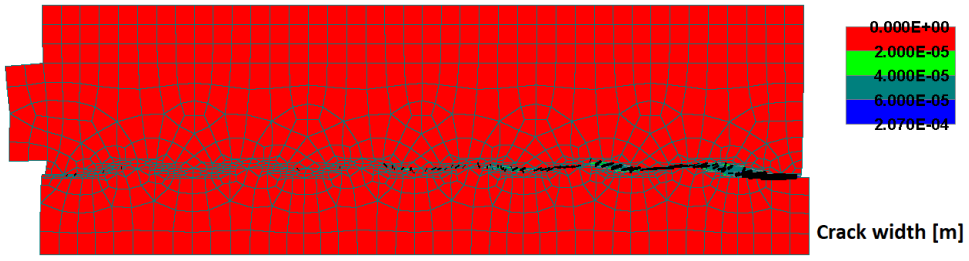

(a) At peak load step (SR-I)

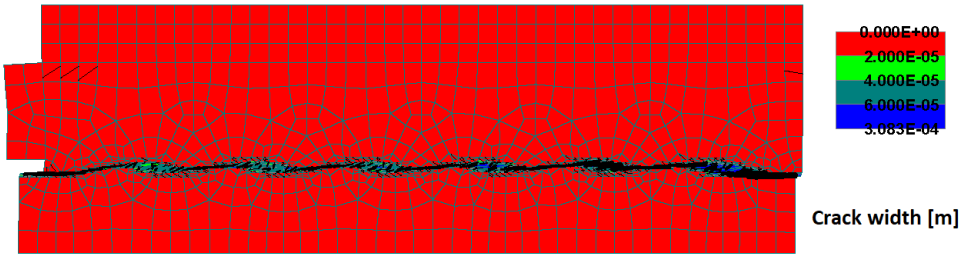

(b) At final load step (SR-II)

Figure A.11: Crack distribution when smooth interface (straight element) is modelled using BC2 (Displacement Multiplier = 100)

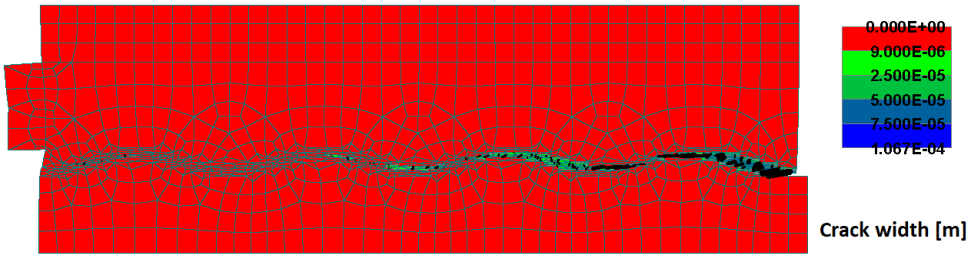

(a) At peak load step (R-I)

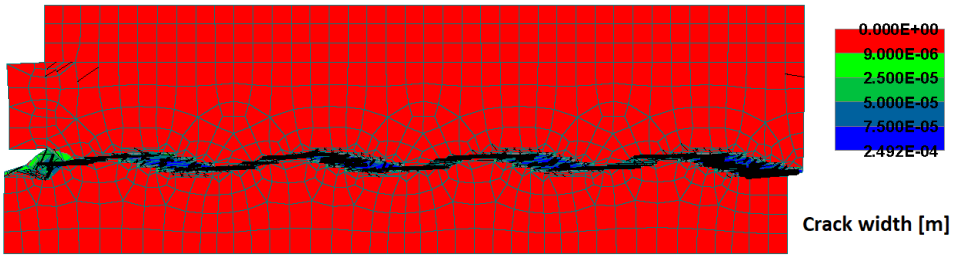

(b) At final load step (R-II)

Figure A.12: Crack distribution when smooth interface (straight element) is modelled using BC2 (Displacement Multiplier = 100)

The crack distribution shown in Figures A.10 - A.12 clearly shows that in every roughness condition, cracks are always localized in the interface element. However, by using BC2, the cracks initiate at the right most end of the interface unlike in case of BC1, where cracks initiated at a weaker section somewhere near the left end of the interface because of the stress flow following the strut-tie model. Here, no such stress distribution is observed and hence, no diagonal cracks develop.

B

Validation of the model

Length of the reinforcement (RF) bars crossing the interface/anchorage length is an important aspect in designing the numerical model. In the experimental set-up the bars run through the entire height of the composite concrete specimen. However, while designing the numerical models, various different techniques are undertaken to model the reinforcement bars (**section**). In some techniques, it is practically not possible to maintain full length of the bars, for example, in case of cross pattern bars, small length is necessary to ensure encasing of the RF bars into the concrete elements. While in case of RF bars designed as macro-elements, since meshing is provided to the bars in addition to the concrete and steel plate elements, a fine mesh takes a considerable amount of computation time to run the analysis. Thus, to decrease the computation time, small length of the RF bars needs to be chosen. Hence, a small test is simulated to select the appropriate length of the RF bar.

A numerical model as shown in Figure 5.4, is used for the simulation. According to the Eurocode 2 guidelines, the anchorage length should not be less than 5ϕ (ϕ is diameter of the RF bar). Nevertheless a total length of 200 mm is chosen for the short RF bar design (100 mm anchorage on both sides of interface, diameter of RF bar being 9.5 mm).

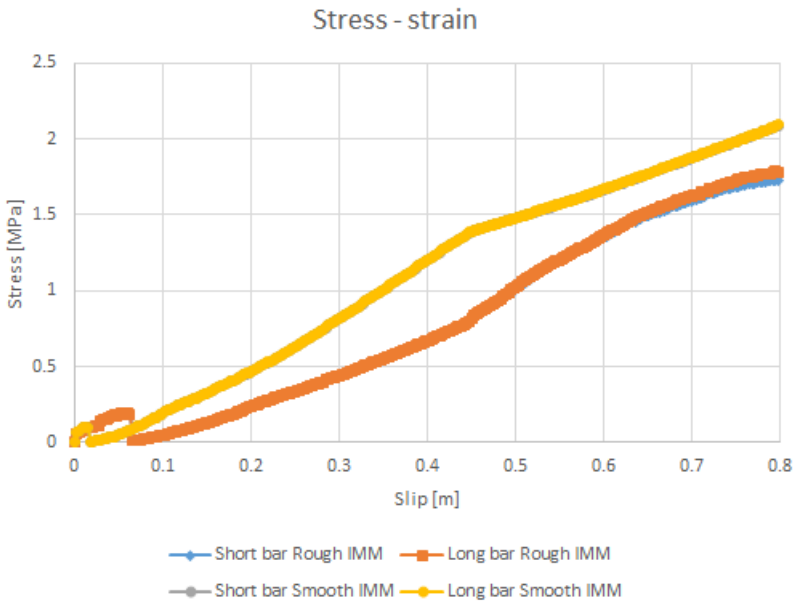

Figure B.1: Stress - strain curve for smooth and rough interface using ATENA IMM

Figure B.1, shows that the responses for both the lengths, chosen for the RF bars, are exactly same. Hence,

a shorter length of the bar is appropriate for simulating any other model using different RF modelling technique.

Bibliography

[1] T. Paulay, R. Park, and M. Phillips, *Horizontal construction joints in cast-in-place reinforced concrete,* Special Publication **42**, 599 (1974).

[2] H. Ir. Borsje and G. Ir. Dieteren, *Onderzoek naar de technische oorzaak van de gedeeltelijke instorting van de in aanbouw zijnde parkeergarage P1 Eindhoven Airport,* , 104 (2017).

[3] T. Bjerrum and W. Gladrow, *Bezwijken Parkeergarage Eindhoven Airport,* , 1 (2017).

[4] C. Zanotti and N. Randl, *Are concrete-concrete bond tests comparable?* Cement and Concrete Composites **99**, 80 (2019).

[5] N. Randl, M. Steiner, and M. Peyerl, *Sustainable strengthening of rc members with high performance concrete overlays,* Maintenance, Monitoring, Safety, Risk and Resilience of Bridges and Bridge Networks , 370 (2016).

[6] J. Walraven and H. Reinhardt, *Concrete mechanics. part a: Theory and experiments on the mechanical behavior of cracks in plain and reinforced concrete subjected to shear loading,* NASA STI/Recon Technical Report N **82** (1981).

[7] C. E. De Normalisation, *Eurocode 2: Design of concrete structures—part 1-1: General rules and rules for buildings,* Brussels, Belgium (2004).

[8] P. M. D. Santos and E. N. B. S. Júlio, *Factors affecting bond between new and old concrete,* ACI Materials Journal **108**, 449 (2011).

[9] N. Randl, *Design recommendations for interface shear transfer in fib model code 2010,* Structural Concrete **14**, 230 (2013).

[10] C. Republic, *ATENA Program Documentation Part 1 Theory,* (2018).

[11] A. S. Code, *Building code requirements for reinforced concrete and commentary,* in *American Concrete Institute* (2008) p. 473.

[12] P. Santos and E. N. Júlio, *Interface shear transfer on composite concrete members.* ACI Structural Journal **111** (2014).

[13] P. W. Birkeland and H. W. Birkeland, *Connections in precast concrete construction,* in *Journal Proceedings*, Vol. 63 (1966) pp. 345–368.

[14] A. H. Mattock and N. M. Hawkins, *Shear transfer in reinforced concrete-recent research,* PRECAST/PRESTRESSED CONCRETE INSTITUTE. JOURNAL **17** (1972).

[15] R. Loov, *Design of precast connections,* in *a seminar organized by Compa International Pte, Ltd* (1978).

[16] J. Walraven, J. Frenay, and A. Pruijssers, *Influence of concrete strength and load history on the shear friction capacity of concrete members date: January-february, 1987,* (1987).

[17] S. Tsoukantas and T. Tassios, *Shear resistance of connections between reinforced concrete linear precast elements,* Structural Journal **86**, 242 (1989).

[18] P. M. D. Santos and E. N. B. S. Júlio, *Effect of filtering on texture assessment of concrete surfaces,* Materials Journal **107**, 31 (2010).

[19] B. Rasmussen, *Strength of transversely loaded bolts and dowels embedded in concrete,* Meddelelse Laboratoriet for Bugningastatik, Denmark Technical University **34**, 39 (1962).

[20] E. Vintzēleou and T. Tassios, *Mathematical models for dowel action under monotonic and cyclic conditions,* Magazine of concrete research **38**, 13 (1986).

[21] K. Zilch and A. Müller, *Grundlagen und anwendungsregeln der bemessung von fugen nach en 1992-1-1,* (2007).

[22] B. Belletti, C. Damoni, M. Hendriks, and J. Den Uijl, *Nonlinear finite element analysis of reinforced concrete slabs: Comparison of safety formats,* in *FraMCos-8: Proceedings of the 8th International Conference on Fracture Mechanics of Concrete and Concrete Structures, Toledo, Spain, 10-14 March 2013* (International Center for Numerical Methods in Engineering, 2013).

[23] D. Pryl, *ATENA Program Documentation Part 11 Troubleshooting Manual,* (2017).

[24] H. Kupfer, H. K. Hilsdorf, and H. Rusch, *Behavior of concrete under biaxial stresses,* in *Journal Proceedings*, Vol. 66 (1969) pp. 656–666.

[25] H. Schlangen, *Experimental and numerical analysis of fracture processes in concrete,* HERON, 38 (2), 1993 (1993).

[26] P. M. Santos and E. N. Júlio, *A state-of-the-art review on roughness quantification methods for concrete surfaces,* Construction and Building Materials **38**, 912 (2013).